

EXPERIMENTAL STUDY ON THE EFFECT OF LOW
WATER SALINITY AND IONIC COMPOSITION ON
WETTABILITY ALTERATION IN CARBONATES.

GBADEBO NAFIU ADEJUMO

June 10th, 2021.

Abstract

Rock wettability plays an important role in oil production. A slight change in rock wettability towards more water wetness will have a significant change in the oil production. Carbonate rocks tend to be preferentially oil-wet or mixed-wet. Altering the ionic composition of the injected brine and lowering the salinity has proven to be an efficient way to improve the water wetness of carbonate rocks. This claim has been supported by several laboratory and field tests.

This masters thesis is a continuation of the work done as part of the specialization project by Adejumo (2020). The objective of this thesis is to explore the efficiency of two aging methods and to investigate the influence of brines with varying salinity and ionic composition on oil recovery in a spontaneous imbibition (SI) experiment. The SI tests are conducted at an elevated temperature of 96°C using high temperature Amott cells.

Two outcrop cores, one from Angola and one from Ainsa in Spain, were used in this study. They are considered as representatives of carbonate fields in Brazil. The same Ainsa cores were previously used by Azizov (2019). The Ainsa cores have higher porosity, and are more homogeneous than the Angola cores. The Angola cores are heterogeneous and tight. Both core materials are classified as anhydrite free limestones. From the mineralogy experiments, traces of magnesium were found in the Angola cores, but not enough to classify them as dolomite cores.

The dynamic aging method proved to be more efficient in core restoration. The interplay between the potential determining ions, SO_4^{2-} , Mg^{2+} and Ca^{2+} in seawater (SW) was able to improve the water wetness of the carbonate samples. Also, an NaCl reduced SW brine, resulted in an incremental oil recovery of about 5.5 % of original oil in place (OOIP). In addition, all modified versions of NaCl reduced SW brines were able to improve oil recovery in all of the spontaneous imbibition experiments carried out. Results of contact angles and zeta potential measurements are in agreement with those results from the SI experiments. Furthermore, SO_4^{2-} and Mg^{2+} are found to be potential determining ions to a carbonate surface, as they are able to alter wettability towards more water-wet conditions.

Acknowledgement

Firstly, my gratitude to God Almighty, who is the author of life, in his grace I am alive today to pen down this report. Also my sincere appreciation to my parents and siblings with whose permission and blessings I began this journey of pursuing a master's degree in Petroleum Engineering at Norwegian University of Science and Technology (NTNU). They have been supportive in all possible forms.

Sincerely, I will not have completed this thesis and the experimental study without thorough guidance, constant motivation, and supervision from Carl Fredrik Berg and my co-supervisor Antje van der Net. Their constant tutoring and directions to solving the problems I encountered while carrying out this specialization project really kept me going through tough times. I am sincerely thankful for the time they dedicated to sharing their knowledge.

My profound gratitude goes to the representatives of Equinor - Rex M.s Wat and Thomas Ramstad for being kind enough to provide the essential materials we have requested, for the experiment. Furthermore, I am indebted to the Lab engineer-Roger Overa for his support with laboratory procedures. His motivation and constant drive is a joy to behold. I am grateful for him. Special thanks to Alberto Luis Bila as well for always being ready to provide assistance even though he is miles away from Norway. I like to thank Haili Long-Sanouiller for her assistance. Working with her was quite seamless and I appreciate the comfort she offers.

Special mention to Jon Runar Drotninghaug and Gunner, who helped with the core cutting. Finally, to my friends home and abroad who understand the meaning of true friendship, I thank them for the good and bad days. You are the best!

Thank you all.
Gbadebo Nafiu Adejumo.

Contents

Abstract	vii
Acknowledgement	ix
Contents	xi
Figures	xv
Tables	xxi
Acronyms	xxiii
1 Introduction	1
2 Background	5
2.1 Wettability	5
2.1.1 Carbonate reservoir rock family	7
2.2 Wetting in carbonate rocks	7
2.2.1 Initial wetting conditions in carbonate reservoirs	8
2.3 Acid number	9
2.4 Core aging	11
3 Surfaces forces and mechanisms	17
3.1 Role of surface forces on wettability	17
3.1.1 Disjoining pressure	17
3.1.2 van der Waals interaction and Hamaker constant	18
3.1.3 Stability of wetting layer film and DLVO theory	20
3.1.4 Electric double layer model	22
3.2 Mechanisms	24
3.2.1 Multi-ion exchange	25
3.2.2 Electric double layer	26
3.2.3 Rock dissolution	27
3.2.4 Fines migration	28
3.2.5 Interfacial tension reduction	28
3.3 Zeta potential and electric double layer	28
4 Effect of brine composition on wettability	31
4.1 Oil recovery in limestone cores	31
4.1.1 Effect of ionic composition	31
4.1.2 Effect of divalent ions on interfacial tension	36
4.1.3 Effect of divalent ions on zeta potential	37
4.1.4 Effect of divalent ions on contact angle measurements	40
4.2 Effect of brine salinity	41

4.2.1	Presence of anhydrite	44
4.2.2	Effect of brine salinity on interfacial tension	46
4.2.3	Effect of brine salinity on contact angle measurements	47
4.2.4	Effect of brine salinity on zeta potential	50
4.3	Oil recovery in other carbonate cores	51
4.3.1	Chalk	51
4.3.2	Dolomite	55
5	Methods and materials	57
5.1	Liquids preparation	57
5.1.1	Oil preparation	57
5.1.2	Brines preparation	58
5.2	Liquid properties	59
5.2.1	Density measurements	59
5.2.2	Viscosity measurements	60
5.2.3	Interfacial tension measurements	61
5.3	Core analysis	61
5.3.1	Core cutting and dimensions	61
5.3.2	Core cleaning, drying and storage.	62
5.3.3	Porosity measurements	63
5.3.4	Permeability measurements	64
5.3.5	Thin sections and scanning electron microscope	65
5.4	Core plug saturation	66
5.4.1	Formation water saturation	66
5.4.2	Contact angle measurements	66
5.4.3	Zeta potential measurements	67
5.4.4	Oil saturation	70
5.5	Core aging	71
5.5.1	Component set-ups	71
5.5.2	Experimental set-up	72
5.6	Spontaneous Imbibition experiment.	74
5.6.1	Experimental and component set-up.	74
6	Results and discussion	79
6.1	Fluid data	79
6.1.1	Density	80
6.1.2	Viscosity	80
6.2	Core data	80
6.2.1	Core cutting and core dimensions	80
6.2.2	Porosity	81
6.2.3	Permeability	82
6.2.4	Core mineralogy	85
6.2.5	Saturation of core plug	87
6.2.6	Contact angle	89
6.2.7	Zeta potential	96
6.3	Core aging	100

6.4	Spontaneous imbibition	100
6.4.1	Static and dynamic aging results.	101
6.4.2	Examining the individual roles of NaCl, magnesium and sulphate.	104
6.4.3	Spontaneous imbibition results on varying magnesium content	107
7	Conclusion and future work	109
7.0.1	Future work	110
	Bibliography	113
A	Additional material	119
A.1	Raw measurement data	119
A.1.1	Core dimensions	119
A.1.2	Porosity and permeability measurements	120
A.2	Porosity measurements	121
A.3	Viscosity and irreducible water saturation data	122
A.4	Contact angle data	123
A.5	Zeta potential data	124
A.6	Spontaneous imbibition data	125

Figures

2.1	Wetting in pores. Figure from Abdallah et al. (1986)	6
2.2	SI results of brines, into a core sample, using different oils with varying acid number (AN). Figure from Standnes and Tor Austad (2000).	10
2.3	Spontaneous imbibition of FW into limestone cores with a varying AN at 110° C. Figure from Austad et al. (2012).	11
2.4	Comparison between static and dynamic Aging. Figures from Fernø et al. (2010).	12
2.5	Static Aging. Figures from Standnes and Tor Austad (2000).	13
2.6	Cross sectional view of statically aged cores, showing non uniform wettability distribution, after being halved following a statically aged process. Figure from Standnes and Tor Austad (2000).	14
2.7	Dynamic aging: No visible induction time and uniform wettability distribution due to aging type. Figures from Standnes and Tor Austad (2000).	14
3.1	Spreading of reservoir fluid on a flat horizontal surface, resulting in primary film with thickness, h. Figure from Donaldson and Alam (2013, p.84).	18
3.2	Schematic showing the relationship between V_T and H_0 . Figure from Han (2002, p.53).	21
3.3	Interaction energy between two identical spherical particles. Figure from Butt, Graf and Kappl (2013, p.104).	21
3.4	The electric double-layer model. Figure from Han (2002, p.25).	22
3.5	Schematic of diffuse electric double-layer. Figure from Butt, Graf and Kappl (2013, p.46).	24
3.6	Suggested wettability alteration mechanism in carbonate surface to illustrate the interplay between Mg^{2+} and Ca^{2+} at high temperatures. Figure from Peimao Zhang, Tweheyo and Tor Austad (2007).	25
3.7	Diagrammatic representation of electric double layer. Figure from Google Images.	26
3.8	A schematic diagram showing the effect of NaCl interaction with other ions on the chalk surface. Figure from Seyed Jafar Fathi, Tor Austad, Strand et al. (2012).	27

3.9	A diagrammatic representation of the potential at the slipping plane. Figure from Zetasizer Nano series Manual.	29
4.1	Contact angle measurements with varying brine salinities and temperature. Figure from Gupta and Mohanty (2011).	32
4.2	Contact angle measurements with varying brine salinities at 90°C. Figure from Gupta and Mohanty (2011).	33
4.3	Results from spontaneous imbibition of limestone cores at a temperature of 120°C by brines with and without SO_4^{2-} . Figure from Strand, Tor Austad et al. (2008).	33
4.4	Oil recoveries made in a SI experiment, with varying imbibing brines at 120°C. Figure from Karimi et al. (2016).	35
4.5	interfacial tension (IFT) results for varying salinity brines with different divalent concentrations. Figure from Tetteh, Janjang, Barati et al. (2018).	36
4.6	Zeta potential results for varying salinity brines with different divalent concentrations. Figure from Tetteh, Janjang, Barati et al. (2018).	37
4.7	Zeta potential of brines with varying composition and pH values of measurement. Figure from Gopani et al. (2021).	39
4.8	Zeta potential of brines with varying ionic strengths. Figure from Gopani et al. (2021).	39
4.9	Contact angle measurements at 40°C, using brines of varying Ca^{2+} and Mg^{2+} concentrations. Figure from Tetteh, Janjang, Barati et al. (2018).	40
4.10	Contact angle measurements at 40°C, using brines of varying ionic composition. Figure from Tetteh, Janjang, Barati et al. (2018).	41
4.11	Coreflooding results of a composite carbonate core which had been injected with brines diluted 2, 10, 20 and 100 times the salinity of Gulf SW. Figure from Yousef, Al-Saleh, Al-Kaabi et al. (2010).	42
4.12	Spontaneous imbibition results for a limestone with varying brine salinities. Figure from Romanuka et al. (2012).	43
4.13	Spontaneous imbibition results for a limestone with varying brine salinities at temperatures of 70°C and 120°C. Figure from Romanuka et al. (2012).	44
4.14	Oil recovery test of a core with anhydrite in the pore space. Figure from Tor Austad, Seyed Farzad Shariatpanahi et al. (2015).	45
4.15	IFT measurement results live oil and brines with varying degree of dilution compared to levels in ordinary SW. Figure from Yousef, Al-Saleh, Al-Kaabi et al. (2010).	46
4.16	Images of wettability measurements when using brines of varying salinities Yousef, Al-Saleh, Al-Kaabi et al. (2010).	47
4.17	Contact angle measurements when using brines of varying salinities Karimi et al. (2016).	48

4.18	Contact angle measurements when using brines of varying salinities (FW) and (SW) on limestone (left) and dolomite (right) patches right. Mahani et al. (2015).	49
4.19	Contact angle measurements when using brines of varying salinities (FW) and 25dSW on limestone (left) and dolomite (right) patches right. Mahani et al. (2015).	49
4.20	Zeta potential of two carbonate rocks in varying brine salinities. Figure from Mahani et al. (2015).	50
4.21	Spontaneous imbibition into oil saturated chalk cores using different imbibing fluids, with different salinities and ionic composition. $S_{wi}=10\%$. Figures from Seyed Jafar Fathi, Tor Austad, Strand et al. (2012).	51
4.22	Spontaneous imbibition into oil saturated chalk cores at 110°C using different imbibing fluids, with different SO_4^{2-} concentrations, Oil with AN=2.1, $S_{wi}=26\% - 28\%$. Figure from Strand, Høgnesen and Tor Austad (2006).	52
4.23	Combined Interaction between Mg^{2+} and Ca^{2+} . Figure from Peimao Zhang, Tweheyo and Tor Austad (2007).	53
4.24	The effect of PDIs on spontaneous imbibition into chalk core at several temperatures. Figure from Peimao Zhang, Tweheyo and Tor Austad (2007).	54
4.25	Chromatography test results on dolomite core. Figure from S. Shariatpanahi et al. (2016).	55
4.26	Spontaneous imbibition results on dolomite core with varying brine compositions. AN=0.52 mgKOH/g. Figure from S. Shariatpanahi et al. (2016).	56
5.1	An image of the oil filtration set-up.	58
5.2	Pycnometer.	59
5.3	Brookfield rotational viscometer.	60
5.4	A schematic of the pendant drop method set-up.	61
5.5	Angola whole core as provided by Equinor.	62
5.6	Core cleaning by Soxhlet extraction.	63
5.7	Helium Porosimeter.	64
5.8	Permeability measurement set-up. Figure 5.8b is from Torsæter and Abtahi (2003).	65
5.9	A schematic of vacuum pump apparatus.	66
5.10	Contact angle measurement experimental set-up.	67
5.11	Zeta potential measurement experimental set-up.	68
5.12	One of the solutions being stirred on the magnetic stirrer.	68
5.13	Checking for asphaltene precipitation, using the microscope.	69
5.14	Centrifuge apparatus.	70
5.15	Components set-up for the centrifuging process	70
5.16	Schematic of dynamic aging set-up without sleeve pressure.	73

5.17	Schematic of dynamic aging set-up with sleeve pressure.	73
5.18	Some of the components used in the high temperature imbibition experiments.	75
5.19	Schematic of spontaneous imbibition (SI) setup.	76
5.20	Schematic of spontaneous imbibition (SI) setup for the replacement of brines with comparative densities.	78
5.21	Images of the imbibition rig.	78
5.22	External view of the imbibition rig.	78
6.1	Gas permeability against inverse of mean pressure plot for core plugs B1, B2 and B3.	84
6.2	Gas permeability against inverse of mean pressure plot for core plugs B5, B6 and B8.	84
6.3	Gas permeability against inverse of mean pressure plot for core plug C1.	85
6.4	Gas permeability against inverse of mean pressure plot for core plug C2.	85
6.5	Core mineralogy.	86
6.6	SEM analysis of section E1.1.	87
6.7	Produced FW, after the centrifuging process.	88
6.8	Problems encountered during the oil saturation of Angola cores. . .	89
6.9	Contact angle (CA) measurements after calcite surface contact with SW and then, SW-0.1NaCl brine.	90
6.10	Contact angle (CA) measurements to determine the impact of selective dilution NaCl in seawater (SW).	91
6.11	Contact angle measurements after calcite surface were aged in varying salinity and ionic brine concentrations at 96°C.	92
6.12	Contact angle measurements with chip 2, brine (FW and then aged at 96°C.	92
6.13	Contact angle measurements with chip 2, have contact with FW, SW, SW-0.1NaCl-2S-4Mg and then SW-0.1NaCl-2S-8Mg aged at 96°C.	92
6.14	Contact angle measurements after calcite surface were aged in varying salinity and ionic brine concentrations at 23°C.	93
6.15	Contact angle measurements with chip, brine (FW and then aged at 23°C.	94
6.16	Contact angle measurements with chip 2, have contact with FW, SW, SW-0.1NaCl-2S-4Mg and then SW-0.1NaCl-2S-8Mg aged at 23°C.	94
6.17	Contact angle measurements, after 3 drops on a calcite surface, exposed to SW-0.1NaCl-2S-8Mg, after contact with FW. Brine aging was done at 96°C.	95
6.18	Contact angle measurements with chip, brine (FW and then SW-0.1NaCl-2S-8Mg) aged at 96°C.	95

6.19	ζ potential results of pure limestone powder in varying brines, temperature and pH. 4Mg represents SW-0.1NaCl-2S-4Mg and 8Mg represents SW-0.1NaCl-2S-8Mg.	97
6.20	ζ potential results of crude-oil aged limestone powder in varying brines, temperature and pH. 4Mg represents SW-0.1NaCl-2S-4Mg and 8Mg represents SW-0.1NaCl-2S-8Mg.	99
6.21	Segregation due to density difference, seen when changing to brines with lower salinity.	101
6.22	Spontaneous imbibition experimental results of two limestone cores, after being imbibed by FW and SW successively and aged statically (B8) and dynamically (B1).	102
6.23	Observation of oil droplet spread on the surface of core sample B1.	103
6.24	Oil recovery by spontaneous imbibition into cores B2 and B3 using different imbibing brines.	105
6.25	Oil recovery by spontaneous imbibition (SI) into cores C1 and C2 using different imbibing brines.	107
A.1	Core Dimensions for all cores used in the experiment.	119
A.2	Permeability measurement data for Ainsa cores B1, B2 and B3.	120
A.3	Permeability measurement data for Ainsa cores B5, B6 and B8.	120
A.4	Permeability measurement data for Angola cores.	121
A.5	Porosity measurement data for all cores.	121
A.6	Final porosity measurement data for all cores.	122
A.7	Liquid Porosity Measurements	122
A.8	Viscosity measurement data	123
A.9	Irreducible water saturation results	123
A.10	Contact angle measurement results for SW, then SW-0.1NaCl sequence	123
A.11	Contact angle measurement results for FW - SW-0.1NaCl-2S-8Mg sequence at high temperature.	124
A.12	Contact angle measurement results for FW - SW-0.1NaCl-2S-8Mg sequence at room temperature.	124
A.13	Contact angle measurement results for direct FW - SW-0.1NaCl-2S-8Mg sequence	124
A.14	Zeta potential data for pure limestone powder.	125
A.15	Zeta potential data for crude oil aged powder.	126
A.16	Spontaneous Imbibition data for cores B1 and B8	127
A.17	Spontaneous Imbibition data for cores C1 and C2	127
A.18	Spontaneous Imbibition data for cores B2 and B3	128

Tables

4.1	Results of adsorption tests on limestone surface. Data source: Strand, Tor Austad et al. (2008).	34
4.2	Results of IFT measurements on limestone surface. Source: Tetteh, Janjang, Barati et al. (2018).	47
4.3	Results of Zeta potential measurements in Tetteh, Janjang, Barati et al. (2018).	50
5.1	Synthetic formation water and seawater composition.	59
5.2	Modified seawater compositions.	59
6.1	Heidrun oil parameters.	79
6.2	Formation water (FW) parameters.	79
6.3	Results from density measurements at room temperature.	80
6.4	Results from viscosity measurements.	80
6.5	Core dimensions	81
6.6	Data for old and new helium and liquid porosity measurements for the Ainsa cores. The old values are those gotten in (Azizov, 2019), while the new values are results from this experiment. PV is pore volume.	82
6.7	Data for pore volume (PV) and helium porosity measurements for the Angola cores.	82
6.8	Data of permeability measurements. The old values are those gotten by (Azizov, 2019) while the new values are results from this experiment.	83
6.9	Pore volume and liquid permeability results for core materials.	83
6.10	Elements by weight percentage from SEM analysis.	86
6.11	A table showing the SWIRR calculation results.	88
6.12	Contact angle measurement sequence and aging conditions for phase 1.	89
6.13	Contact Angle: Measurement sequence and conditions for phase 2.	91
6.14	Petrophysical properties of the Ainsa cores used for SI experiments at elevated temperature.	102
6.15	Petrophysical properties of the Ainsa cores, B2 and B3, used for SI experiments at elevated temperature.	104

6.16 Petrophysical properties of Angola cores, C1 and C2 used for SI
experiments at elevated temperature. 107

Acronyms

- A** cross-sectional area. 62
- AN** acid number. xv, xvii, 8–11, 51, 52, 56, 57, 109, 110
- BN** basic number. 51
- CA** contact angle. xviii, 91
- CT** computerized tomography. 62
- DI** Deionized water. 58
- EDL** electric double layer. xv, 3, 22, 25–27, 37, 56, 97
- EOR** enhanced oil recovery. 2–4, 8, 9, 24, 31, 33, 55
- FB** formation brine. 2, 8, 27, 31, 34–37, 41, 46–48, 51
- FW** Formation water. xv, xvii–xix, xxi, 8, 10, 11, 34, 40–45, 47–50, 55, 58, 59, 66, 71, 76, 77, 79, 80, 87, 88, 91–98, 101–105, 107, 109, 110
- IFT** interfacial tension. xii, xvi, xxi, 4, 5, 25, 28, 36, 37, 46–48, 61, 79
- LSW** low salinity water. 36, 37, 40, 41, 47, 49, 50
- MIE** multi-ion exchange. 3, 25, 26, 28, 34, 37, 54
- NTNU** Norwegian University of Science and Technology. ix
- OOIP** original oil in place. vii, 1, 2, 33, 35, 36, 43, 45, 51, 52, 55, 103–108, 110
- PDI** potential determining ion. vii, xvii, 2, 3, 7, 9, 24–26, 31–35, 37, 38, 40, 41, 43, 44, 46, 48, 51, 53–55, 91, 93, 97, 98, 103, 105, 106, 108, 110
- PPM** parts per million. 41

PV Pore volume. 102, 104, 107

RPM rotations per minute. 62, 70, 80, 88, 89

SEM scanning electron microscope. xxi, 65, 66, 85–87

SI spontaneous imbibition. vii, xv, xvi, xviii, xix, xxi, xxii, 1–4, 8, 10, 13, 14, 27, 33, 35, 41, 44, 54, 57, 74–84, 100–102, 104–107, 109–111

SW seawater. vii, xvi–xix, xxi, 2, 9, 24, 27, 28, 31, 33–38, 41–51, 53–56, 58, 59, 76, 77, 80, 89–99, 101–110

SWIRR irreducible water saturation. xxi, 6, 88, 102, 104, 107

VDW Van der Waals. 17–21, 96

Chapter 1

Introduction

Oil production in Brazil has been on an upward trending pattern since 2008, when it produced about 2 million barrels for each day. From that point, forward production has expanded almost 53 %, arriving at a normal of 3.10 million barrels for each day in 2019 Bruna Alves (2020). Campos Basin, the main production province in Brazil, was discovered in 1974. It is located on the North coast of the Rio de Janeiro State (Costa Fraga et al., 2003). As of 2008, only about 10 % of the original oil in place (OOIP) had been recovered (Lucia, 2007). This low oil recovery is a general characteristics of carbonate reservoirs, i.e, dolomite, limestone and chalk. More than 50 % of world oil reserves are located in carbonate reservoirs (Strand, Tor Austad et al., 2008). The average worldwide oil recovery from carbonate reservoirs is estimated at 30 % (Strand, Høgnesen and Tor Austad, 2006).

Carbonate rocks tend to be preferentially oil-wet or mixed wet because of the positive zeta potential of the rock surface, solubility of anhydrite and presence of organic acids in oil (Gandomkar and Rahimpour, 2017; Strand, Høgnesen and Tor Austad, 2006; Peimao Zhang, Tweheyo and Tor Austad, 2007). As at 2016, Al-Hadhrami and Blunt (2001) reported that after 20 years of production, only 2 % of oil recovery has been made in Ghaba North Field in Oman which is considered to be a carbonate reservoir. Generally, carbonate reservoirs are considered to be fractured and having low permeability, i.e, being tight. Hence, the oil recovery from these kind of reservoirs is a great challenge in the industry today (Peimao Zhang and Tor Austad, 2006).

Spontaneous imbibition is a process where a wetting phase displaces a non-wetting phase by capillary action (Sriram Chandrasekhar, 2013). The ability of imbibing brines to recover oil can be accessed by the SI process. The SI is relatively easy to conduct in the laboratory, as not large cores sizes are needed and experiments can be carried on wide ranges of samples simultaneously (Romanuka et al., 2012). The wettability alteration by the low salinity brines is assessed by the incremental oil recovered during the SI experiments after replacing the current brine with

a low salinity brine (Song et al., 2020). The SI of water into the oil containing matrix is a key process for oil recovery in carbonate reservoirs. The matrix permeability and wettability, play very vital roles in oil production from carbonate reservoirs. The injection of water has been considered as an option for improved oil recovery, however this technique has been unsuccessful in carbonate reservoirs as a lot of residual oil saturation is left behind. Because of the initial wetting state of carbonate rocks, it is imperative for such reservoirs to produce from the rock matrix, therefore majority of laboratory experiments on wettability in carbonate rocks are carried out through the spontaneous imbibition process (Sohal, Thyne and SØgaard, 2016).

Water injection into carbonate reservoirs tends to follow through the path of the fractures and only displace the little oil contained therein. Because of the negative capillarity of oil-wet rocks, the water is unable to imbibe into the matrix blocks which are the source of oil in carbonate reservoirs (Strand, Tor Austad et al., 2008; Karimi et al., 2016). This is attributed to their natural wettability states which is either mixed-wet or oil-wet (Sriram Chandrasekhar, 2013; Gandomkar and Rahimpour, 2017; Strand, Høgenesen and Tor Austad, 2006; Zhang, Tor Austad et al., 2005). The reason for these types of wettability is their net surface charge density, which is usually positive (Donaldson and Alam, 2013, p.227). Wettability is the general attraction of liquids to a surface. In this way, for a water/oil/rock framework, the term wettability alludes to the normal, in general, relative wetting inclination of the interstitial surfaces of the rock (Donaldson and Alam, 2013, p.2).

To date, quite a number of publications, including but not limited to (Sriram Chandrasekhar, 2013; Yi, Sarma et al., 2012; Tor Austad, Seyed Farzad Shariatpanahi et al., 2015; Strand, Høgenesen and Tor Austad, 2006; S Jafar Fathi, Tor Austad and Strand, 2011; S. Shariatpanahi et al., 2016; Yousef, Al-Saleh, Al-Kaabi et al., 2010; Strand, Tor Austad et al., 2008) have focused on how the wettability of the carbonate reservoirs can be altered to more water-wet thereby increasing the ultimate oil recovery. Altering the wettability can be done by reducing the salinity or modifying the ionic composition of the injected brine. Modifying the ionic composition involves varying the quantities of the potential determining ion (PDI), in the injected brine. The capacity of an ion to specially break down (dissolve) over its counter ion is classified as PDI. The injected brine is able to alter the existing thermodynamic equilibrium between all the phases present in the porous media. This alteration is birthed by the interaction between the rock surface and the injected brine.

Seawater (SW) has been found to be an effective enhanced oil recovery (EOR) fluid. SW increased oil recovery by around 40 % of original oil in place (OOIP) compared to the initial formation brine (FB) in a spontaneous imbibition process [Strand, Høgenesen and Tor Austad (2006), Seyed Jafar Fathi, Tor Austad, Strand et al. (2012), S. Shariatpanahi et al. (2016), Yousef, Al-Saleh, Al-Kaabi et

al. (2010), Strand, Tor Austad et al. (2008) and Sriram Chandrasekhar (2013)]. Several mechanisms have been discussed to support the oil recovery by modified injected brines. Some of these mechanism include multi-ion exchange (MIE) and expansion of the electric double layer (EDL). The mechanisms are not yet fully understood, hence continued work on this subject would be of great benefit to the oil industry.

The static and the dynamic aging procedures were used in this experimental study, so as to test the effectiveness of both in wettability restoration. The static aging process entails the core plug being fully submerged in the crude oil at a given temperature, while the dynamic aging process ensures the continuous flow of crude oil through the core samples. One Ainsa core was aged statically. Three (3) Ainsa cores were aged dynamically without sleeve pressure, while two (2) Angola cores were aged dynamically with sleeve pressure. All aging process were carried out at an elevated temperature of 96°C.

This masters thesis is a continuation of the work done as part of the specialization project in Adejumo (2020) in the Fall 2020 semester. This project, sees to study the effect of low salinity effect on enhanced oil recovery (EOR) from Ainsa carbonate and Angola carbonates, which are representatives of carbonate fields in Brazil. As part of this project, core analysis experiments have been carried out to quantify the properties of the reservoir. Hence, the objectives of this specialization project are;

1. To build a spontaneous imbibition set up at an elevated temperature of 96°C.
2. To look at the possibilities of using the built SI set up to understand the controlling factors behind the oil recovery from core materials by using the knowledge of the PDI on the carbonate surface, to develop varying salinity and ionic composition brines in the SI experiment.
3. To test the effectiveness of the static and dynamic aging process on wettability restoration by building a high temperature dynamic aging set up.

Furthermore, to achieve the aforementioned objectives, several core analysis experiments have been carried out to have a deeper understanding of the reservoir properties, which would serve as guidelines to develop a suitable *smart water* to optimize oil recovery from the core samples. "Smart Water" is an adjusted injection brine which is designed to alter wettability to improve oil recovery Mamonov, Puntervold, Strand et al. (2017). The use of smart waters have improved oil recovery, eliminated the use of expensive chemicals, thereby reducing accompanying environmental and logistical problems Karimi et al. (2016).

In the following chapters, the *Introduction* presents initial knowledge of the study, states the object of the masters thesis and also provides the overall structure of the report. In the *Background*, the literature reviewed are summarized. The chapter

discusses initial wetting in carbonates, types of carbonates and their distinct features and how they respond to low salinity EOR in terms of oil recovery. Furthermore, in the *Surfaces forces and mechanisms* section, effect of different brine composition on contact angle, spontaneous imbibition, zeta potential, interfacial tension (IFT) as discussed in literature are briefly summarised. The *Methods and materials* discusses all materials and methods used for the wettability alteration study on the core samples. The newly built imbibition and dynamic aging rig are also discussed in this chapter. In the *Results and discussion* section, all results obtained from laboratory experiments are discussed. In the *Conclusion and future work* section, final notes and recommendations are made concerning the experimental study as well as the way forward for future works.

Chapter 2

Background

2.1 Wettability

The preference of one fluid in the presence of another, to spread on the surface of the rock in a rock-fluid system can be termed **rock wettability**. Reservoir wettability is determined by complex interface boundary conditions acting within the pore space of rocks (Morrow et al., 1990). Typically, when two immiscible fluids contacts a solid surface, one of the fluids tends to spread more over the solid surface than the other. Interfacial tension (IFT) is the attractive force (adhesive), occurring at the interface, between two immiscible liquids Torsæter and Abtahi (2003). Wettability is a reservoir property that depends on rock-fluid interfacial tension, thus in an oil/water/rock system in equilibrium, the following equation (Young's equation) can be derived;

$$\sigma_{so} - \sigma_{sw} = \sigma_{wo} \cos\theta \quad (2.1)$$

σ_{so} is the interfacial tension between the oil and the solid.

σ_{sw} is the interfacial tension between the water and the solid.

σ_{wo} is the interfacial tension between the water and oil.

$\cos\theta$ is the contact angle measured through the aqueous face.

Adhesion tension A_T ; Equation 2.2, determines which fluid adheres to the solid surface. A positive A_T indicates a water-wetting, a zero A_T indicates mixed-wetting while a negative A_T indicates oil-wetting.

$$A_T = \sigma_{so} - \sigma_{sw} = \sigma_{wo} \cos\theta \quad (2.2)$$

Rock wettability plays an important role in oil production, and for this reason, this subject is widely discussed in the industry. Most reservoirs are usually classified as either water-wet, mixed-wet, or oil-wet. Water-wet means that the rock surface has a preference for water in the presence of oil, while the rock surface has a preference for oil in the case of oil-wetting conditions. When more than 50 % of the surface of a water/oil/rock system is occupied by water, the system is considered as water-wet. That is, water is considered as the continuous phase, while oil, which is the non-wetting phase, is the discontinuous phase. At irreducible water saturation (SWIRR), water remains as the continuous phase through the smaller pores in the porous medium but also, the oil saturation is now sufficient to also act as a continuous phase through the larger pores. The wetting phase ceases to be one, at saturations less than SWIRR. If a water preferring surface is first saturated with oil, and then exposed to water, the water imbibes into the rock pores to displace the oil until a balance is reached between the capillary and surface forces of the fluid and rock (Donaldson and Alam, 2013, p.2).

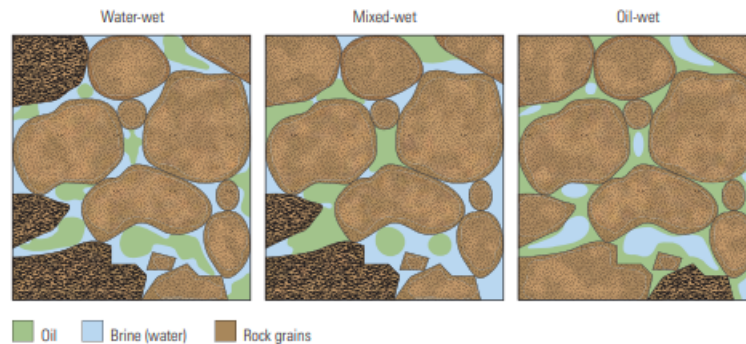


Figure 2.1: Wetting in pores. Figure from Abdallah et al. (1986)

Making the assumption that a reservoir is water-wet, when it is not, can lead to irreversible reservoir damage (Morrow et al., 1990). As shown in Figure 2.1, in a water-wet case, oil remains in the center of the pores. In the case of the oil wetting, the positions of the oil and water, are the reverse of those of the water-wet conditions. Also, oil ceases to be a continuous phase (water is the continuous phase in the water wet conditions), for all saturations less than residual oil saturation (Donaldson and Alam, 2013, p.3). In the mixed-wet case, oil has displaced water from some of the surfaces, but is still in the centers of water-wet pores. The little pores in the rock have a preference for water, while the bigger pores have a preference for oil. The capillary and viscous forces as well as the displacement energies are about the same (Donaldson and Alam, 2013, p.201).

Carbonate reservoirs are usually water-wet prior to oil migration. Wettability affects the amount of oil that can be produced at the pore level. Because the impact of wettability extends from pore scale to reservoir scale, wettability can affect project economics. Satisfactory estimation of rock wettability involves laboratory

experiments. Two most widely discussed methods for estimating rock wettability are contact angle method and the Amott method. Contact angle is the most universal measure of the wettability of surfaces because it provides information about the solid-liquid interaction (Morrow et al., 1990). A water-wet rock would have a contact angle of 0° - 75° ; mixed-wet would have 75° - 115° ; and oil-wet would have 115° - 180° (Santos et al., 2006).

2.1.1 Carbonate reservoir rock family

Carbonates begin from the calcareous skeletons of creatures. These parts are solidified via carbonate precipitating from water. The greater part of the living organisms stayed on the base in shallow marine water, where algae were available. After the death of these organisms, they fall into deeper depth, where they are accumulated (Darling, 2005). One of the most important parameters in classifying carbonate reservoirs, is the network between all porosity types. Because sometimes, the overall porosity can be large enough but the permeability is too low due to tiny pore throats, owned by chains of interconnected pores (Donaldson and Alam, 2013, p.184). The voids within the three kinds of carbonates, ranges and the general guidance for the porosity classifications are extensively discussed in Chilingar and Yen (1992). The types of reservoir rocks found in the carbonate family are chalk, dolomite and limestone. These rocks have their unique features and the affinities of the potential determining ions on the surface of these rocks varies as well. Chalks are the consequence of compaction and cementation of marine creatures, limestone is a combination of carbonate mud and pieces of biogenic materials (Jordan, Sjursather, Collins et al., 2004).

In similarities, all carbonate rock types are all made up of the same chemical composition which is the $CaCO_3$ and same carboxylic materials adsorb on their surfaces. Chalk is a soft, friable and light-coloured version of limestone. Chalk is believed to have more reactive surfaces and having a larger surface area than limestone. The specific surface area of chalk and limestone as measured in Seyed Farzad Shariatpanahi, Strand and Tor Austad (2010), results to 1.70 m²/g, and 0.29 m²/g respectively. Limestone is less homogeneous in porosity and permeability when compared to chalk Strand, Tor Austad et al. (2008). Dolomite is a type of limestone. The magnesium carbonate $MgCO_3$ concentration makes the difference between the two rock types. When the $MgCO_3$ concentration approaches 45 % it is called dolomite, which is a double carbonate of calcium and magnesium. Thus, the term 'limestone' in a general sense, includes dolomite (Bowles, 1956).

2.2 Wetting in carbonate rocks

According to Thomas, Clouse and Longo (1993), the mixed or oil wetness of the carbonate reservoir can be credited to the adsorption of the carboxylic materials on the rock surface. The carboxylic materials in crude oil are characterised by the

acid number (AN). These carboxylic materials are negatively charged and they adsorb to the positive sites of the calcite surface (Seyed Jafar Fathi, Tor Austad, Strand et al., 2012).

Water based EOR is significantly affected by the initial wetting properties of the carbonate rocks. The low concentration of SO_4^{2-} in formation brine (FB) is a result of high concentration of Ca^{2+} and the precipitation of anhydrite at high temperatures (Seyed Farzad Shariatpanahi, Strand and Tor Austad, 2011). The composition of FW have an ability to improve or impede recovery actory when it interacts with other inhect brines Sohal, Thyne and Sjøgaard (2016). Seawater (SW) has been found to be an effective EOR fluid [(Strand, Høgnesen and Tor Austad, 2006; Seyed Jafar Fathi, Tor Austad, Strand et al., 2012; S. Shariatpanahi et al., 2016; Yousef, Al-Saleh, Al-Kaabi et al., 2010; Strand, Tor Austad et al., 2008; Sriram Chandrasekhar, 2013)]. Excessive concentration of SO_4^{2-} in injected brines can make a once sweet oil field to become sour, therefore producing corrosive and toxic H_2S gas (Sohal, Thyne and Sjøgaard, 2016). Seawater differs from formation water primarily by having a lesser salinity content, which is about 35,000 ppm compared to 247,000 ppm for FB.

2.2.1 Initial wetting conditions in carbonate reservoirs

In principle, the flow of oil through the porous medium is supported by capillary, viscous, and gravity forces. The SI process is dependent on its capillary force, which is related to the wetting state of the rock. Capillary force is the driver that enhances the imbibition of injected brines into the pore matrix (Sohal, Thyne and Sjøgaard, 2016). The displacement of oil is thus dependent on the capillary force, which reduces with reducing water-wetness of the rock (Peimao Zhang, Tweheyo and Tor Austad, 2007). Altering the wettability towards more water wet, reduces the capillary action and thereby there is an improvement in the oil recovery (Karimi et al., 2016). One of the factors that determine the success rate of any EOR methods is wettability. Porosity, wettability and permeability, are some of the key parameters in determining the value of a petroleum reservoir. The wettability of a particular reservoir will have an effect on the fraction of recoverable oil (Thomas, Clouse and Longo, 1993). According to a study in Puntervold, Strand and Tor Austad (2007), a 19 % increase in the water wetness of the rock improved the oil recovery by 25 %.

The thickness of the water film between the oil phase and the rock surface also affects the wettability in carbonate rocks. The thicker the water film, the more stable the system (Seyed Farzad Shariatpanahi, Strand and Tor Austad, 2011). Activation energy is another parameter that affects wettability, as discussed in Strand, Tor Austad et al. (2008). The wetting condition in carbonate rocks is also controlled by the acid number Section 2.3, which is characterized by the carboxylic materials and fatty acids present in the crude oil.

The capacity of an ion to break down (dissolve) over its counter ion is classified as potential determining ion (PDI). The most common PDIs over a carbonate surface are Sulphate, Calcium and Magnesium. The properties of these ions are unequivocally identified with the surface potential of the corresponding ion (Han, 2002). Understanding the symbiotic interplay between the three PDIs in injected fluid is a good start to develop a 'smart water' to act as a wettability modifier in carbonate rocks. Therefore, injected fluids should have sufficient negatively charged ions to make the positively charged rock surface, less positive to enable the desorption of the negatively charged carboxylic material from the rock surface. This would in turn improve the water wetness of the rock (Peimao Zhang and Tor Austad, 2006).

Previous literature [Seyed Farzad Shariatpanahi, Strand and Tor Austad (2011), Peimao Zhang, Tweheyo and Tor Austad (2007) and Austad et al. (2012)] have established the effectiveness of seawater as a wettability modifying fluid to alter carbonate rocks into more water wet, especially at high temperatures. A recent study have also shown that not only is presence of active ions in SW important in the wettability alteration process; the amount of non-active salt, NaCl also have an impact (S Jafar Fathi, Tor Austad and Strand, 2011).

A detailed study of the mechanisms occurring in the interactions between rock and fluids must be thoroughly understood, to have a successful EOR projects. The idea behind these mechanisms is how a positively charged carbonate surface is made less positively charged by PDIs contained in the injection brine, which results in the desorption of the carboxylic materials contained in the crude oil, thereby increasing water wetness of the carbonate surface.

2.3 Acid number

The chemical properties of crude oil include but not limited to asphaltenes, resins, acid, and base numbers (Standnes and Tor Austad, 2000). Acid number is the most important wettability modifier according to Standnes and Tor Austad (2000) and Seyed Farzad Shariatpanahi, Strand and Tor Austad (2010). The acid number (AN) has a unit of milligrams of KOH per gram of oil. For an acid number y , it means that y mg of KOH is needed to neutralise the acidic material present in 1g of oil Hopkins et al. (2016).

Base number is also discussed in some literature, such as Seyed Farzad Shariatpanahi, Strand and Tor Austad (2010), but acid number is the most important. Crude oils contain acidic components (carboxylic materials) which are characterised as AN. The ability of a crude oil to alter wettability tallies with its AN. The higher the AN, the lower the water wetness of the rock. However, a strongly water-wet cores might not necessarily result in optimal oil recovery due to capillary trapped oil Austad et al. (2012). The carboxylic materials are usually present

in the molecules of the heavy end of the crude oil [(Seyed Farzad Shariatpanahi, Strand and Tor Austad, 2011; Peimao Zhang, Tweheyo and Tor Austad, 2007)].

In an adsorption test carried out by Thomas, Clouse and Longo (1993), it was concluded that carboxylic materials adsorb most strongly to carbonate surface and the adsorption is stabilized by long, straight chains. According to Standnes and Tor Austad (2000), there is a relationship between AN and the capacity to modify the wetting condition of the porous media, as estimated by unconstrained imbibition of brine. Experimental results from same literature agrees with the works in Austad et al. (2012) which states that high AN guarantees stronger adsorption of the carboxylic materials on the rock surface which makes it more oil-wet. From Figure 2.2, which is the layout of the SI experiment in Standnes and Tor Austad (2000), where varying AN oils were used.

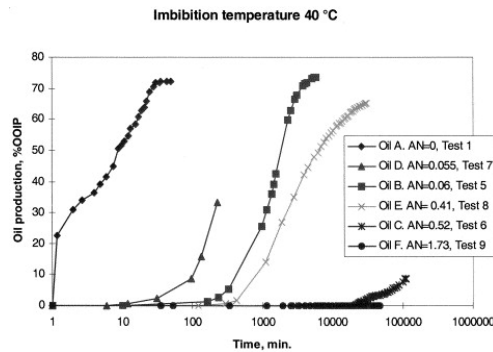


Figure 2.2: SI results of brines, into a core sample, using different oils with varying acid number (AN). Figure from Standnes and Tor Austad (2000).

For oil A, which is a pure n-heptane, a water-wet core, its imbibition rate is in clear contrast to oils B-F. Furthermore, it can be suggested that all oils are able to alter wettability to an extent, so far they contain some amount of carboxylic group components. Also, there seem to be a correlation between the AN and the percentage % of oil production. Oil F, with the highest AN, seem to make the core sample most oil-wet and no imbibition of brine was recorded, after 33 days as reported in Standnes and Tor Austad (2000). It should be noted that oils D and E, contains 2.6 wt % and 0.19 wt % of asphaltene respectively. However, no trend between the asphaltene level and wettability modification was established. This further reinstates that, when the carboxylic materials present in the crude oil, interact with a rock surface, they are able to modify the wettability of the particular rock surface. The acid number of the oil used in this masters' thesis is 3.3 mg KOH/g.

Furthermore, in a spontaneous imbibition test carried out in Austad et al. (2012), using limestone cores with FW as the imbibing fluid. Core 16A and 11B were saturated with oil AN = 0.08 and 0.07 respectively. The results shown in Figure 2.3 depicts that the water wetness decreases with increasing AN. According

Rao (1999), the water wetness of carbonate rocks, increases with increasing temperature. And the higher the acid number, the lower the water wetness of the rock. Therefore, temperature and AN are dependent parameters. Because, AN decreases with increasing temperature. This is due to decarboxylation of acidic material contained in the crude oil, due to geologic time (Zhang, Tor Austad et al., 2005). The quantity of carboxylic materials and its effect on wettability was explored in (Seyed Jafar Fathi, Tor Austad, Strand and Puntervold, 2010). They took out the carboxylic materials from different samples of crude oil and reported that the higher the quantity of carboxylic materials present, the higher the oil wetness characteristics exhibited by the sample of crude oil.

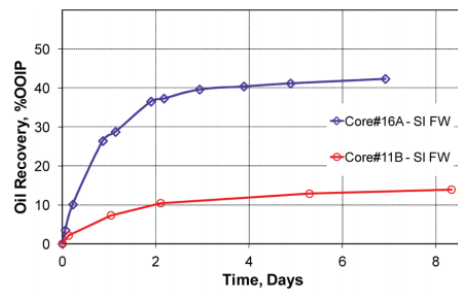


Figure 2.3: Spontaneous imbibition of FW into limestone cores with a varying AN at 110°C. Figure from Austad et al. (2012).

2.4 Core aging

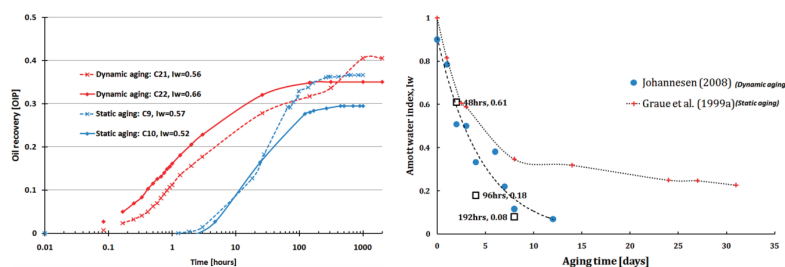
Aging is a widely used method for altering core wettability. The aging process is required to restore the core samples to their initial reservoir state as much as possible, since a lot of changes (mechanical, wettability e.t.c) must have occurred to reservoir rocks, during coring and transportation from the field to the laboratory. Mechanical damages, which could result from coring programs of reservoir rocks, have made outcrop cores one of the commonly used samples for laboratory experiments. Outcrop cores are usually drilled from the earth surface, thus commonly water-wet. The process of restoring these samples to oil-wet is called aging.

Aging tends to have an effect on wetting, since the oil is made to make contact with the core surface (Hopkins, 2016). Aging is able to alter wettability of a rock sample while maintaining the initial state of the pore network structure and mineralogy (Graue, 1999). During the aging process, the core samples are made to make contacts with crude oil samples, at elevated temperature and a period of time. According to Standnes and Tor Austad (2000), the acid number (AN), Section 2.3 of the crude oil and the homogeneous distribution of the surface active agents contained therein, effective aging condition and initial water saturation are some of the factors that impact the wetting state of a core sample.

Fernø et al. (2010) reported that, the wetting state of a rock sample affects its ultimate oil recovery method of fluid flow e.t.c

The two major kinds of aging are static aging and the dynamic aging. The static aging process entails the core plug being fully submerged in the crude oil, in an enclosed aging cell, for a period of time and at a given temperature, while the dynamic aging process ensures the continuous flow of crude oil flowing through the core samples, placed in an hassler core holder with a confining pressure, at an elevated temperature. Unlike the static aging, fresh oil, with new surface active agents are available to get attached to the rock surface. Al-Mahrooqi et al. (2005) investigated the changes in wettability by aging at a pore scale using a series of electrical impedance and NMR T2 measurements. 3 outcrop core samples were aged at varying pressure, time and temperature conditions and the results were compared with non-aged plugs from the same outcrop sample. The T2 distributions changed as more oil came in contact with the samples and this was inferred as a result of wettability changes.

In a work by Fernø et al. (2010), the wettability alteration established by both aging methods was compared using consolidated, porous chalk samples, with initial water present in the pore space, at constant temperature of 90°C. Wettability change during the aging process was assessed by the reduction in water imbibition rate, total volume of spontaneously imbibed water, and the Amott-Harvey water index. Two sets of dynamic aging were carried out; constant aging time (96 hours) with varying flow rate (1, 3, and 5) cm^3/h and constant flow rate (3 cm^3/h) with varying aging times (48, 96, and 192) hours. The static aging was carried out for 72 hours. At shorter aging times (72 hours or less), both aging methods performed equally well. At longer aging times, the dynamic aging process was more effective, as it takes the static aging 3 times as long aging time to match the same level of effectiveness. Also, at a constant aging time of 96 hours, there exist an optimal flooding rate at which the greatest wetting can occur.



(a) Induction and production rates of (b) Amott water index vs time, when two aging types.

Figure 2.4: Comparison between static and dynamic Aging. Figures from Fernø et al. (2010).

Furthermore, the induction time (time of cores, making contact with water in the Amott cell and when the first oil production is noticed) was faster for cores aged dynamically. The production rate of statically aged cores was 15 times slower for the first 40 % of oil recovery during the spontaneous imbibition process. Figure 2.4a show results of the comparison of the production rate and the induction times of the two aging types. The statically aged cores (C9 and C10) show slower production rates and longer induction times. The wettability change is sensitive to the flooding rate, especially when the flooding time is constant. In the work in Fernø et al. (2010), with a constant aging time of 96 hours, the flooding rate of $1\text{cm}^3/\text{hr}$, $3\text{cm}^3/\text{hr}$ and $5\text{cm}^3/\text{hr}$ gave an average wetting of 0.53, 0.31 and 0.44 respectively. Figure 2.4b, shows the comparison of both aging methods compared to Amott water index, reached at a given time. It is evident that the most significant change, as measured by the water index, occurs with the dynamic aging method.

To achieve a uniform wettability state throughout the core is beneficial for a good interpretation of spontaneous imbibition (SI) experimental results Standnes and Tor Austad (2000). Dubey, Waxman et al. (1991) and Graue, Bognø, Baldwin et al. (2001) experienced a radial wettability distribution while using the static aging method. More aging occurred in the circumference of the core plug than the inner central axis of the sample. In a SI experiment by Standnes and Tor Austad (2000), where the core were statically aged for four days at 50°C , no oil production was recorded until after 600 minutes, which was at a slow rate. This observation is consistent with those made in Fernø et al. (2010), where the cores aged statically exhibited long induction times. In the work in Standnes and Tor Austad (2000), after 1600 minutes, the production rate increased rapidly and the oil peaked at 74 % as shown in Figure 2.5a.

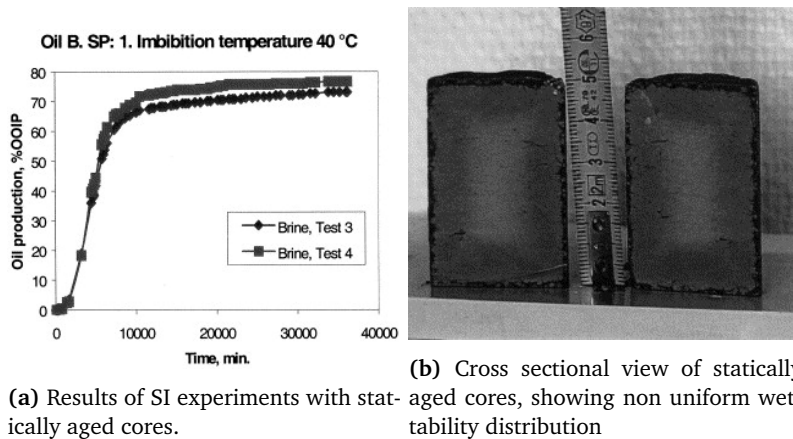


Figure 2.5: Static Aging. Figures from Standnes and Tor Austad (2000).

The long induction times can be attributed to a nearly oil-wet core surface and a more water-wetness of the core centre. This was confirmed when the core sample

was halved, after the SI experiment. The observation was, the core surface was darker and the centre of the core as shown in Figure 2.5b. That is, as the oil moves from the surface of the core, towards the center, the adsorption of surface active agents are so fast such that, not enough reaches the center of the core. This causes a non-uniform distribution, which is not a good wettability restoration characteristics. Further confirmation was made, when a core with similar petrophysical properties, was statically aged for 4 days at 50°C. The core was then halved after the aging process as shown in Figure 2.6. Similar observation was made, the centre of the colour contains a colourless fluid, while the core surface, have a darker colour which shows the deposits of more surface active agents. Graue, Bognø, Moe et al. (1999) also reported poor wettability distribution, while aging core samples, at irreducible water saturation, at a high temperature.

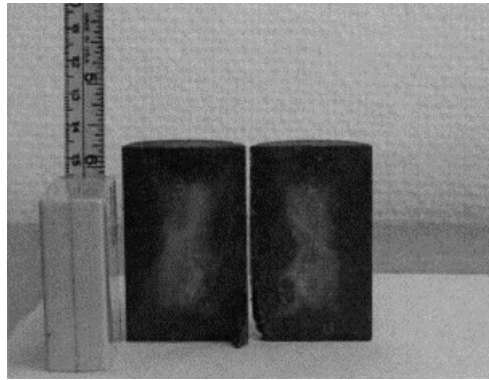
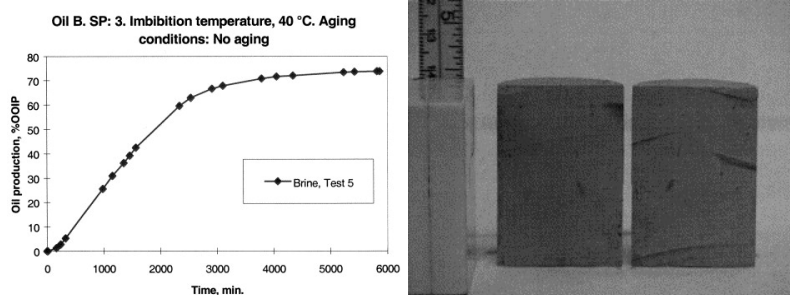


Figure 2.6: Cross sectional view of statically aged cores, showing non uniform wettability distribution, after being halved following a statically aged process. Figure from Standnes and Tor Austad (2000).



(a) Results of SI with cores first dynamically aged, then aged statically. **(b)** Cross sectional view of the core, after the experiment.

Figure 2.7: Dynamic aging: No visible induction time and uniform wettability distribution due to aging type. Figures from Standnes and Tor Austad (2000).

On the contrary, dynamically aged cores showed no visible induction time and also uniform wettability distribution was established as illustrated in Figure 2.7.

One of the disadvantages of the dynamic aging is the high volume of crude oil used in the process. A study in Johanssen, (2008) shows that dynamically aged cores, longer than 6 days exhibits better wettability changes and result in lower Amott Harvey water indices than statically aged cores. One of the reasons for the distinction in the results of the two aging processes can be attributed to the contact between the crude oil, surface of the pore wall and the interior of the core. Because of the limited amount of crude oil used during the static aging method, there is also a limited amount of surface active agents contained in the crude oil that can alter the wettability whereas in the dynamic aging, the constant supply of crude oil ensures that more surface active agents are available.

Chapter 3

Surfaces forces and mechanisms

3.1 Role of surface forces on wettability

Surface forces play vital roles in determining the wettability state of reservoir rocks. The molecular interaction, i.e., the preference of a reservoir rock for oil or water, is largely dependent on the distance between the mineral surface and the liquid. Examples of the applicability of surface forces can be seen in the interaction of two solid surfaces in a liquid medium, two liquid-gas interface interactions in a liquid layer and also oil/gas/rock system in oil reservoirs Butt, Graf and Kappl (2013, p.6). Surface forces control the wetting of mineral surfaces by liquids Hirasaki et al. (1991).

3.1.1 Disjoining pressure

Disjoining pressure Π , can be defined as the difference in pressure within a film, spreading between two surfaces and the pressure in the bulk phase. It is characterized as the adjustment of Gibbs free energy with distance and per unit area at steady cross-sectional area, temperature, and volume Butt, Graf and Kappl (2013, p.95). In a three-phase system, which forms three contact lines, when they interact, the distance between these interfaces, as a function of energy is expressed by the disjoining pressure that separates the interfaces. A negative disjoining pressure leads to attraction of the two interfaces Hirasaki et al. (1991).

The disjoining pressure is made up of Van der Waals (VDW) forces (attractive), electrostatic forces (could be attractive or repulsive), and hydration or structural forces, caused by the inter-molecular structure of the solvent or water. The hydrogen forces are not as prevalent as the others. In a gas/liquid/solid system, Figure 3.1, say a reservoir fluid spreading on a solid surface, the liquid creates a film whose thickness is dependent on the total interacting fluid and the surface forces acting on the system. There is an interaction between all three interfaces. Repulsive interaction between these interfaces stabilises the thin film, while the attractive interaction destabilises the thin films, spreading on the surface of the

rock.

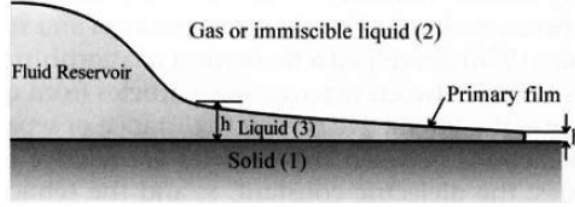


Figure 3.1: Spreading of reservoir fluid on a flat horizontal surface, resulting in primary film with thickness, h . Figure from Donaldson and Alam (2013, p.84).

The pressure that keeps the film from the surface is called the disjoining pressure Donaldson and Alam (2013, p.85). Hirasaki et al. (1991) reported that, when the disjoining pressure is positive, there is a repulsion of the interfaces, and the liquid film becomes stable. According to Donaldson and Alam (2013, p.85), the adherence of a liquid to a flat and horizontal surface or its rise along a tube with height H , can be expressed in Equation 3.1. At equilibrium, the rate of change in free energy with the thickness (h) of the liquid film is zero.

$$\frac{\delta G}{\delta h} = 0 = \frac{A}{6\pi h^3} + \rho gH = -P_h \quad (3.1)$$

With increasing thickness of h , Figure 3.1, the VDW pressure keeps diminishing to zero and Equation 3.1, results to the capillary pressure equation but with a decreasing value of h , as applicable on an horizontal flat surface, the gravity term diminishes to zero and the VDW, repulsive disjoining pressure, $\Pi_{vdW(h)}$ becomes Equation 3.2.

$$\Pi_{vdW(h)} = -\frac{A_{12}}{6\pi h^3} \quad (3.2)$$

A_{12} is called the Hamaker constant.

3.1.2 van der Waals interaction and Hamaker constant

The Hamaker constant (A) is a coefficient that provides a relationship between the thickness of two interacting interfaces and the Van der Waals (VDW) energy Donaldson and Alam (2013, p.82). According to Hirasaki et al. (1991), the knowledge of the dielectric constant ϵ , refractive index n and the absorption potential of the interfaces is sufficient to calculate the Hamaker constant. The long-range and short-range forces, which arise from the electrostatic interactions between molecules, atoms, and particles, do have an influence on wettability. The interactions occurring at space (commonly less than one nanometer), which are controlled by short range forces while the London dispersion forces, Keesom forces and Debye-Induced forces, which comprise of the long-range forces, are jointly

described as the VDW forces (Donaldson and Alam, 2013, p.67) and this is expressed in equation 3.3.

$$E_{vdw} = E_{disp} + E_{elec} + E_{ind} \quad (3.3)$$

E_{vdw} is VDW Energy, E_{disp} is London dispersion forces, E_{elec} is Keesom forces and E_{ind} : Debye-Induced Energy. For two molecules with polarization α , and dipole moment, μ :

$$E_{vdw} = \frac{1}{4\pi\epsilon\epsilon_0} \frac{1}{r^6} \left\{ \frac{3}{4} \alpha^2 h\nu + \frac{2\mu^4}{3K_B T} + 2\mu^2 \alpha \right\} \quad (3.4)$$

T : Absolute Temperature K : Boltzmann approximation ν : Electron frequency. The conventional methodology of VDW interaction is built on the Hamaker hypothesis, which accepts that the connections are pair-wise attractive substance and free of the mediating media. However, a more modern hypothesis, called the Lifshitz theory, is based on the quantum field theory. This modern theory, is not in total agreement with the Hamaker's hypothesis. According to Hirasaki et al. (1991), the Lifshitz theory agrees that the assumptions by Hamaker are only true, when the interactive forces are E_{disp} .

The Hamaker constant for the solid (1), gas (2) and liquid phase (3), shown in Figure 3.1 is approximately, Equation 3.5.

$$A \approx \frac{3}{4}KT \left\{ \frac{\epsilon_1 - \epsilon_3}{\epsilon_1 - \epsilon_3} \right\} \left\{ \frac{\epsilon_2 - \epsilon_3}{\epsilon_2 - \epsilon_3} \right\} + \frac{(0.265h\nu)(n_2^2 - n_3^2)(n_2^2 - n_3^2)}{\left\{ (n_1^2 + n_3^2)^{0.5}(n_2^2 + n_3^2)^{0.5}(n_1^2 + n_3^2)^{0.5} \right\} + \left\{ (n_2^2 + n_3^2)^{0.5} \right\}} \quad (3.5)$$

The first term results from Keesom and Debye force which depends on temperature, T while the second term results from London forces and it depends on the electron frequency, ν , and refractive index, n . The Hamaker constant A , is positive when the interactive forces are repulsive and negative when the interactive forces are positive as summarized in Donaldson and Alam (2013, p.83). The Hamaker constant for two dissimilar phases (1 & 2) interacting, across a third phase (3) with the identity of the materials being unknown is given as Equation 3.6 in Hirasaki et al. (1991).

$$A_{132} = \left(\sqrt{A_{11}} \right) - \left(\sqrt{A_{33}} \right) \left(\sqrt{A_{22}} \right) - \left(\sqrt{A_{33}} \right) \quad (3.6)$$

According to Figure 3.1, in a scenario with a solid (1), and a gas (2) with an absorbed liquid layer with thickness δ on a solid (4) and liquid film (3) with thickness, h , the Hamaker constant is estimated by Equation 3.7, as given in Donaldson and Alam (2013, p.84):

$$W = \frac{\left(A_{11}^{0.5} - A_{44}^{0.5} \right) \left(A_{22}^{0.5} - A_{33}^{0.5} \right)}{12\pi(\delta + h)^2} + \frac{\left(A_{44}^{0.5} - A_{33}^{0.5} \right) \left(A_{22}^{0.5} - A_{33}^{0.5} \right)}{12\pi h^2} \quad (3.7)$$

When the δ is negligible in comparison with h , the interaction is equivalent to that of a liquid film between solid and gas phases. When δ is large, the interaction between gas and solid, across phase 3 becomes applicable. These scenarios are capable of changing the a repulsive force in the system to attractive forces and vice versa. The interactive forces in play have a significant effect on the wettability of the system Donaldson and Alam (2013, p.84).

3.1.3 Stability of wetting layer film and DLVO theory

The inter-molecular surface force concept stem from the DLVO (Derjaguin, Landau, Verwey, and Overbeek) theory, which was first used to explain the stability of a colloid system. The theory provides the required knowledge of double layer repulsive and VDW attractive forces and how they affect the stability of colloid system Donaldson and Alam (2013, p.81). The DLVO was later used to explain the stability of the water layer film. The assumptions for both stability conditions (colloid system and water films) differ, as described in Hirasaki et al. (1991). A sufficient energy is required between the thick wetting film with approximately zero contact angle and the think water film, with a significant contact angle, for there to be a stability for the thick water film. The stability of a water film with zilch capillary pressure, is reached when the summation of the electrostatic and VDW forces are at a maximum, at the thick wetting area. The stability of the thin water film is compromised when energy between the thick and thin wetting films is not sufficient enough. This condition is feasible, once the capillary pressure increases significantly Hirasaki et al. (1991). According to Butt, Graf and Kappl (2013, p.95), the shape, material type, and distance between two bodies are some of the criteria that determines the energy between two bodies.

According to Han (2002, p.52), the ultimate potential, V_T , is the summation of the attractive and repulsive potentials. For two parallel plates,

$$V_T = \frac{64nkT\gamma^2}{k} \exp(-kH_0) - \frac{A}{12\pi H_0^2} \left(\frac{erg}{cm^2} \right) \quad (3.8)$$

The first term is the repulsive force between the parallel plates while the second term is the attractive force between them. For two spheres plates,

$$V_T = \frac{\varepsilon a \psi_0}{2} \ln[1 + \exp(-\kappa H_0)] - \frac{Aa}{12H_0} [erg] \quad (3.9)$$

Likewise, in Equation 3.9, the first term is the repulsive force between the spheres while the second term is the attractive force. H_0 is the distance between two plates, ψ is the electrical potential, ε is the permittivity of the medium, T is the temperature of the system, κ is the Boltzmann constant = 1.38066×10^{23} , $J K^{-1}$, λ is the surface tension, A is the Hamaker constant and a is the radius of the sphere. Equations 3.8 and [3.9] are not valid for when H_0 is about 0.1λ . Figure 3.2, is shows the plot of V_T against H_0 . According to Han (2002, p.51), at shorter distances, a

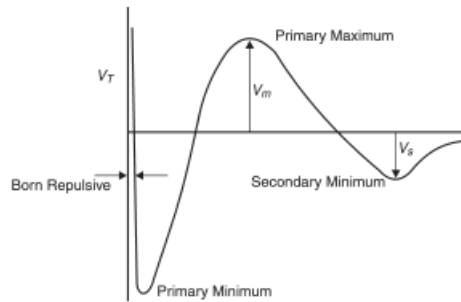


Figure 3.2: Schematic showing the relationship between V_T and H_0 . Figure from Han (2002, p.53).

secondary minimum, V_s is reached. And as the gap between both molecules closes, V_m , the primary minimum is attained. As the gap closes further, attractive VDW forces, further dominates and the V_m becomes more apparent. A significant repulsive force comes into play, when two molecules are made to forcefully approach each other.

Aqueous dispersion tend to precipitate with increasing salt concentrations. Compared to other ions, divalent ions tend to precipitate at smaller salt concentrations of 0.5 to 2 mM. Butt, Graf and Kappl (2013, p.103) used the DLVO theory Equation 3.9, to calculate the interaction energy between two identical spherical particles, the results are illustrated in Figure 3.3.

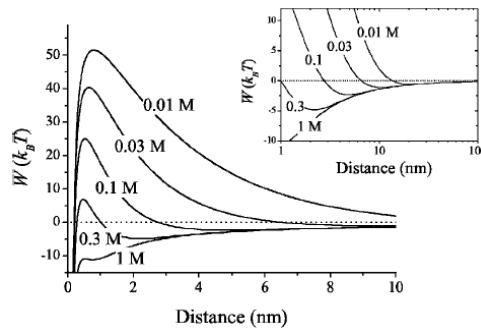


Figure 3.3: Interaction energy between two identical spherical particles. Figure from Butt, Graf and Kappl (2013, p.104).

Fragile attractions are experienced at lengthy distances, while repulsive forces are evident at intermediate distances. However, significant attractions are experienced at much shorter distances. At high salt concentrations, the energy limit reduces and the VDW forces become evident, and reverse is the case for low salt concentrations Butt, Graf and Kappl (2013, p.103).

3.1.4 Electric double layer model

The electric double layer (EDL) is made up of the diffuse and the stern layer. This theory provides substantial knowledge as to why most solids become charged when they come in contact with a polar medium, like liquids, especially water, which has a high dielectric constant and a good solvent for ions Butt, Graf and Kappl (2013, p.42). When solid surfaces become charged, an electric field is established. The liquid phase contains counter ions that attract the ions in the solid surface, this overall charge in the system becomes neutral and an electric double-layer is formed in the solid-liquid interface. The ions in the solution rearrange themselves often to keep this electroneutrality at the interface Han (2002, p.23).

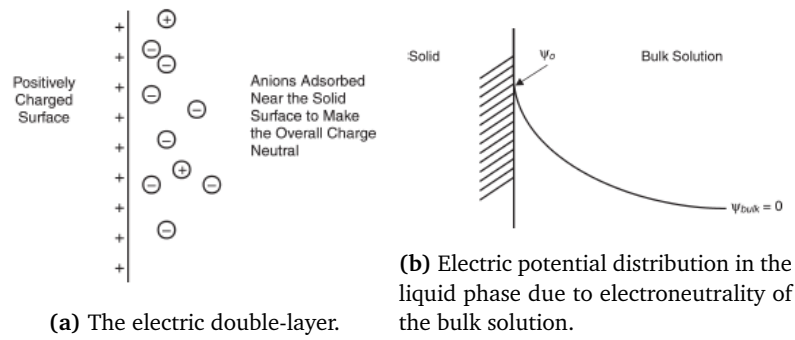


Figure 3.4: The electric double-layer model. Figure from Han (2002, p.25).

In the double layer, the liquid and solid phases are each charged as shown in Figure 3.4a. The result of electrical potential distribution in the liquid phase, as a result of surface charge is illustrated in Figure 3.4b. The Gouy-Chapman and Grahmme theories have been used to explain the double layer theory using planar surfaces, afterwards, Debye and Huckel used spherical surfaces.

According to the Gouy model, the electrical potential distribution in the bulk solution is expressed with the Poisson's equation 3.10:

$$\nabla^2\psi = -\frac{4\pi\rho}{\epsilon} \quad (3.10)$$

For one dimension along the x-axis, Equation 3.10, becomes Equation 3.11:

$$\frac{d^2\psi}{dx^2} = -\frac{4\pi\rho}{\epsilon} \quad (3.11)$$

ψ is the electrical potential, ρ is the charge density, ϵ is the permittivity of the medium. D is the dielectric constant of the medium and ϵ_0 is the permittivity of the vacuum. ϵ_w is the permittivity of water = $4\pi 78 \times 8.85 \times 10^{-14}$ coul²/J.cm. ρ is the charge density and expressed by:

$$\rho = \sum z_i n_i \exp \quad (3.12)$$

z_i is the valence of ions, present in the solution and n_i is the number of moles of the ionic species of i and e is the electronic charge. The permittivity of the medium, ϵ , is expressed by:

$$\epsilon = 4\pi D\epsilon_0 \quad (3.13)$$

Boltzmann equation, 3.14, can be used to show the ion distribution.

$$n_i = n_i^0 \exp\left(-\frac{z_i e \psi}{kT}\right) \quad (3.14)$$

The expression $\epsilon e z_i$, can be used to determine the number of ionic specie, i , at any position close to the solid surface, n . By substituting Equations 3.12 and 3.14 into Equation 3.11, The analytical expression 3.15 is gotten, which is the Poisson equation for a monovalent ion present in the solution. Boundary condition, $\varphi = 0$ at $x = \infty$ and $\varphi = \varphi_0$ at $x = 0$ is applied.

$$\psi = \frac{2kT}{z_i e} \ln\left(\frac{1 + \gamma e^{-kx}}{1 - \gamma e^{-kx}}\right) \quad (3.15)$$

$$\gamma = \frac{e^z/2 - 1}{e^z/2 + 1}, z = \frac{z_i e \psi_0}{kT} \quad (3.16)$$

$$k = \sqrt{\frac{8\pi n z_i^2 e^2}{\epsilon kT}}$$

$$k = \sqrt{\frac{8\pi e^2 N_{avo}}{1000} \sum \frac{1}{2} z_i^2 C_i} \quad (3.17)$$

N_{avo} is the Avogadros number and C_i is the ion molar concentration in the system. For conditions of $z \ll 1$ or $\psi_0 < 25\text{mV}$, Equation 3.15 becomes Equation 3.18:

$$\psi = \psi_0 e^{-kx} \quad (3.18)$$

For surface potentials as high as +/- 100 mV, Equation 3.18, has proven to be more accurate than Equation 3.15, according to Han (2002, p.25). The inverse of Equation 3.17 is called the Debye length λD , which is also known as the electric double-layer thickness and can be simplified to Equation 3.19, at 25°C. The double-layer thickness decreases drastically with increasing salt concentration and this phenomenon is called double-layer compression. As illustrated in Figure 3.5, the exponential decrease of potential becomes steeper with increasing salinity content.

$$\frac{1}{k} = \frac{4.3}{\sqrt{I}} \times 10^{-8} \text{cm} \quad (3.19)$$

The Guoy model is applicable for systems containing only NaCl. As long as the electroneutrality of the system is maintained, NaCl moves freely in the system.

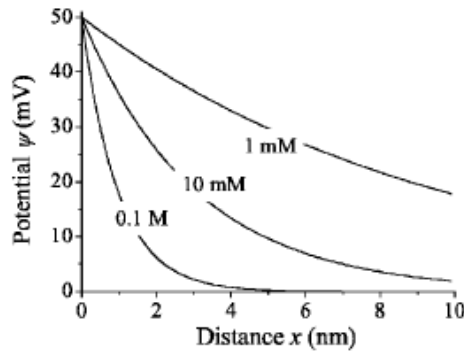


Figure 3.5: Schematic of diffuse electric double-layer. Figure from Butt, Graf and Kappl (2013, p.46).

However, not all systems are this way, therefore the Guoy model becomes in-applicable. Furthermore, this model does not consider the size of the ions. For aqueous solutions, the Guoy model is valid for salt concentrations of up to 0.2 M and potentials less than 50 - 80 mV. According to Butt, Graf and Kappl (2013, p.51), the limitations of the Poisson-Boltzmann theory are:

1. Ionic sizes are neglected.
2. Surface charge is homogeneous and smeared out.
3. Between ions and the surface, the image forces are ignored.

Regardless, this theory provides a good approximation.

3.2 Mechanisms

A detailed understanding of the mechanisms birthed by the interactions between rock and fluids must be thoroughly understood, to have a successful EOR process. As at 2015, there was an average 80,000 - 120,000 barrels/day over a 3 year period additional recovery, from the Ekofisk chalk field, after the injection of SW (Sohal, Thyne and Søgaaard, 2016). The unexpectedly high recovery have triggered several laboratory tests to determine the underlying mechanism.

In this section, a detailed analysis is given as to how a positively charged carbonate surface is made less positively charged by PDIs contained in injection brines, which results in the desorption of the carboxylic materials contained in the crude oil, thereby increasing water wetness of the carbonate surface. Different mechanisms have been suggested in the literature to aid this process and some of these mechanism are discussed here. It is noteworthy that a consistent explanation of the exact mechanism that causes wettability in carbonate rocks is yet to materialise in literature.

It is quite possible that different mechanisms could be in effect at the same time with each proving its own contribution. Some of the proposed mechanisms are Multi-ion exchange (MIE) and Electric double layer EDL. Others include fine migration, rock dissolution, increase in pH and IFT reduction and a low salinity recovery hypothesis called salting-in effect in RezaeiDoust et al. (2009). While, a generally accepted mechanism is yet to be available in the literature, a widely accepted idea is that low salinity brines creates an environment, which is convenient for additional oil recovery.

3.2.1 Multi-ion exchange

Multi-ion exchange (MIE) has been discussed and supported in Strand, Høgnesen and Tor Austad (2006), Peimao Zhang, Tweheyo and Tor Austad (2007), Seyed Farzad Shariatpanahi, Strand and Tor Austad (2011), Yousef, Al-Saleh, Al-Kaabi et al. (2010) and Tor Austad, Seyed Farzad Shariatpanahi et al. (2015). MIE in carbonates is discussed in terms of anion exchange and cation exchange as discussed in sandstone. MIE involves the process where SO_4^{2-} is adsorbed onto the positively charged rock surface, thereby allowing the co-adsorption of Ca^{2+} and/or Mg^{2+} which facilitates the desorption of the negatively charged carboxylic group from the rock surface which then results in the less oil wetness of it, as illustrated in Figure 3.6. This process is temperature sensitive. At higher temperatures, the process becomes more active and Mg^{2+} is able to displace Ca^{2+} and form carboxylate complexes (Sohal, Thyne and Søggaard, 2016). SO_4^{2-} just serves as a catalyst to enable the co-adsorption of Ca^{2+} and/or Mg^{2+} by reducing the electrostatic repulsive force (Yi, Sarma et al., 2012). For an effect MIE process, the following conditions should be met.

1. Presence of SO_4^{2-} and another PDI.
2. Preferable temperature should be $> 90^\circ C$ Austad et al. (2012).

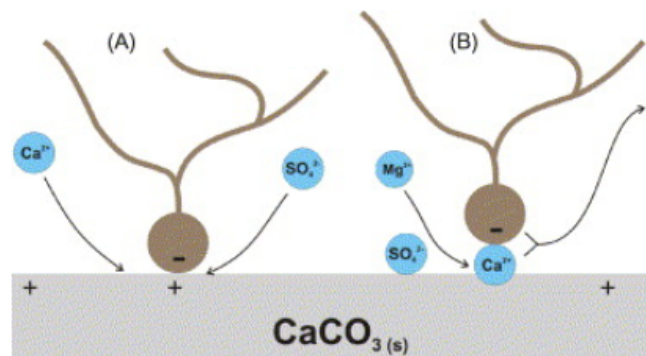


Figure 3.6: Suggested wettability alteration mechanism in carbonate surface to illustrate the interplay between Mg^{2+} and Ca^{2+} at high temperatures. Figure from Peimao Zhang, Tweheyo and Tor Austad (2007).

Figure 3.6 illustrates the interplay between the anion SO_4^{2-} and cations Ca^{2+} and/or Mg^{2+} at high temperatures on the chalk surface. The MIE is also valid for dolomite S. Shariatpanahi et al., 2016 and limestone with traces of anhydrite.

3.2.2 Electric double layer

The electric double layer (EDL) is made up of the stern layer and the diffuse layer. The EDL was referred to in the work in Seyed Jafar Fathi, Tor Austad, Strand et al. (2012). The principle behind the EDL explains that just right beside a strongly charged solid surface as shown in Figure 3.7, there are layers of negatively charged ion particles that adsorb to the surface of the positively charged solid surface to form an immobile later of ions called the Stern layer. That is, the stern layer is a static area containing counter ions. The diffuse layer is situated between the stern layer and the ionic equilibrium area, which is where several ions of different charges are allowed to move freely. The diffuse layer is an area of co and counter ions repelled by the stern layer. The charge density at any point from the solid surface is given by the difference in the concentration of these co and counter ions. Thus, the charge density is negligible at the point of electroneutrality. The concentrations of these ions increase with the distance to the surface until electroneutrality is reached.

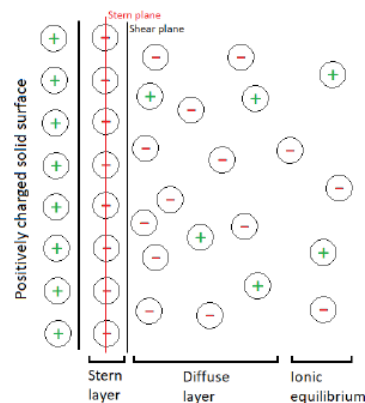


Figure 3.7: Diagrammatic representation of electric double layer. Figure from Google Images.

Na^+ and Cl^- are not potential determining ion (PDI)s though they belong to the double layer. The PDI are contained in the stern layer while the Na^+ and Cl^- are contained in the diffuse layer. Both layers make up the double layer. When the cations contained in the double layer, mainly consist of the PDI, they tend to have better access to the rock surface as shown in Figure 3.8 to alter wettability. Same principle applies in the presence of SO_4^{2-} , if the concentration of Cl^- is decreased, SO_4^{2-} would have an unconstrained access to the rock surface. This is why depleting the injected fluid of NaCl would result in increased oil recovery Seyed Jafar Fathi, Tor Austad, Strand et al. (2012).

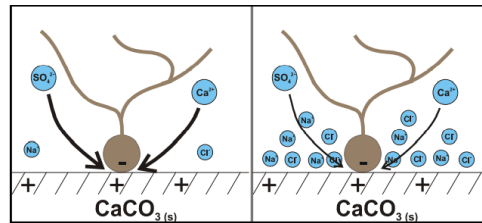


Figure 3.8: A schematic diagram showing the effect of NaCl interaction with other ions on the chalk surface. Figure from Seyed Jafar Fathi, Tor Austad, Strand et al. (2012).

Electric double layer expansion

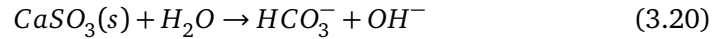
The impact of low salinity brines on wettability alteration depends on the interaction between the EDLs at the oil/brine and the brine/rock interface. The interaction between the ions of the low salinity brine and the ions on the rock surface leads to the expansion of the EDL. Higher pH resulting from rock dissolution results to negatively charged brine/rock interface which is largely repelled by the negatively charged oil/brine interface. The reduction in brine salinity leads to the expansion in the interface of the two EDLs. This expansion means that there is a greater repulsion between the rock and oil interfaces and leads to the desorption of the organic components from the rock surface Karimi et al. (2016). Reduction of salinity in the injected brine, will enhance the solubility of organic compounds in the aqueous phase (Salting-in effect) which will in turn enable more desorption of the carboxylic materials from the rock surface (RezaeiDoust et al., 2009).

3.2.3 Rock dissolution

Although there are still several debates about this mechanism which was first introduced in Hiorth et al. (2008). where a geothermodynamic model was developed with some pre-existing experimental data. Simulation experiments could not find a correlation between surface charge changes and the oil recovered by SI of SW. The geo-model was then applied to compute the change of chalk to other different minerals. This new results was able to provide some positive findings between rock disintegration and oil recovery. Furthermore, the model further clarified the low salinity impacts in carbonates by contending that reducing the Ca^{2+} concentration in the injected brine that would result in the dissolution which would restore equilibrium within the brines. This dissolution would deliver strongly adsorbed carboxylic materials from the rock surface and this will improve the water wetness Yi, Sarma et al. (2012).

The NMR results in Yousef, Al-Saleh, Al-Kaabi et al. (2010) confirmed the effect of this mechanism. The differences in the concentration of Ca^{2+} ion in the FB and the low salinity brine would lead to mineral dissolution which will in turn enable the removal of the adsorbed oil components form the rock surface according to

Equation 3.20, Karimi et al. (2016). Equilibration is one of the reasons why this mechanism might not be applicable at reservoir scale as noted in Mahani et al. (2015). Also Tor Austad, Strand and Puntervold (2009) via series of experiments have rejected the effectiveness of this mechanism.



3.2.4 Fines migration

This mechanism is more common in sandstone and is a phenomenon linked with MIE. However, some previous studies like Tang and Marrow, Bernard et. al; have suggested that this mechanism could play a part in carbonates. The idea behind the fines migrations is that moving particles (usually clay, in the case of sandstone), released by low salinity water, tend to block pore-throats. This particle tend to re-direct flow of water, into unswept regions and this increases microscopic sweep RezaeiDoust et al. (2009). The dissolution of anhydrites and dolomite Yousef, Al-Saleh, Al-Kaabi et al. (2010), Tor Austad, Seyed Farzad Shariatpanahi et al. (2015), Austad et al. (2012) and S. Shariatpanahi et al. (2016) will result in fine migration. A lot of work is currently ongoing concerning this mechanism.

3.2.5 Interfacial tension reduction

The effect of reducing injected water salinity and varying ionic composition keeps raising several doubts in literature. Residual oil saturation is usually controlled by the capillary number which is a ratio of the capillary force to the viscous force [NTNU TPG4160 2021 notes]. The composition of injected brine has a marginal effect on the viscous forces which means the effect on capillary force is pronounced. Yousef, Al-Saleh, Al-Kaabi et al., 2010 noticed a little interfacial tension (IFT) change between diluted SW and live oil. Okasha et. al. suggested otherwise. Therefore, there is no form of conclusion yet concerning the effect of brine salinity on IFT. The effect could be attributed to brine and crude oil composition.

3.3 Zeta potential and electric double layer

When liquids are not intentionally deionized, they usually contain ions which could be negatively charged, also called anions, or positively charged, also called cations. Particles are also charged, therefore when positively charged particles comes in contact with negatively charged ions, attraction of ions occur and vice versa. The ions which are far off of surface of the particles, form a diffuse layer. These ions could be seen as free ions and tend to move with the particles as they move with the incoming liquid. outside of the diffuse layer are the static ions, and this is called the slip plane (stern layer), as discussed in Section 3.2.2. The potential at the slip plane is called the zeta potential (ζ).

A potential exists between the molecule surface and the scattering fluid which changes as indicated by the separation from the molecule surface. Several literature, Mahani et al. (2015), Song et al. (2020), Tetteh, Janjang, Barati et al. (2018) and Peimao Zhang and Tor Austad (2006) have reported that the knowledge of zeta potential measurements are useful for understanding rock wettability.

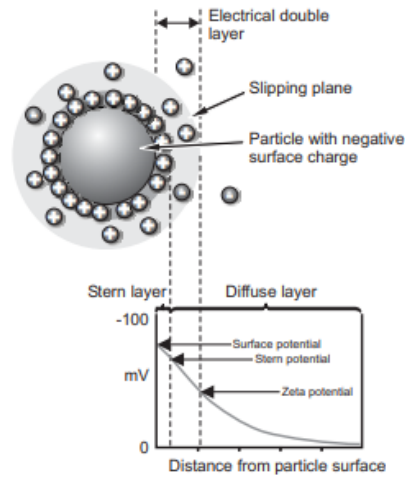


Figure 3.9: A diagrammatic representation of the potential at the slipping plane. Figure from Zetasizer Nano series Manual.

The ζ measurement gives an idea about the stability of the particle suspended in the solution. Low zeta potential measurements indicate the absence of forces, to hold the particle from flocculating. ζ measurements are made with the knowledge of the electrophoretic mobility, which is defined as the velocity of the particle in an electric field. ζ is calculated using Henry's equation which is given as;

$$U_E = \frac{2\varepsilon\zeta f(K_a)}{3\eta} \quad (3.21)$$

U_E is the electrophoretic mobility, ε is the dielectric constant, ζ is the zeta potential, $f(K_a)$ is the Henry's function and η is the viscosity.

Chapter 4

Effect of brine composition on wettability

4.1 Oil recovery in limestone cores

4.1.1 Effect of ionic composition

Effect of SO_4^{2-}

The concentration of SO_4^{2-} in the formation brine (FB) is almost negligible due to the high concentration of Ca^{2+} . However, about 2,689 mg/l of SO_4^{2-} can be found in seawater (SW). Limestone is a less reactive surface, compared to chalk. Strand, Tor Austad et al. (2008). Therefore, the effectiveness of SW as an EOR fluid and the affinities of the PDIs to the limestone surface need to be investigated.

The chromatographic separation technique is used to determine the adsorption of an ion on a solid surface. The principle of the test is the chromatographic separation of the non adsorbing tracer (in this case SCN^-) and adsorbing ions (in this case SO_4^{2-}) contained in a chromatographic liquid (SW); on the water-wet site of the rock surface. The region between the emanating bend of tracer and the PDI is legitimately corresponding to the water-wet surface. Utilizing a totally water-wet condition as a source of perspective framework, the proportion between the two zones will give a wetting list, which portrays the water-wet part of the real center surface zone. Strand, Tor Austad et al. (2008). The larger the area between the effluent tracer and the ion, the stronger the affinity of that ion towards the surface being investigated. The area is calculated using the trapezoid method.

Results of chromatographic tests carried out in Strand, Tor Austad et al. (2008), confirms that SO_4^{2-} adsorb equally to the surface of limestone as it does for chalk surface and the adsorption increases with an increasing temperature. At elevated temperatures, (Above 100°C), the adsorption of SO_4^{2-} tends to increase due to the breakage of hydrogen molecules which would lead to sulphate being more

strongly desolvated by the water molecules Strand, Høgnesen and Tor Austad (2006).

Combined interaction between SO_4^{2-} and other potential determining ion (PDI)

SO_4^{2-} alone cannot act as a wettability modifier in the absence of other PDIs. Gupta and Mohanty (2011) scrutinized the effect of SO_4^{2-} on a calcite surface, with an initial contact angle between 150° - 170° . The base concentration SO_4^{2-} , Ca^{2+} and Mg^{2+} were kept at 0.025, 0.013 and 0.045 M respectively. As represented in Figure 4.1, at room temperature, MgCa2S and MgCa4S couldn't significantly alter the contact angle below 150° . At an elevated temperature of $70^\circ C$, same brines were able to alter the wettability to a resulting average contact angle of a 86° (Intermediate-wet). MgCa2S and MgCa4S made the calcite surface water-wet with contact angle measurements of 54° and 36° respectively, at $90^\circ C$. Therefore, at higher temperatures, SO_4^{2-} is able to act as a catalyst, to desorb the carboxylic materials contained in crude oil, from the solid surface, thereby making the surface more water-wet.

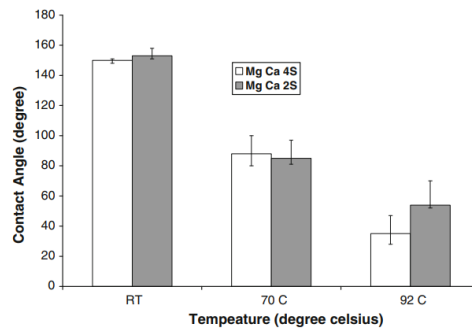


Figure 4.1: Contact angle measurements with varying brine salinities and temperature. Figure from Gupta and Mohanty (2011).

Further contact angle measurements as reported in Gupta and Mohanty (2011), carried out at $90^\circ C$, made the following observations as shown in Figure 4.2;

1. High SO_4^{2-} concentrations in the presence of other two PDI, was able to greatly alter the calcite surface to water-wet. In comparison, presence of SO_4^{2-} alone, in the absence of other PDI, was less effective in altering wettability.
2. Likewise, the absence of sulphate was unable to significantly alter the wettability of the calcite surface, as in the case of MgCa0S and 4Mg0Ca0S.
3. Mg^{2+} alone is unable to alter wettability 4Mg0Ca0S, except in the presence of SO_4^{2-} , as in 4Mg0CaS.
4. High concentration of Ca^{2+} alone, is able to alter wettability, but performed slightly better in the presence of SO_4^{2-} 0Mg5CaS.

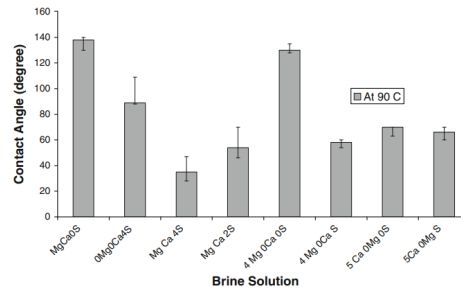


Figure 4.2: Contact angle measurements with varying brine salinities at 90°C. Figure from Gupta and Mohanty (2011).

As reported in Gupta and Mohanty (2011), SO_4^{2-} is an effective wettability modifier towards a limestone surface. Its affinity towards the solid surface increases with temperature and oil recovery increases with increasing sulphate concentration in the injection brine, though there exist an optimal concentration Hognesen, Strand, Tor Austad et al. (2005). Furthermore, Hognesen, Strand, Tor Austad et al. (2005) carried out a spontaneous imbibition (SI) experiment at a temperature of 120°C, using modified SW with varying concentrations of SO_4^{2-} . The oil recovery when the injection brine was SW and SW without sulphate are 30 % and 15 % respectively.

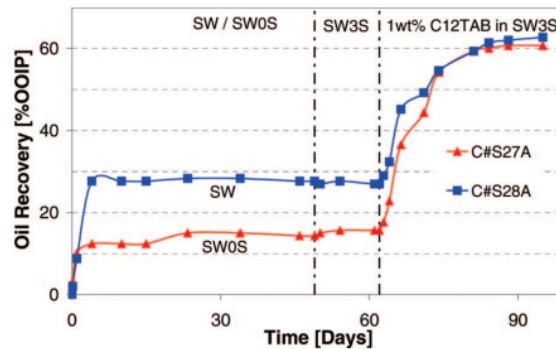


Figure 4.3: Results from spontaneous imbibition of limestone cores at a temperature of 120°C by brines with and without SO_4^{2-} . Figure from Strand, Tor Austad et al. (2008).

In an oil displacement test, whose results are shown in Figure 4.3, the oil recovery at 120°C was about 15 % higher when the limestone core was imbibed with SW compared to SW without SO_4^{2-} (SW0S). It can therefore be seen that SW is a suitable EOR fluid in limestone as it is in chalk. Also, in a SI experiment (120°C), carried out in Sriram Chandrasekhar (2013), to investigate the lone effect of SO_4^{2-} in the absence of other PDI in SW, (0Mg0Ca4S). A total oil recovery of 22 % of OOIP was made. Furthermore, an additional 19 % of oil was recovered when brine MgCa4S was used Sriram Chandrasekhar (2013).

The mechanism responsible for this recovery can be attributed to multi-ion exchange (MIE) Sriram Chandrasekhar (2013). SO_4^{2-} tend to adsorb strongly on the limestone surface which then allows for the co-adsorption of Ca^{2+} and thereby displace the negatively charged carboxylic materials contained in the crude oil. This process increases the water-wetness of the calcite surface. Though, sulphate is a PDI to carbonate surface, it is also regarded as a problem because precipitation of $BaSO_4$ can result to reservoir souring and scaling Strand, Høgenesen and Tor Austad (2006).

Effect of Mg^{2+} and Ca^{2+}

The concentration of Mg^{2+} in the initial brine FB; and SW are 27.41 mg/l and 1279 mg/l respectively. Mg^{2+} has the highest concentration in SW amongst all the potential determining ion (PDI)s. The concentration of Ca^{2+} in the FW is usually high which stands at about 27,118 mg/l and 409 mg/l in SW. Amongst other conditions, the degree of success of a wettability alteration process is supported by the concentrations of PDIs in the injection fluid and the temperature. The affinities of Mg^{2+} and Ca^{2+} onto the limestone surface were investigated in Strand, Tor Austad et al. (2008) using the chromatographic tests described in Section 4.1.1. The results from Strand, Tor Austad et al. (2008), are presented in Table 4.1.

Temperature °C	Ca^{2+} adsorption area	Mg^{2+} adsorption area
20	0.19	0.16
70	0.16	0.18
100	0.14	0.26
130	0.15	0.29

Table 4.1: Results of adsorption tests on limestone surface. Data source: Strand, Tor Austad et al. (2008).

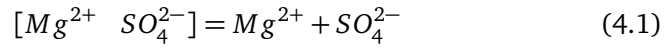
At lower temperatures, the adsorption of both PDIs were quite similar. However, at higher temperatures, the adsorption of Mg^{2+} became more evident. The reasons are, according to Strand, Tor Austad et al. (2008);

1. Mg^{2+} ion is quite small with a high charge density, hence it is more solvated in water.
2. Hydration energy of both ions. -459 Kcal/Mol and -380 Kcal/Mol for Mg^{2+} and Ca^{2+} respectively. Hence, Mg^{2+} is more reactive than Ca^{2+} due to partial dehydration of the ions.

Furthermore, to study the interaction between all the PDIs, and the limestone surface, results showed that in the presence of SO_4^{2-} , the concentration of Ca^{2+} decreases while the concentration of Mg^{2+} increases Strand, Tor Austad et al. (2008). This is attributed to;

1. The adsorption of Ca^{2+} on the limestone surface and the desorption of Mg^{2+} from the surface.

2. When SO_4^{2-} adsorb onto the rock surface, it makes the surface less positive charge, so Ca^{2+} is able to adsorb on the surface due to less electrostatic repulsion.
3. Mg^{2+} forms an ion pair with SO_4^{2-} in the aqueous phase.



This ion pair lowers the effectiveness of the Mg^{2+} and thus allow it desorb from the carbonate surface.

Results of adsorption tests carried out in Seyed Farzad Shariatpanahi, Strand and Tor Austad (2010) are in agreement with those carried out in Strand, Tor Austad et al. (2008). As the concentration of SO_4^{2-} increases on the solid surface, the co-adsorption of Ca^{2+} increases, thereby increasing the water-wetness of the carbonate surface. The presence of SO_4^{2-} , decreases the equilibrium condition of the Ca^{2+} ion and this allows for the desorption of Mg^{2+} . As observed in chalk, there was a substitution of Ca^{2+} by Mg^{2+} , though the rate of substitution is lower for limestone. Furthermore, no substitution was noticed at temperatures below $80^\circ C$. However, the substitution increased with increasing temperature Seyed Farzad Shariatpanahi, Strand and Tor Austad (2010).

Combined interaction between Mg^{2+} , Ca^{2+} and other potential determining ion (PDI)

Mg^{2+} is able to substitute Ca^{2+} from the rock surface at elevated temperatures, and this is called the dolomization process. The rate of substitution increases as the temperature increases. In a SI experiment, carried out at a temperature of $120^\circ C$ in Sriram Chandrasekhar (2013), to investigate the lone effect of Mg^{2+} in the absence of other PDI in a SW. A total oil recovery of 23 % of OOIP was made. The phenomenon responsible for this recovery can be attributed to dolomization process Sriram Chandrasekhar (2013).

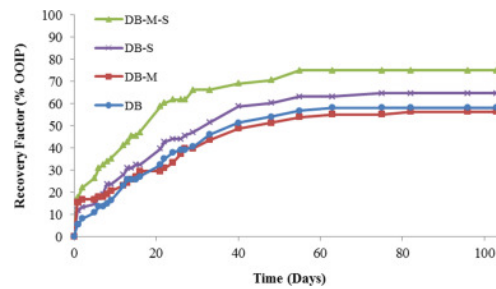


Figure 4.4: Oil recoveries made in a SI experiment, with varying imbibing brines at $120^\circ C$. Figure from Karimi et al. (2016).

Karimi et al. (2016) examined the impact of Mg^{2+} and SO_4^{2-} in injected brines, on oil recovery using a limestone sample in a spontaneous imbibition experiment whose results are illustrated in Figure 4.4. The recoveries for 100 times diluted FB

(DB), and DB spiked with 5 times the concentration of magnesium in FB (DB-M), are 58 % and 56 % of OOIP respectively. DB spiked with 10 times the concentration of sulphate in FB (DB-S), had a recovery of 60 % of OOIP. And 75 % of OOIP was recovered with DB spiked with 5 times magnesium and 10 times sulphate concentration in FB (DB-S-M). Though all brine combinations improved the water wetness of the rock surface, but brines with higher concentration of SO_4^{2-} , than Mg^{2+} were more effective. At low temperatures, Mg^{2+} tends to be strongly hydrated in water, and this impedes its reactivity with other minerals. However, at higher temperatures, it is dehydrated and therefore its reactivity with other minerals also increases.

The results of coreflooding experiment in Tetteh, Janjang, Barati et al. (2018), shows that brines depleted of Ca^{2+} , i.e., SW0Ca and LSW0Ca reduced oil recovery potential by about 0.2 % and 3.4 % respectively when compared to baseline results when using ordinary SW and LSW in tertiary mode.

4.1.2 Effect of divalent ions on interfacial tension

Interfacial tension (IFT) is the contractile tendency of a liquid surface when exposed to another immiscible liquid Torsæter and Abtahi (2003). The chemical reactions happening at the interface of the oil and brine has been found to be connected with wettability alteration. Therefore, the contributions of divalent ions to these chemical reactions has been investigated in various literature Tetteh, Janjang, Barati et al. (2018) and Gandomkar and Rahimpour (2017).

In an IFT measurements in Tetteh, Janjang, Barati et al. (2018), Mg^{2+} had the most significant effect on IFT. In SWS0Mg, i.e., SW without Mg^{2+} , the absence of Mg^{2+} resulted in the initial and final IFT values of 26.38 mN/m and 21.63 mN/m respectively. This trend is in agreement with the work of Gandomkar and Rahimpour (2017), where the single brine with $MgCl_2$ resulted in the greatest wettability change towards water-wet.

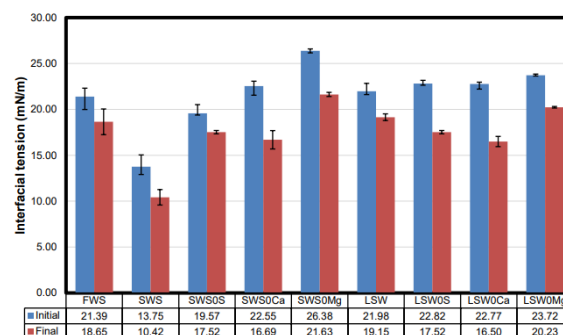


Figure 4.5: interfacial tension (IFT) results for varying salinity brines with different divalent concentrations. Figure from Tetteh, Janjang, Barati et al. (2018).

Furthermore, as shown in Figure 4.5, the absence of divalent ions such as SWS0Ca, SWS0S, LSW0S, LSW0Ca, and LSW0Mg resulting in series of high IFT values. Therefore presence of divalent ions have tendencies to reduce IFT. SWS contains the highest of concentration of divalent ions amongst all the brines tested, hence the reason for the least IFT value. Other reasons for the IFT values for FB, SW and LSW are further explained in Section 4.2.2. Al-Attar et al. reported that, with decreasing concentration of SO_4^{2-} and Ca^{2+} in injected brines, there was also a decreasing trend in , and also mentioned that the maximum recovery was not recorded with this brine.

4.1.3 Effect of divalent ions on zeta potential

Similar to interfacial tension (IFT), the surface charge of a carbonate surface, will give a strong indication of its wettability. Disjoining pressure [3.1.1] is a key ingredient in the wettability alteration process and electrostatic forces are the most pre-dominant determinant in the disjoining pressure required to result in wettability alteration Tetteh, Janjang, Barati et al. (2018). Furthermore, these forces between the solid/brine and oil/brine interfaces are responsible for the expansion of the electric double layer (EDL), which in turn results in the occurrence of stable water film at the oil/rock interface. Ionic strength and multi-ion exchange (MIE) between the PDI are responsible for surface charge reduction Tetteh, Janjang, Barati et al. (2018).

To quantify the effectiveness of Mg^{2+} and Ca^{2+} on the surface charge of a limestone surface, four brines (FWS0Ca, SWS0Ca, FWS0Mg, SWS0Mg) were tested with both divalent ions being isolated in varying salinity brines. Mg^{2+} has been found to be more effective at higher temperatures, therefore Ca^{2+} is expected to be more effective in this test temperature of $25^{\circ}C$ in Tetteh, Janjang, Barati et al. (2018). Experimental results are illustrated in Figure 4.6.

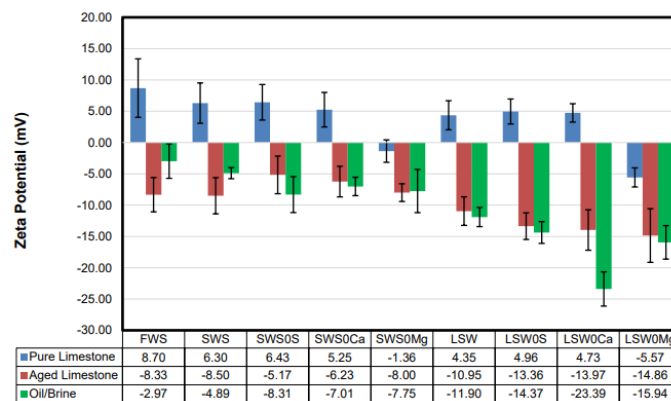


Figure 4.6: Zeta potential results for varying salinity brines with different divalent concentrations. Figure from Tetteh, Janjang, Barati et al. (2018).

For pure limestone, the reduction in the zeta potential values between SWSOMg and LWSOMg can be attributed to the excessive reactivity of calcium and the remainder of SO_4^{2-} concentrations in the brines. For the case of the aged limestone, the negative zeta potential values are caused by the higher influence of the brine/oil interface over the solid/brine interface. Carboxylic acid present in the crude oil is the reason for -23.39 mV value recorded at the brine/oil interface for the LSWOCa brine. Wettability alteration is expected to occur when a similar polarity is measured at the oil/brine and solid/brine interface, therefore the most significant wettability change to more water-wet is expected to occur with brines SWSOMg and LSWOMg. To investigate the effect of SO_4^{2-} on surface charge, SO_4^{2-} concentration was isolated in varying brine salinities while keeping their ionic strength constant. The surface charge without sulphate became more positive for both brines for the pure limestone, Figure 4.6, this is because the absence of sulphate will give room for extra activity for other PDI on the solid surface Tetteh, Janjang, Barati et al. (2018).

Song et al. (2020) carried out several zeta potential measurements at 25°C, using single electrolyte based and different sea water modified brines, to investigate the interactions of the PDI on an Indiana limestone surface. Though, the test temperature might not represent the reality of the rock/brine and oil/brine interfaces at 96°C but it gives perspective to the temperature effect on ion interactions with limestone surface. Sufficient electrostatic repulsion at the oil/brine and rock/brine interface is necessary for the disjoining pressure required to stabilize the brine film between rock and oil Song et al. (2020). The reduction of Na^+ from injection brines and the addition of sulphate concentration, enables the rock surface towards water-wet conditions. Furthermore, Mg^{2+} alone is unable to alter the wettability alteration, to favourable conditions Song et al. (2020).

Gopani et al. (2021) performed several zeta potential analysis using varying salinity brines and ionic compositions. Zeta potential increases with increasing level of dilution and this is attributed to the double layer mechanism Gopani et al. (2021). Figure 4.7, shows zeta potential vs pH plot for several brines used in the zeta potential analysis. Within the pH range of 6.5-7.5, the carbonate surface tends to be net positive and attach to the carboxylic materials contained in the crude oil Mahani et al. (2015). Figure 4.8 illustrates zeta potential results for varying ionic strength brines, to demonstrate the effect of the potential determining ion (PDI). The following conclusions were drawn from Figures [4.7] and [4.8] as per, Gopani et al. (2021).

1. Zeta potential values becomes more negative as brine salinity moves from 25 % dilution to 1 % dilution compared to SW. The implication of negative potential, is a negative rock surface, which is beneficial to the double layer expansion.
2. The addition of Ca^{2+} and Mg^{2+} , renders the carbonate surface more positive. That is, more positive zeta potential values.

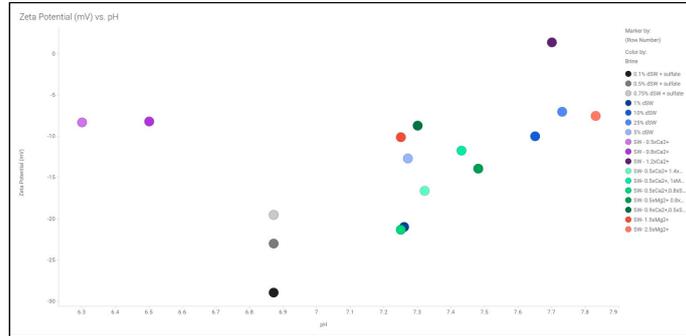


Figure 4.7: Zeta potential of brines with varying composition and pH values of measurement. Figure from Gopani et al. (2021).

3. The addition of SO_4^{2-} renders the carbonate surface more negative. This is due to the chemical affinity of sulphate on rock surface to form $CaSO_4$ precipitates. This affinity thus, increases the force of repulsion between the rock/brine and oil/brine interfaces.
4. To enable the desorption of carboxylic materials from the rock surface, it is beneficial to keep the zeta potential value either more negative or near zero. A near zero value insinuate a reduction in the attractive forces, keeping the oil attached to the rock surface, while a more negative zeta potential value, means an increment in repulsion forces between the negatively charged oil and rock surface.
5. With more adsorption of Ca^{2+} and Mg^{2+} on the rock surface, the electrostatic force reaches a minimum between the rock/brine and oil/brine interfaces, this results to the release of oil molecules from the rock surface.

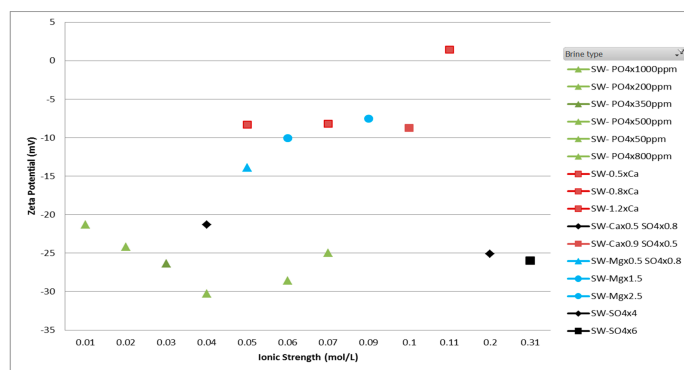


Figure 4.8: Zeta potential of brines with varying ionic strengths. Figure from Gopani et al. (2021).

4.1.4 Effect of divalent ions on contact angle measurements

Contact angle is one of the numerous ways to quantify rock wettability. Contact angle measurements in Tetteh, Janjang, Barati et al. (2018), using the same brines as in sections 4.5 and 4.1.3, the contact angle measurements, as shown in Figure 4.9a, reduced from 168° to 156° to 137° , when changing from brines FWS to SWS0Ca and LSW0Ca respectively.

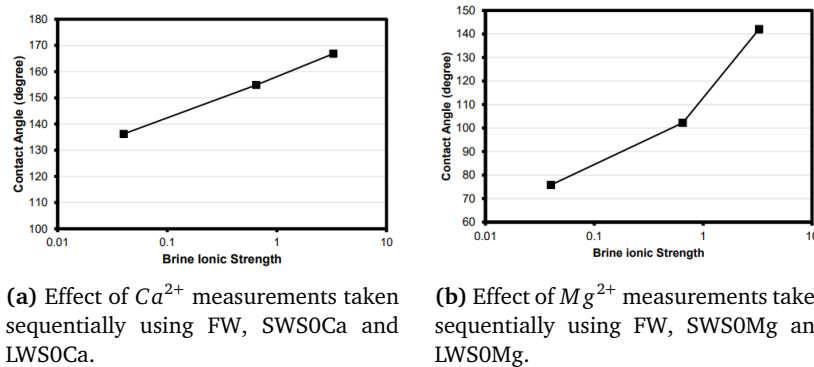
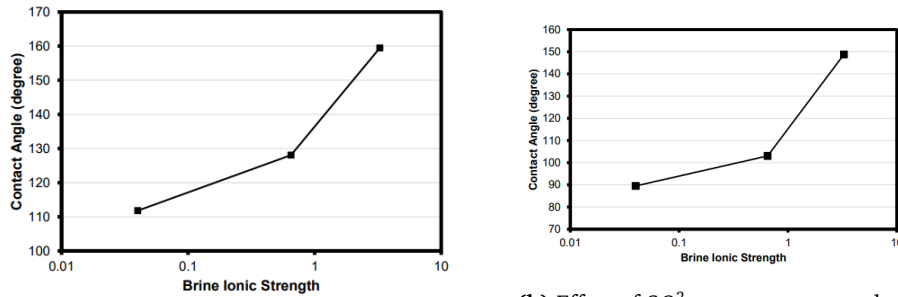


Figure 4.9: Contact angle measurements at 40°C , using brines of varying Ca^{2+} and Mg^{2+} concentrations. Figure from Tetteh, Janjang, Barati et al. (2018).

Also, the contact angle measurements reduced from 142° to 102° to 76° ; Figure 4.9b, when changing from brines FWS to SWS0Mg and LWS0Mg respectively. Therefore as explained in Section 4.1.3, the most significant wettability changed occurred with brines SWS0Mg and LWS0Mg because similar polarity measurements were recorded at the oil/brine and oil/rock interfaces which leads to the increased elastic forces to the gross disjoining pressure Tetteh, Janjang, Barati et al. (2018). It should also be noted that, due to the test temperature of 40°C , Ca^{2+} is expected to be more reactive to the limestone surface than Mg^{2+} .

In the case of SO_4^{2-} , the reduction of SO_4^{2-} concentration in the testing brines will have no much significance to the wettability alteration. As shown in Figure 4.10, the contact angle measurements in Figure 4.10b, are similar to Figure 4.10a, which are the baseline results.

Contact angle measurements in Gandomkar and Rahimpour (2017), to test the affinity of ions on limestone surface as they affect wettability alteration, results that increasing the SO_4^{2-} in the presence of Mg^{2+} , reduced the contact angle from 43° to 32° . Increasing SO_4^{2-} concentration in the LSW, changes the wettability of the limestone to a more intermediate wetness and increasing the SO_4^{2-} concentration in the LSW, in the presence of other PDIs, changes the wettability from intermediate wetness to strongly water-wet, i.e., 87° to 30° . When the concentration of Ca^{2+} in the LSW, was increased in the presence of other PDIs, the contact angle measurements varied from 128° to 132° .



(a) Baseline measurements taken sequentially using FW, SW and LSW.

(b) Effect of SO_4^{2-} measurements taken sequentially using FW, SWSOS and LWSOS.

Figure 4.10: Contact angle measurements at 40°C , using brines of varying ionic composition. Figure from Tetteh, Janjang, Barati et al. (2018).

Similar contact angle measurements in Sriram Chandrasekhar (2013) confirms that SW with added concentrations of SO_4^{2-} and Mg^{2+} are able to alter the wettability of an initially oil-wet limestone sample to more water-wet. These results were further validated by SI experiments. The test temperature is 100°C . The ranges of selected brines contains different combinations and insulation of all the PDI in reference to ordinary SW. Brines MgCa2S, MgCa4S, 0Mg0Ca4S, 0Mg0Ca2S, Mg0Ca0S and Mg0Ca4S showed promising results while 0MgCa0S, 0MgCa4S and MgCa0S were unsuccessful combinations.

As in MgCa2S and MgCa4S, the presence of all the PDIs in SW have the ability of altering wettability. Increasing the concentration of SO_4^{2-} by two times and four times in SW and the absence of other PDI (0Mg0Ca4S and 0Mg0Ca2S) improved the wettability of the calcite surface to more water-wet. Mg^{2+} alone in the absence of other PDI (Mg0Ca0S) and in the presence of four times concentration of SO_4^{2-} (Mg0Ca4S), proved to be an effective wettability modifier. This can be largely based on the effect of the test temperature; which means Mg^{2+} becomes more reactive.

4.2 Effect of brine salinity

The effect of water saltiness and particle structure on oil recuperation has been a region of examination as of late. Proof from research facility considers upheld by some field tests focusing on principally sandstone, has particularly demonstrated that infusing low saltiness water significantly affects oil recovery. New series of experiments are being carried out on carbonate reservoirs. The salinity of ocean SW is about 30,000 parts per million (PPM) while the salinity of FB is about 250,000 PPM. However the salinity of Gulf SW is about 58,000 PPM. The mechanism behind the effectiveness of reducing salinity has been explained in Section 3.2.2.

In a core flooding experiment in Yousef, Al-Saleh, Al-Kaabi et al. (2010) to investigate the effect of low salinity on oil recovery in carbonate reservoirs, using composite core with six individual cores. The average porosity and permeability of the individual cores are about 25 % and 39.6 mD respectively. The composition of the rock material is 80 % of calcite, 13 % of dolomite, 6 % of anhydrite and less than 1 % of quartz. X-ray Computerized Tomography (CT) scans helped to identify cores with fractures and permeability barriers.

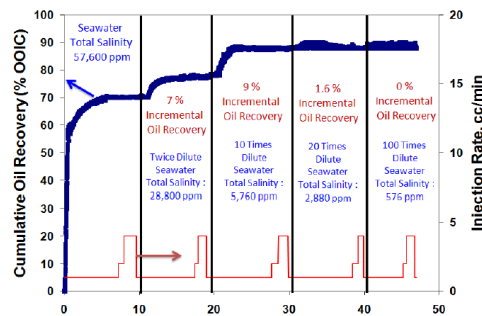


Figure 4.11: Coreflooding results of a composite carbonate core which had been injected with brines diluted 2, 10, 20 and 100 times the salinity of Gulf SW. Figure from Yousef, Al-Saleh, Al-Kaabi et al. (2010).

From Figure 4.11, oil recovery after the injection of Gulf SW peaked at 67 %. A 9 % incremental recovery was made when the brine was switched from 2 times diluted Gulf SW to 10 times diluted Gulf SW. Most notably, no much was recovered when the brine was switched to 100 times diluted Gulf SW. A similar experiment was carried out in Yousef, Al-Saleh, Al-Kaabi et al. (2010), using a different composite core to validate the results of the first experiment. The results of this new coreflood test affirmed and approved the considerable extra oil recuperation seen with past coreflood experiments.

In accordance with Yousef, Al-Saleh, Al-Kaabi et al. (2010), Feldmann et al. (2020) carried out several spontaneous imbibition experiments at 20°C to quantify low salinity effects on limestone samples. In the first test, the highest oil recovery (3.1 %) was recorded when the initial and the imbibing water was diluted SW. Feldmann et al. (2020) noted that not a lot of oil recovery should be expected if the same fluid is used as the initial as well as the imbibing fluid. In group 2 experiments, the highest oil recovery (36.1 %) was recorded when FW and diluted seawater were used as connate water and imbibing brine respectively. The sulphate concentration (about 3.5 g/l) of the SW is more than that of the FW, and also 4 times less saline, therefore the oil recovered when the cores were initially imbibed with SW, after FW could be a combined effect of high sulphate concentration and low salinity. Hence, the huge recovery (36.1 %) when the cores were then imbibed with diluted seawater, after using FW as the connate water will be attributed to the effect of low salinity. As the diluted seawater, is 400 times less

saline and the sulphate concentration is about 0.035 g/l. Diluted SW showed to be more efficient than smart water for oil recovery.

Alongside Yousef, Al-Saleh, Al-Kaabi et al. (2010) and Feldmann et al. (2020), Nasralla et al. (2018) examined the effect of low salinity on oil recovery in limestone cores, in series of spontaneous imbibition experiments. Three samples with varying permeability values were imbibed with FW, SW and 10 times diluted SW in secondary and tertiary modes. In all experiments carried out in Nasralla et al. (2018), the 10 times diluted SW showed more potential for oil recovery. In the secondary mode, the approximate oil recovery of 9 % and 5 % by SW and FW respectively shows that SW is a better wettability modifier than the FW. While in the tertiary mode, the imbibition of SW resulted in an oil recovery of 5 %, and 7 % when the cores were imbibed with 10 times diluted SW in the same mode. This further shows the efficiency of low salinity of injected brine. However, Nasralla et al. (2018) noted that the optimal level of dilution varies from section to section in the reservoir.

The results of Nasralla et al. (2018) are in agreement with those of Romanuka et al. (2012), where limestone cores were used for spontaneous imbibition tests at temperatures of 70°C and 120°C. As shown in Figure 4.12 Romanuka et al. (2012) reported about 6 % - 10% OOIP after the sample was imbibed with FW, 1 % oil recovery was made when the initial brine was replaced with a higher salinity brine (PW) and 3 % incremental recovery was made when a type of the FW was spiked with Ca^{2+} , SO_4^{2-} and Mg^{2+} [$FW - CaMgSO_4$]. The ionic strength of [$FW - CaMgSO_4$] was significantly lower than FW, hence, an affirmative reason can not be given for the change in wettability, i.e, whether its because of the lower ionic strength or the introduction of potential determining ion (PDI).

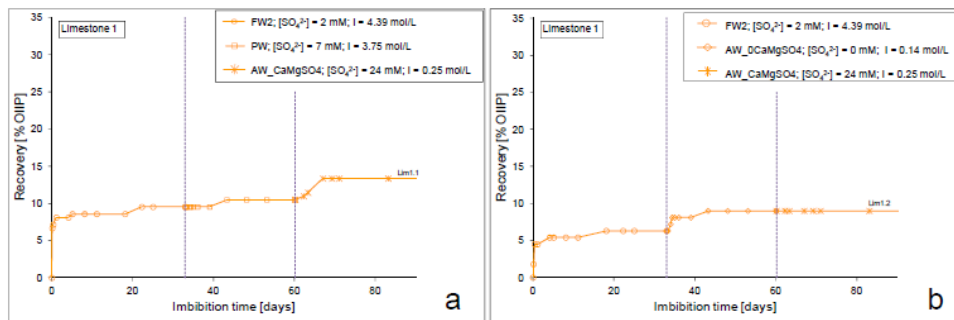


Figure 4.12: Spontaneous imbibition results for a limestone with varying brine salinities. Figure from Romanuka et al. (2012).

Similar experiments with same core in Romanuka et al. (2012), was imbibed with a lower ionic strength brine with no PDI and there was an incremental 3 % recovery compared to when 0 % when PDIs were later introduced. These results were further validated with another limestone but with only SO_4^{2-} . Romanuka

et al. (2012) concluded that, the wettability of the limestone core was altered by reducing the ionic strength and not by the introduction of potential determining ion. The introduction of sulphate could lead to plugging of reservoir rock, scale formation and souring of oil fields Romanuka et al. (2012). All these problems, can be eliminated by low salinity brines.

Romanuka et al. (2012) reported higher oil recoveries at a 120°C, during SI tests using limestone cores as seen in Figure 4.13. Therefore, oil recoveries are higher at elevated temperatures.

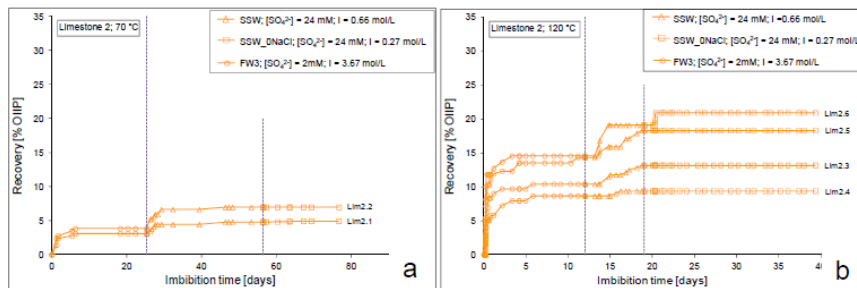


Figure 4.13: Spontaneous imbibition results for a limestone with varying brine salinities at temperatures of 70°C and 120°C. Figure from Romanuka et al. (2012).

Seyed Jafar Fathi, Tor Austad, Strand et al. (2012) reported a reduction in oil recovery with decreasing salinity. The difference in results compared to Yousef, Al-Saleh, Al-Kaabi et al. (2010), this has been attributed to rock type, reservoir fluids, injection practices e.t.c most notably is the presence of anhydrite.

4.2.1 Presence of anhydrite

Majority of carbonate reservoirs exist at a very high temperature. The initial brine contains a lot of Ca^{2+} , hence sulphate is present through the solubility of anhydrite, $CaSO_4(s)$. But the solubility of anhydrite decreases with increasing temperature and for this reason, the sulphate dissolved in the FW is usually low Austad et al. (2012). The solubility of anhydrite in pure water is about 2.01 g/L at 20°C and 1.62 g/L at 100°C.

According to Tor Austad, Seyed Farzad Shariatpanahi et al. (2015), tertiary oil recovery was observed with limestone reservoir cores with a given amount of dis-solvable anhydrite, no recovery was made from cores which are dis-solvable anhydrite free when same experiments were carried out. Hence, the presence of dis solvable anhydrite in limestone cores is essential for low salinity effect.

It is established that SW contains all the active ions to improve the wettability of a carbonate surface Seyed Jafar Fathi, Tor Austad, Strand et al. (2012) and

Tor Austad, Seyed Farzad Shariatpanahi et al. (2015). However, the combination of the presence of anhydrite in the pore space and the injection of diluted SW, could result in a better wettability modifying process. To investigate these conditions, Tor Austad, Seyed Farzad Shariatpanahi et al. (2015) carried out two sets of test. In the first test, at a temperature of 100°C, a core was successively flooded with sulphate depleted FW (FWOS), Gulf SW (GSW) and 10x diluted Gulf SW (d10GSW). The oil recovery peaked at 33 % of OOIP after the injection of d10GSW, the recovery after the injection of FWOS was about 25 % as shown in Figure 4.14.

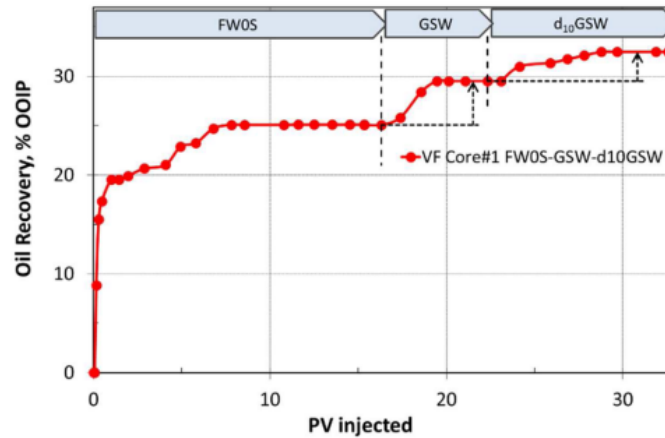
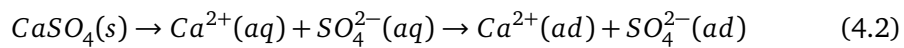


Figure 4.14: Oil recovery test of a core with anhydrite in the pore space. Figure from Tor Austad, Seyed Farzad Shariatpanahi et al. (2015).

The effluent of the d10GSW fluid used in test Figure 4.14, was analysed for the concentration of SO_4^{2-} and Ca^{2+} which were initially 4.5mM and 1.6 mM respectively. The concentrations of both ions in the d10GSW increased to about 10mM. The importance of sulphate in imbibing fluid cannot be over emphasised. SO_4^{2-} acts as a catalyst for the desorption of carboxylic materials from the carbonate surface. If SO_4^{2-} is absent in the injection fluid, the dissolution of anhydrite, $CaSO_4(s)$, could act as an 'emergency' or 'in-place' source of SO_4^{2-} Tor Austad, Seyed Farzad Shariatpanahi et al. (2015). Hence, the presence of dissolvable anhydrite is important. The chemical mechanism to understand the low salinity effect in carbonate rocks is suggested in Tor Austad, Seyed Farzad Shariatpanahi et al. (2015) in Equation 4.2;



$Ca^{2+}(aq) + SO_4^{2-}(aq)$ tend to dissolve in pore water while $Ca^{2+}(ad) + SO_4^{2-}(ad)$ are ions which are dissolved on the carbonate surface. As mentioned earlier, solubility of anhydrite is the source of $SO_4^{2-}(aq)$ and this is a function of the brine composition, temperature and salinity of the injected fluid. The solubility of

anhydrite increases with a decreasing concentration of Ca^{2+} and NaCl but with increasing temperature. The shortfall in solubility of anydrite in high temperatures can be compensated for if there is a significant amount of anhydrite distribution in the pore space Tor Austad, Seyed Farzad Shariatpanahi et al. (2015).

Mahani et al. (2015) investigated the impact of reduced brine salinity using two types of carbonate rocks. The limestone became less oil wet after it was successively flooded with FB, SW, 25 times diluted SW (25dSW) and 25 times diluted SW equilibrated with calcite (25dSWEQ). In this experiment in Mahani et al. (2015), low salinity effects were seen when the injected brine was diluted with deionized water, i.e, the concentrations of PDIs are now reduced. Therefore, low salinity effect can also be achieved even with little concentration of PDIs present in the injected brines. This further validates that wettability alteration in carbonates is majorly as a result of brine salinity and ionic composition of injected brines. Furthermore, the results of the zeta potential measurements were consistent with the wettability alteration of the limestone surface to more water-wet. That is, the limestone-brine interface because less positively charged.

4.2.2 Effect of brine salinity on interfacial tension

interfacial tension (IFT) is the contractile tendency of a liquid surface when exposed to another immiscible liquid Torsæter and Abtahi (2003). According to Yousef, Al-Saleh, Al-Kaabi et al. (2010), variation in salinity insignificantly affects the IFT, and therefore on liquid-Liquid connections. A further investigation was done to quantify the effect of varying salinities on IFT. The experiment was carried out at reservoir conditions, which is similar to that of the the core flooding experiments.

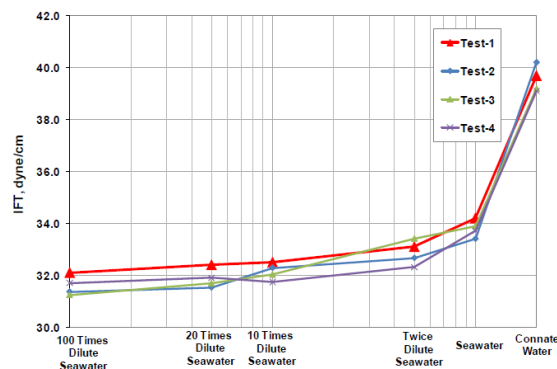


Figure 4.15: IFT measurement results live oil and brines with varying degree of dilution compared to levels in ordinary SW. Figure from Yousef, Al-Saleh, Al-Kaabi et al. (2010).

Results of the IFT measurements are depicted in Figure [4.15]. The lower the salinity, the lower the IFT values. However, the greatest change occurred between

switching from the connate water (FB) to the Gulf SW. Not much significant change in IFT was noticed between the diluted brines.

Though IFT measurements tend to decrease with decreasing salinity, However, Lashkarbolooki, Ayatollahi and Riazi (2014), have reported that this trend is not always true. Results of IFT measurement in Tetteh, Janjang, Barati et al. (2018), using limestone samples are illustrated in Table 4.2.

	FW	SW	LSW
Initial (mN/m)	21.39	13.75	21.98
Final (mN/m)	18.65	10.42	19.15

Table 4.2: Results of IFT measurements on limestone surface. Source: Tetteh, Janjang, Barati et al. (2018).

Since divalent ions tend to have significant effect on IFT, the reduced values shown in SW is quite understandable. This can be attributed to the presence of more divalent ions compared to other two brines and strong inter-molecular forces at the oil/brine interface. The dilutions in LSW reduced the concentrations on divalent ions present therein, and this leads to LSW, having identical IFT measurements as FW.

4.2.3 Effect of brine salinity on contact angle measurements

Yousef, Al-Saleh, Al-Kaabi et al. (2010) used the contact angle method in his investigation to address the effect of infusing distinctive saltiness slugs of seawater on carbonate rock wettability. The same rock sample and brine injection sequence was used for this experiment as the previous ones described above in Yousef, Al-Saleh, Al-Kaabi et al. (2010) and the pendant drop instrument method was utilized. All experiments are carried out at reservoir conditions and monitored for 2 days to ensure a proper impact of all injected brines. A water-wet rock would have a contact angle of 0° - 75° ; intermediate would have 75° - 115° ; and oil-wet would have 115° - 180° Santos et al. (2006).

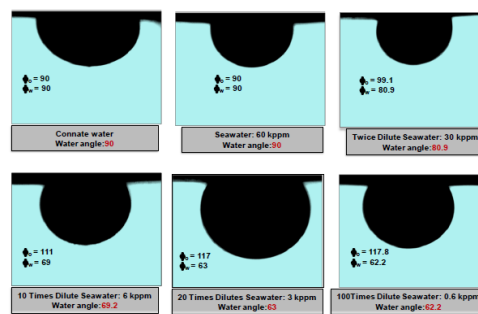


Figure 4.16: Images of wettability measurements when using brines of varying salinities Yousef, Al-Saleh, Al-Kaabi et al. (2010).

The contact angle results, Figure 4.16, are consistent with the oil recovery from the core flooding results in Yousef, Al-Saleh, Al-Kaabi et al. (2010) as more oil was recovered during the injection of 2x and 10x diluted SW. These contact angle measurements are consistent with those carried out in Mohanty, Chandrasekhar et al. (2013). Therefore, since the IFT measurements confirmed that, diluted SW have no effects on fluid-fluid interaction, then it can be concluded that the additional oil recovered during the injection of diluted SW, is as a result of rock-fluid interactions.

Karimi et al. (2016) investigated the ability of different salinity brines to alter the wettability of a limestone sample through contact angle measurements. Before the introduction of brines, the sample was aged and the contact angle measurement results to 149° , which shows an oil-wet state. And this can be attributed to the adsorption of the organic materials on the surface of the sample, during the aging process. As shown in Figure 4.17, the contact angle reduced from 149° to 146° to 81° to 61° and finally 47° after the introduction of the calcite surface to 100 times diluted FB (DB), DB spiked with 10 times the concentration of sulphate in FB (DB-S), DB spiked with 5 times the concentration of magnesium in FB (DB-M), and DB spiked with both magnesium and sulphate concentration (DB-M-S) respectively. The dilution of the FB is done to reduce the concentration of the nonactive salts NaCl. However, the low concentrations of PDIs in FB makes the dilution ineffective, i.e., unable to remove the adsorbed carboxylic materials on the surface of the calcite. The calcite surface became more water wet with the introduction of magnesium and sulphate. Therefore, they can be considered as wettability modifiers for oil-wet limestone.

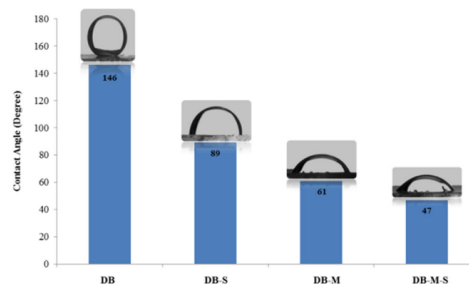


Figure 4.17: Contact angle measurements when using brines of varying salinities Karimi et al. (2016).

Mahani et al. (2015) examined how the contact angle measurement changes when it contacts brines of varying salinity with carbonate (Limestone and dolomite) patches with oil droplets. More contact angle changes were noticed in the limestone cores compared to the dolomite cores. And this is also in alliance with the zeta potential results where positive charges were seen at higher salinities with lower rate of change at lesser salinities. The contact angle measurements reduced after the introduction of SW. The carbonate patches were first exposed to FW for

about 40 hours. Results are shown in Figure 4.18.

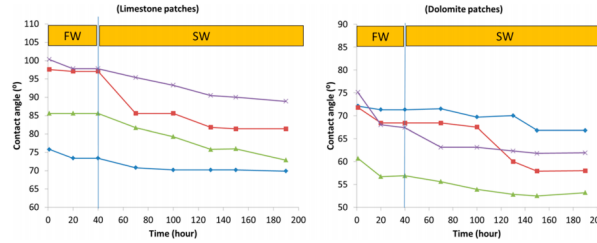


Figure 9. Contact angle of four different oil droplets (with different curve colors) on (left) limestone and (right) dolomite patches as a function of time in FW and SW.

Figure 4.18: Contact angle measurements when using brines of varying salinities (FW) and (SW) on limestone (left) and dolomite (right) patches right. Mahani et al. (2015).

However, in similar experiment in Mahani et al. (2015), where 25 times diluted SW (25dSW), Figure 4.19, was using as the brine phase after the exposure to FW, reduction in contact angle, measurements were only noticed in the limestone cores as shown in Figure . This was as a result of mineral dissolution. These results were enough for Mahani et al. (2015), to conclude a low salinity effect on wettability alteration in carbonates.

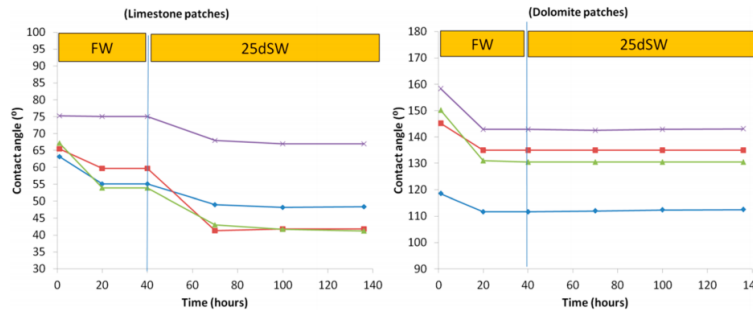


Figure 4.19: Contact angle measurements when using brines of varying salinities (FW) and 25dSW on limestone (left) and dolomite (right) patches right. Mahani et al. (2015).

Contact angle measurements carried out in Tetteh, Janjang, Barati et al. (2018), where 3 brines with varying salinity was used. The least saline brine (LSW) reduced the contact angle measurement by about 18 angles, compared to the intermediate brine (SW), which reduced the contact angle measurement by about 31 angles. The contact angle measurement of the initial brine (FW) was about 160°. These reduction in contact angle values with decreasing salinity brine are in agreement with results in Yousef, Al-Saleh, Al-Kaabi et al. (2010) and Mahani et al. (2015).

4.2.4 Effect of brine salinity on zeta potential

Zeta potential measurements provides an information on the surface charge of a solid (Karimi et al., 2016). It is a function of pH and particle size. Mahani et al. (2015) investigated the impact of salinity changes on the surface charge of oil/water and water/rock interface of two kinds of carbonate rocks. The results of the zeta potential measurements as a function of brine salinity and pH values are shown in Figure 4.20a.

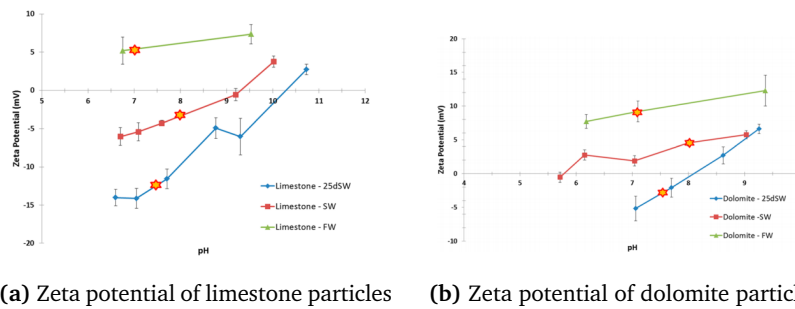


Figure 4.20: Zeta potential of two carbonate rocks in varying brine salinities. Figure from Mahani et al. (2015).

For the limestone core, the zeta potential values increase with increasing pH values for all salinities. The zeta potential remained positive for the FW, while the difference in composition of SW made the zeta potential less positive. The least saline brine tends to be much more negative as seen from the illustration. Therefore, the higher the salinity of the brine, the lower the gradient of the zeta potential with pH values.

In zeta potential experiments in Tetteh, Janjang, Barati et al. (2018), where 3 salinity brines FW, SW and LSW were used. The SW is 5 times diluted FW, while LSW is 82 times diluted FW. The zeta potential value shift in the case of pure limestone as illustrated in Table 4.3, from 8.70 mV to 4.35 mV, shows the effectiveness of low salinity water in the reduction of surface charge in a calcite surface. The negative values gotten at the oil/brine interface can be attributed to the strongly adsorbed carboxylic materials which are present in the crude oil. For the aged limestone, the values are -8.33 mV, -8.50 mV and -10.95 mV for FW, SW and LSW respectively. This trend is in agreement with those in Karimi et al. (2016).

	FW	SW	LSW
Pure Limestone (mV)	8.70	6.30	4.35
Aged Limestone (mV)	-8.33	-8.50	-10.95
Oil/brine (mV)	-2.97	-4.89	-11.90

Table 4.3: Results of Zeta potential measurements in Tetteh, Janjang, Barati et al. (2018).

4.3 Oil recovery in other carbonate cores

4.3.1 Chalk

Effect of ionic composition and brine salinity

In comparison to other carbonate rocks, a lot more research have been done concerning wettability alteration in chalk Seyed Jafar Fathi, Tor Austad, Strand et al. (2012), Peimao Zhang and Tor Austad (2006), Strand, Høgnesen and Tor Austad (2006) and Peimao Zhang, Tweheyo and Tor Austad (2007), compared to limestone and dolomite. However, our focus in this thesis is limestone. It has been reported in literature that PDIs that adsorb unto a limestone also apply to chalk. In an adsorption test in Strand, Høgnesen and Tor Austad (2006), the adsorption of sulphate to the chalk surface increases with increasing temperature which is similar to limestone.

Seyed Jafar Fathi, Tor Austad, Strand et al. (2012) investigated the effectiveness of SO_4^{2-} as a PDI on a carbonate surface. At $70^\circ C$, 50 % of OOIP was recorded when an NaCl depleted SW was spiked with 4 times sulphate concentration of original SW. Ordinary SW gave a recovery of 38 % of OOIP. Hence, the concentration of sulphate has a big impact on the oil recovery as seen in Figures 4.21a and 4.21b.

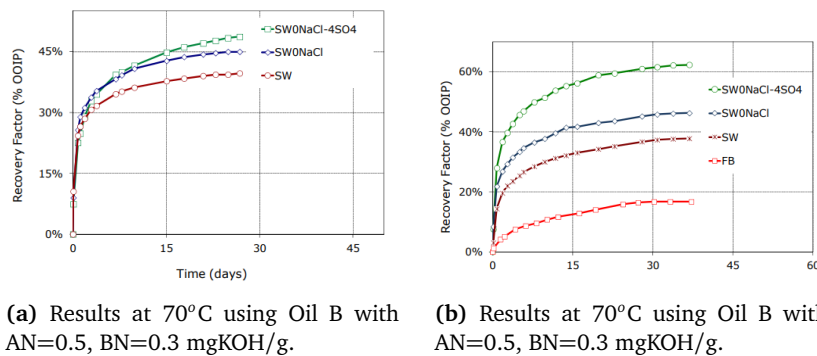


Figure 4.21: Spontaneous imbibition into oil saturated chalk cores using different imbibing fluids, with different salinities and ionic composition. $S_{wi}=10\%$. Figures from Seyed Jafar Fathi, Tor Austad, Strand et al. (2012).

At $90^\circ C$, similar trend was noticed as shown in Figure 4.21b. formation brine which has a low SO_4^{2-} content gave the least recovery of about 17 % of OOIP while NaCl depleted SW which was spiked with 4 times sulphate concentration of original SW gave the maximum recovery of 62 % of OOIP. This is attributed to more activity of the active ions in the double layer. Ordinary SW recovered about 38 % of OOIP. Similar experiment carried out in Strand, Høgnesen and Tor Austad (2006) resulted in akin trend as noticed in Seyed Jafar Fathi, Tor Austad, Strand et al. (2012). The result is depicted in Figure 4.22. The effect of additional

sulphate concentration is quite evident.

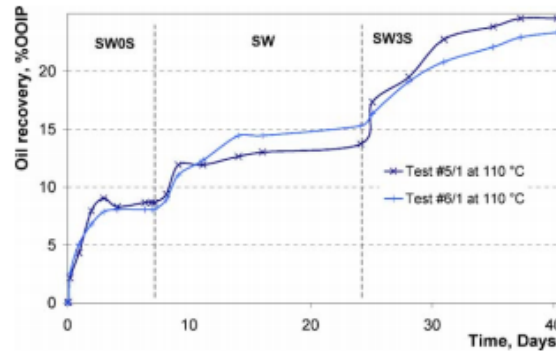
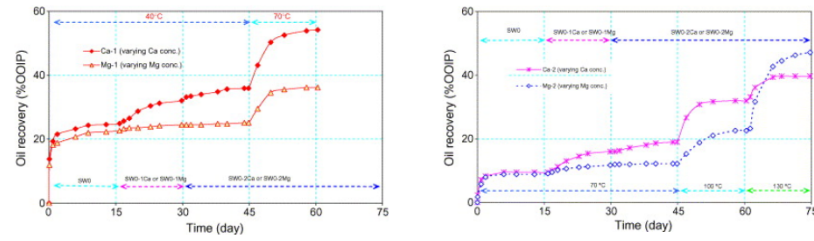


Figure 4.22: Spontaneous imbibition into oil saturated chalk cores at 110°C using different imbibing fluids, with different SO_4^{2-} concentrations, Oil with AN=2.1, S_{wi} =26% - 28 %. Figure from Strand, Høgnesen and Tor Austad (2006).

The affinity of Ca^{2+} to a chalk surface was investigated in Strand, Høgnesen and Tor Austad (2006). Results show that co-adsorption of Ca^{2+} on the rock surface increases with increasing temperature and SO_4^{2-} concentration. The more Ca^{2+} adsorbed onto the chalk surface, the more the negatively charged carboxylic materials are removed from the chalk surface which in turn improves the water-wetness. Ca^{2+} is an active wettability modifier in the presence of SO_4^{2-} at temperatures less than 100°C when approaching temperatures greater than 125°C, the precipitation of $CaSO_4$ is initiated but this can be mitigated by the increased concentration of Mg^{2+} Peimao Zhang, Tweheyo and Tor Austad (2007).

In a series of spontaneous imbibition experiments in Peimao Zhang, Tweheyo and Tor Austad (2007), to investigate the interplay between Mg^{2+} and Ca^{2+} . The oil with the lower AN was used at the lower temperatures (40°C and 70°C) to ensure a reasonable oil recovery. As shown in Figure 4.23a, at 40°C, about 20 % to 25 % of the OOIP was recovered. At 40°C, when 0.025 mol/l of Mg^{2+} and Ca^{2+} were separately added to individual cores; after 30days, the core with additional Ca^{2+} had an increase in oil recovery of up to 33 % of the OOIP and negligible oil recovery for the core with Mg^{2+} . When 0.045 mol/l of Mg^{2+} and Ca^{2+} were added to the cores, there was a 4 % recovery in the core with additional Ca^{2+} but the core with Mg^{2+} still had a negligible recovery.

At 70°C, the core with Ca^{2+} concentration reached an oil recovery of 55 % and the one with Mg^{2+} peaked at 33 %. Hence, Ca^{2+} appeared to be a more efficient wettability modifier in the presence of SO_4^{2-} at temperatures less than 70°C. Similar experiment carried out in Peimao Zhang, Tweheyo and Tor Austad (2007) at elevated temperatures $\geq 100^\circ C$ results that Ca^{2+} is a better wettability mod-



(a) A representation of how equal concentration of Mg^{2+} and Ca^{2+} and constant SO_4^{2-} concentration performed at low temperatures, i.e., $< 70^\circ\text{C}$.

(b) A representation of how equal concentration of Mg^{2+} and Ca^{2+} and constant SO_4^{2-} concentration performed at high temperatures, i.e., $> 100^\circ\text{C}$.

Figure 4.23: Combined Interaction between Mg^{2+} and Ca^{2+} . Figure from Peimao Zhang, Tweheyo and Tor Austad (2007).

ifier than Mg^{2+} at a temperature of 100°C as depicted in Figure 4.23b. At 130°C , the core which was imbibed with Mg^{2+} had more recovery (48 %) than the core imbibed with Ca^{2+} (40 %). The solubility limit of $CaSO_4$ was confirmed to have been exceeded at a temperature of 125°C and this was further confirmed virtually by precipitated materials beneath the imbibition cells. Hence, the effectiveness of Mg^{2+} and Ca^{2+} in the presence of SO_4^{2-} is limited by the precipitation of $CaSO_4$ at high temperatures. In a zeta potential measurement in Peimao Zhang, Tweheyo and Tor Austad (2007), the positive charge on the chalk surface increases with an increasing concentration of Mg^{2+} while the pH is kept constant at 8.4. Therefore, it was verified that Mg^{2+} is a PDI to chalk surface which in turn can act as a wettability modifier towards more water-wet.

The adsorption of Mg^{2+} on the chalk surface was studied in Peimao Zhang, Tweheyo and Tor Austad (2007) at 23°C and 130°C . The rate of adsorption was more evident at the higher temperature. After the effluent was analysed, the concentration of Ca^{2+} significantly increased by 60 % from the initial concentration and the concentration of Mg^{2+} was reduced compared to the initial concentration. This shows a possible occurrence of dolomization process.

These results are similar to those gotten in Karimi et al. (2016). No significant substitution was noticed at temperatures lower than 80°C , but a similar molar increase and decrease of both ions were noticed at temperatures of 90°C , 110°C and 130°C . According to Petrovich and Hamouda (1998), in the Ekofisk field ($T=130^\circ\text{C}$), decrease in the concentration of Mg^{2+} was noticed after the breakthrough of SW. This can be attributed to dolomization process. It is expected that the substitution reaction is more evident when using SW as the injection fluid, because of its high concentration in Mg^{2+} . Finally, it can be concluded that Mg^{2+} is very active PDI at high temperatures.

The effectiveness of Mg^{2+} in the presence of other PDIs especially at 70°C , 100°C and 130°C is depicted in Figure 4.24, during SI tests carried out in Peimao Zhang, Tweheyo and Tor Austad (2007). At 70°C , the imbibing fluids were totally depleted of Ca^{2+} and Mg^{2+} but concentration of SO_4^{2-} were added at 0, 1, 2 and 4 times the concentration in SW. Oil recovery was low, about 10 % and this could be attributed to partial water wetness of the rock and fluid expansion. At 100°C , the little oil recovered could be attributed to fluid expansion and thus it was concluded that SO_4^{2-} alone is unable to improve oil recovery by SI in chalk cores in the absence of other PDIs. The concentration of $Ca^{2+} = 0.013 \text{ mol/l}$ and Mg^{2+} as in original SW was added to the imbibing fluids. In the case of Mg^{2+} , the oil recovery increased with increasing SO_4^{2-} concentration.

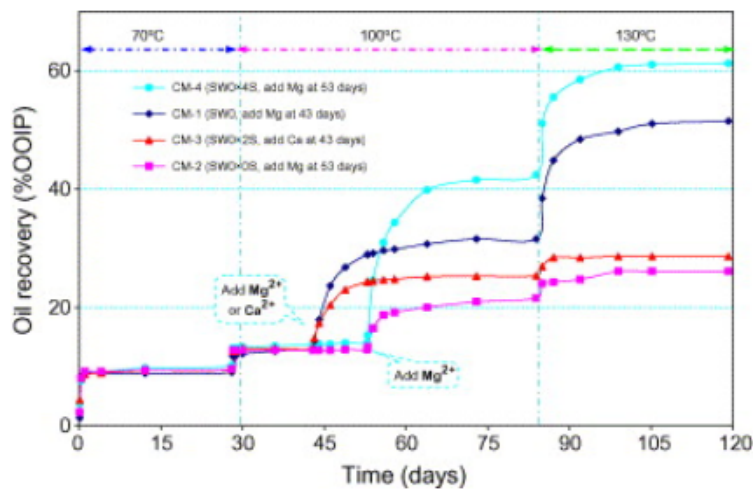


Figure 4.24: The effect of PDIs on spontaneous imbibition into chalk core at several temperatures. Figure from Peimao Zhang, Tweheyo and Tor Austad (2007).

At 130°C , the highest recovery was also made when Mg^{2+} was combined with 4 times the concentration of SO_4^{2-} content in SW. The oil recovery was about 60 % compared to 42 % in the previous temperature. Hence, the effectiveness of the combination of Mg^{2+} and SO_4^{2-} are temperature dependent. The higher the temperature, the higher the oil recovery. When a core was exposed to an injection fluid with Mg^{2+} but depleted of SO_4^{2-} , a marginal oil recovery was made which could be as a result of fluid expansion. Thus, Mg^{2+} is only a wettability modifier at high temperatures in the presence of SO_4^{2-} . The chemical mechanism to explain this oil displacement process is called multi-ion exchange (MIE) which was explained in Section 3.2.1.

4.3.2 Dolomite

A number of field and laboratory experiments have been carried out concerning the effects of 'smart water' on oil recovery in carbonates especially in chalk and limestone [Seyed Jafar Fathi, Tor Austad, Strand et al. (2012), S. Shariatpanahi et al. (2016) and Standnes and Tor Austad (2000)]. However, little attention has been paid to dolomite which is also a member of the carbonate family. S. Shariatpanahi et al. (2016) in series of experiments, studied the affinity of the aforementioned PDIs towards the dolomite surface by using the chromatographic test method, which was initially discussed in Section 4.1.1. Furthermore, spontaneous imbibition studies were carried out using a Silurian outcrop core with up to 235 mD and 20 % permeability and porosity respectively.

The chromatography results, Figure 4.25 shows that the adsorption of sulphate onto dolomite surface is quite low at room temperature which amounts to like 0.08 and then increases to 0.16 at elevated temperature of about 130°C.

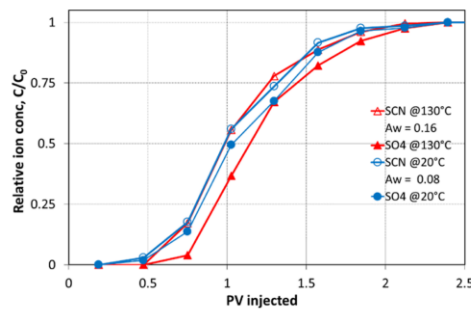


Figure 4.25: Chromatography test results on dolomite core. Figure from S. Shariatpanahi et al. (2016).

This adsorption results are generally low compared to those of chalk and limestone. Further experiments in S. Shariatpanahi et al. (2016) shows that the presence of SO_4^{2-} has negligible effect on the adsorption and co-adsorption of Mg^{2+} and/or Ca^{2+} which is in contrast with other carbonate families, hence there should be questions about the effectiveness of SW as an EOR fluid in dolomites.

To further quantify results of oil recovery by spontaneous imbibition in dolomite, S. Shariatpanahi et al. (2016) conducted a test on two dolomite cores with similar properties. The results from both cores show a similar trend as seen in Figure 4.26. About 8 %, 11 % and 25 % of cumulative OOIP was recovered from core SIL # 9 when flooded successively with FW, SW and 10 times diluted SW (d10SW) respectively. While, about 6 %, 7 % and 16 % of cumulative OOIP was recovered from core SIL # 6 when flooded in the same order. Similar experiment in Romanuka et al. (2012) on two Silurian outcrop dolomite cores resulted in similar results. About 8 %, 9 % and 18 % of cumulative OOIP was recovered from the first core when flooded successively with FW, SW and 10 times diluted SW (d10SW) respectively. While, about 6 %, 8 % and 22 % of cumulative OOIP was recovered

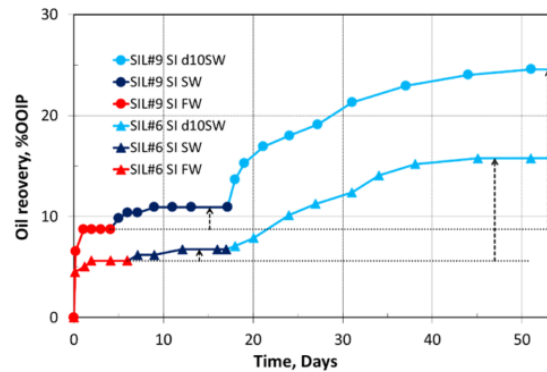


Figure 4.26: Spontaneous imbibition results on dolomite core with varying brine compositions. AN=0.52 mgKOH/g. Figure from S. Shariatpanahi et al. (2016).

from the last core, when brine flooding was done in the same order.

The oil recovered from this dolomite cores are quite low compared to those from limestone and chalk cores which again signifies that SW might not be the most optimum injection brine for dolomite. However, the pronounced jump in oil recovery after the injection of 10 times diluted SW (d10SW) cannot be ignored. This dramatic increase could not be attributed to the presence of dis solvable anhydrite as it was asertain that the cores were anhydrite free at the beginning of the experiments.

In the presence SO_4^{2-} also acts as a catalyst of wettability alteration in dolomite at high temperatures, and by reducing the salt content in brines, it gives room for increased activities of SO_4^{2-} . Furthermore, the results of these outcrop dolomite cores were similar to those gotten in Romanuka et al., 2012 where reservoir cores were used.

In zeta potential measurements for dolomite cores, as Figure 4.20b indicates, more positive surface charges compared to the limestone cores. This shows the difference in the surface reaction of both cores to brine salinities. The higher surface density, due to the presence of excess magnesium which is part of the mineralogy of the dolomite core, could be the basis for the more presence of positive charges when compared to the limestone core Mahani et al. (2015). The EDL structure of the dolomite is highly structured, therefore the ionic strength have not so much impact on the surface density Van Cappellen et al. (1993). Therefore, it was concluded that desorption of carboxylic materials from the dolomite surface are less easy when compared with their limestone counterparts, this is based on the surface charge results gotten from the experiments. Surface charge thus play a role in the wettability alteration of carbonates to more water wet.

Chapter 5

Methods and materials

This chapter describes the experimental setup for the dynamic aging set-up and the spontaneous imbibition (SI) tests. However, before detailing these set-ups, several core analysis experiments were carried out to determine the petrophysical properties of the cores and fluids used in the experiments. Therefore, the materials and methods of these core analysis are also discussed here.

The early subsections of this chapter discuss the preliminary tests carried out to determine core and fluid properties, followed by oil and brine preparations and finally the aging and SI set ups. Two types of core materials were used in this project;

1. Outcrop Ainsa core from the Ainsa Basin in the Spanish Pyrenees which is a representative of a carbonate field in Brazil operated by Equinor. The Ainsa cores are classified as anhydrite free limestone.
2. Outcrop Angola cores which is a representative of a carbonate field in Brazil operated by Equinor. The Angola cores are classified as limestone cores and also anhydrite free.

The Ainsa cores are labelled B1, B2, B3, B5, B6, B7 and B8, which were previously used by Azizov (2019). Angola cores are the newest cores provided solely for this experiment.

5.1 Liquids preparation

5.1.1 Oil preparation

A single type of oil was used for this experiment and it was provided by Equinor. The acid number (AN), Section 2.3 is 3.30 mg KOH/g as provided by Equinor. The oil is called Heidrun oil from the Norwegian oil field called Heidrun. The oil filtration was done in the fumehood under vacuum. It was made to pass through a 5 micrometer filter.



Figure 5.1: An image of the oil filtration set-up.

The purpose of oil filtration is to remove particles from the oil to avoid any form of blockage of the system. The schematic of the crude oil filtration set up can be found in Figure 5.1. The Bucher funnel and flask are connected via a tight clip holder. A rubber tung is placed at the entrance of the buckner flask to prevent any air flow. The white rubber tubing connects the flask to the tap, which also creates vacuum for oil flow through the filter.

5.1.2 Brines preparation

Six (6) types of brines were used in this experiment. FW, SW, SW-0.1, SW-0.1NaCl, SW-0.1NaCl-2S-4Mg, and SW-0.1NaCl-2S-8Mg. The brines were synthesized using deionized water (DI) and various laboratory salts with at least 99.3 % purity from VWR BDH Chemicals-Belgium. The FW have same properties as those of the Ekofisk Field FW. The SW ionic composition is similar to those of the North Sea. The FW and SW compositions are shown in Figure 5.1.

SW-0.1, SW-0.1NaCl, SW-0.1NaCl-2S-4Mg, and SW-0.1NaCl-2S-8Mg are modified SW compositions. SW-0.1 is ten times diluted concentration of SW. SW-0.1NaCl is 10 times diluted NaCl in SW. SW-0.1NaCl-2S-4Mg is 10 times NaCl diluted SW enriched with two and four times the concentration of sulfate and magnesium in SW respectively. SW-0.1NaCl-2S-8Mg is 10 times NaCl diluted SW enriched with two and eight times the concentration of sulfate and magnesium in SW respectively. The composition of all modified brines used are presented in Figure 5.2. To ensure complete dissolution of the solids, the magnetic stirrer was utilized. The stirring was done for 24 hours prior to usage.

Ions	FW (g/l)	SW (g/l)	SW-0.1 (g/l)
NaCl	148.521	23.741	2.374
NaHCO ₃	0.000	0.194	0.019
Na ₂ SO ₄	0.000	0.3976	0.398
KCl	5.510	0.755	0.076
MgCl ₂ ·x6H ₂ O	22.927	10.696	1.070
CaCl ₂ ·x2H ₂ O	99.473	1.500	0.150
SrCl ₂ ·x6H ₂ O	13.3338	0.024	0.002
Salinity (g/ltr)	247.7925	34.8218	3.482
Ionic Strength (mol/ltr)	5.13366	0.69137	0.069

Table 5.1: Synthetic formation water and seawater composition.

Ions	SW-0.1NaCl (g/l)	SW-0.1NaCl-2S-4Mg (g/l)	SW-0.1NaCl-2S-8Mg (g/l)
NaCl	2.371	2.371	2.371
NaHCO ₃	0.1940	0.1940	0.1940
Na ₂ SO ₄	0.3976	7.9520	7.9520
KCl	0.7550	0.7550	0.7550
MgCl ₂ ·x6H ₂ O	10.696	42.7840	85.5680
CaCl ₂ ·x2H ₂ O	1.500	1.500	1.500
SrCl ₂ ·x6H ₂ O	0.024	0.024	0.024
Salinity (g/ltr)	13.45	32.4585	52.4952
Ionic Strength (mol/ltr)	0.32	0.8832	1.51458

Table 5.2: Modified seawater compositions.

5.2 Liquid properties

5.2.1 Density measurements

Density ρ is defined as the mass of a substance per unit volume. The density of a substance varies with temperature and pressure. The units of mass and volume used at a measured temperature must be stated when the density of a substance is being reported. Density measurements were taken at room temperature and values are reported in the unit of g/cc. The pycnometer; Figure 5.2, method of measuring the density of fluids was utilized in this experiment.



Figure 5.2: Pycnometer.

The primary advantages of using the pycnometer method over others (API hydrometer, Westphal balance, Specific gravity balance) for density measurements are: it is a simple method, the instrument is relatively inexpensive, and the measurements are of higher accuracy. However, the pycnometer also has some disadvantages such as density must be calculated (indirect method), and the instrument for measurement is breakable.

The measurement principle of the pycnometer method is that a clean dry pycnometer of known weight is filled with a known volume of the liquid of interest at a known temperature. The opening of the pycnometer is then closed and the weight of the pycnometer plus the fluid is then used in calculating the density of the fluid. The fluid density is calculated using Equation 5.1:

$$\rho_{fluid} = \frac{W_{pyc+fluid} - W_{pyc}}{V_{pyc}} \quad (5.1)$$

ρ_f is the fluid density, W_{pyc} is the weight of the dry pycnometer, $W_{pyc+fluid}$ is the weight of the pycnometer filled with fluid and V_{pyc} is the volume of pycnometer.

5.2.2 Viscosity measurements

Crude oil viscosity was measured using the Brookfield rotational viscometer as shown in Figure 5.3. Viscosity is sensitive to temperature changes, but relatively insensitive to pressure changes until a very high pressure is reached Torsæter and Abtahi (2003).



Figure 5.3: Brookfield rotational viscometer.

The crude oil was poured into the annulus contained in the lower section of the viscometer. Then, the spindle was totally submerged in the crude oil and made to rotate (spin). The torque required to rotate the spindle, can be used to determine the velocity of the fluid contained therein. The test was carried out at 22.3°C and 96°C using spindle 31 and spindle 18, respectively. The value of the viscosity was recorded from the equipment when the readings stabilized.

5.2.3 Interfacial tension measurements

The Kruss Drop Shape Analyzer as shown in Figure 5.4 utilizes the optical pendant drop technique with a climbing drop, was utilized to gauge the interfacial tension between the Heidrun oil and the brine. IFT is determined with the pendant drop technique by utilizing the arch of the drop in the saline solution. The IFT makes the weight in the drop increment. The Laplace equation portrays the connection among IFT and the pressure contrast in the drop.

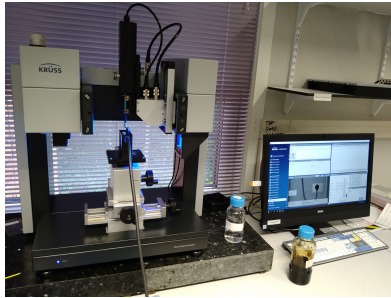


Figure 5.4: A schematic of the pendant drop method set-up.

The chamber is filled with saltwater and a needle is used to drop the oil droplets into the saltwater solution. The entire setup is connected to a computer and the video of the experiment can be viewed on it. A baseline is set to fix and track the formation of the oil droplet and the measurement program on the computer is started. The program automatically performs the measurement by adding volumes to the drop, until the drop finally breaks off from the needle. The program then displays all relevant results for the interfacial tension calculation. The measurement was carried out at room temperature, however a difference of about $\pm 2^{\circ}\text{C}$ could be noticed. About 300 runs were made to determine the IFT results.

5.3 Core analysis

5.3.1 Core cutting and dimensions

A whole Angola outcrop core, Figure 5.5, was provided by Equinor. The core cutting was done at the thin section workshop at the IV faculty building with the help of Kjetil Eriksen and Jon Runar Drotninghaug. A precised saw was used for the core cutting to get the required dimensions of the core plugs. To avoid any form of material damage and salt dissolution as we are making use of a carbonate core, the cutting process was done dry.



Figure 5.5: Angola whole core as provided by Equinor.

Pressurized air was used as the coolant, and a diamond toothed drill bit with a low rotations per minute (RPM) so as to avoid core breakage during cutting. With the help of the computerized tomography (CT) scan provided by Equinor, the best positions for drilling was identified. The CT scan helped identify the presence of fractures and permeability barriers. While cutting, a plastic and duct tape was connected to the cutting equipment to avoid so much dust while drilling dry.

Though a precised saw was used to cut in set-determined dimensions, there could still be some minor deviations from these set dimensions, hence a digital vernier caliper was used to measure the length and diameter of the core plugs so more accurate bulk volumes V_{bulk} , can be obtained. Several length and diameter measurements were taking along the core plug and average values were obtained for calculations. The cross-sectional area (A) was calculated using the Equation 5.2

$$\text{cross-sectional area}[cm^2] = \frac{\pi d^2}{4} \quad (5.2)$$

d is the average diameter of the core plug [cm].

$$\text{Bulk volume} = AL \quad (5.3)$$

L is the average length of the core plug [cm].

5.3.2 Core cleaning, drying and storage.

One of the aims of core cleaning is to ensure that no form of residue is left within the cores before the commencement of the experiment. Weight measurements were taken before and after the cleaning process to note any form of weight difference. The cores were cleaned in the soxhlet extraction set-up as seen in Figure 5.6. At the base of the soxhlet is a heating compartment that warms the fluid used for cleaning which could be toluene or methanol, to its boiling point. Methanol is utilized for salt and water expulsion, while toluene is utilized for oil evacuation.

The methanol will disintegrate and move to the highest point of the instrument, where there is a water-based cooling component or condenser. This makes the methanol consolidate over the center until the soxhlet is filled. The methanol is presently disintegrating and gathering in a nonstop shut framework, until the center is esteemed clean.



Figure 5.6: Core cleaning by Soxhlet extraction.

All Angola cores and two Ainsa cores were cleaned with only methanol. The cleaning was done for a day and when no change in the colour of the methanol was noticed, the cores were moved to the drying oven. The other Ainsa cores (B1, B2, B3 and B8) were cleaned with toluene for about 5 days and drying was done for the same number of days, until constant weight. All drying was done at a temperature of 60°C. All cores were constantly wrapped in aluminium foil while not in use. Ainsa cores which were saturated in crude oil before the cleaning process were still left submerged in a plastic container. All this careful processes were taken to preserve the integrity of the samples.

5.3.3 Porosity measurements

The porosity of the core sample was determined using the Helium Porosimeter method. The set-up is shown in Figure 5.7, all valves are manually operated. This type of porosimeter is suitable for grain volume determination. The Helium gas expansion porosimeter enables the determination of grain and pore volume via an isothermal helium expansion and the application of Boyle's law and Charles law. Subsequently, the porosity and grain density can be calculated. Helium is the preferred gas because of the advantages it has over other gases (Torsæter and Abtahi (2003):

1. It has small molecules, which are able to penetrate small pores rapidly.
2. It is inert and does not absorb on rock surfaces.
3. For pressure and temperature employed in the test, helium can be considered as an ideal gas.
4. It has high diffusivity, hence, it can be used for determining porosity of rocks with low permeability (Torsæter and Abtahi (2003)).

The grain volume is calculated by;

$$V_{grain} = V_1 - V_2 \quad (5.4)$$



Figure 5.7: Helium Porosimeter.

V_{grain} is the grain volume of core sample [cm^3], V_1 is the volume of matrix cup without a core sample [cm^3] and V_2 is the volume of matrix cup with a core sample [cm^3].

$$V_{pore} = V_{bulk} - V_{grain} \quad (5.5)$$

V_{pore} = pore volume of core sample [cm^3].

The effective porosity is calculated using then computed using Equation 5.6;

$$\phi_e = \frac{V_{pore}}{V_{bulk}} * 100 \quad (5.6)$$

ϕ_e is the effective porosity [%].

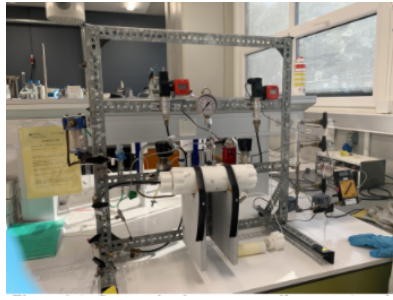
The liquid saturation method of determining porosity was also explored to check the validity of the helium porosity results. With a known weight of a core sample when dried and when saturated with a liquid and finally with the density of the liquid well known, the pore volume can then be determined using Equation 5.7;

$$V_{pore} = \frac{W_{wet} - W_{dry}}{\rho_w} \quad (5.7)$$

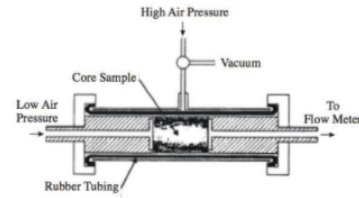
W_{wet} is the wet weight of core, W_{dry} is the dry weight of core and ρ_w is the density of saturating liquid.

5.3.4 Permeability measurements

Air permeability of the core sample was measured using a constant head permeameter as seen in Figure 5.8a. Liquid permeability of the core plugs were found using the Klinkenberg correlations.



(a) Constant Head Permeameter.



(b) Hassler core holder.

Figure 5.8: Permeability measurement set-up. Figure 5.8b is from Torsæter and Abtahi (2003).

The Manometers on both sides of the core measured upstream and downstream pressures, while the airflow was measured by the flow meter. Hassler core holder shown in Figure 5.8b was used with the permeameter. Hassler core holder type was preferred because of its below listed advantages Torsæter and Abtahi (2003):

1. excellent tightness.
2. can be used for measuring relative permeability.
3. can be used for samples of different sizes.

Up to six permeability tests were carried out at varying upstream and downstream pressures. The pressure difference was kept at a minimum of 0.2 bar. The air permeability was then calculated using Equation 5.8,

$$K_g = \frac{2QL\mu P_{atm}}{A(P_1^2 - P_2^2)} \quad (5.8)$$

K_g is the air permeability [D], μ is the air viscosity [cP], P_{atm} is the atmospheric pressure [atm], Q is the flowrate [ml/s], P_1 is the upstream pressure [bar] and P_2 is the downstream pressure [bar].

The Klinkenberg correction factor b , can be calculated by

$$b = \frac{m}{K_l} \quad (5.9)$$

K_l is the liquid permeability [mD], b is the correction factor and m is the slope of the graph.

5.3.5 Thin sections and scanning electron microscope

Two thin sections, E1 and E3 from core samples C1 and C3, respectively, were constructed for the experiment. Scanning electron microscope (SEM) was used for the chemical identification of the rock sample. The SEM test were set up by

setting a little piece of rock on the carbon glue circle mounted on the aluminum stub. A slim platinum layer was applied to prevent charging of the samples. Several points were picked based off from different colour representations. The colours differ by the densities of the elements contained in the sample. Dr. Haili assisted in the SEM analysis of the thin sections.

5.4 Core plug saturation

5.4.1 Formation water saturation

The core plugs were saturated using the vacuum pump in Formation water (FW). The set up is shown in Figure 5.9. The cores were first placed in a beaker, and then placed in the gas container before being completely sealed off.



Figure 5.9: A schematic of vacuum pump apparatus.

The weight of dry and subsequently saturated cores were measured. At a stabilised pressure of 0.1 bar reading on the pump, FW was let into the tank from the overhead storage till the cores were fully submerged in the FW. The vacuum pump was run for about 2 hours and afterwards the cores were removed and submerged in the same brine at room temperature till the drainage process was initiated within 5 days.

5.4.2 Contact angle measurements

A Goniometer Figure 5.10a, was used to carry out series of contact angle measurements to determine the wettability of the calcite plate by. A goniometer is an image system set-up to capture the profile of a liquid drop (in our case, crude oil) on a solid substance (in our case, the rock sample). The profile of one liquid on the solid can be observed in the presence of another liquid (in our case, brines of varying salinities). The angle formed between the oil-brine interface, through the calcite surface is the contact angle.

A high resolution camera was employed to accurately capture this drop and calculate the contact angle. The image is then processed on a computer using a specialised software, called the **attention theta**. The software outputs, the right and left angles of the drops, which was calculated using the Youngs lapace equation. The values displayed on the screen are measured through the oil phase. These values are then subtracted from 180, to determine the contact angles through the denser (more dense) phase, which is water.

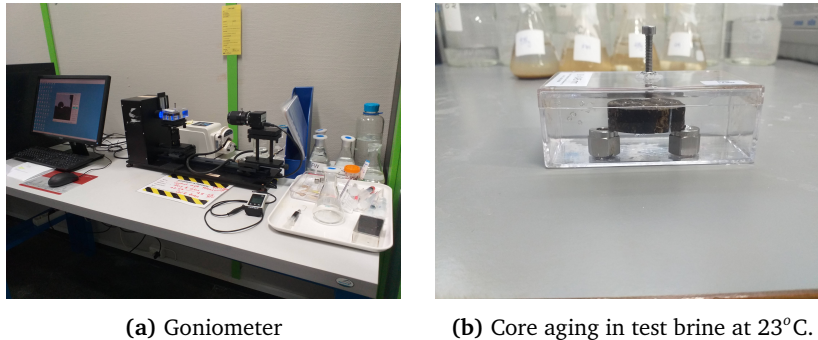


Figure 5.10: Contact angle measurement experimental set-up.

Two calcite plates (Chip 1 and Chip 2) were polished on a diamond plate. The surface of the polished samples is assumed to be non porous and this was confirmed from images where no porosity was seen. Therefore, the chips are expected to be completely sealed samples. The two polished plates were statically aged in crude oil for 20 days, at 96°C , to render them more oil-wet. Afterwards, the chips were aged in each test brine as shown in Figure 5.10b, at varying temperature and time.

Measurements were taking after 24 hours of aging in each test brine at room temperature. The images from the goniometer were taken after the calcite surface was introduced to crude oil droplet. The contact angle was then recorded few minutes after the introduction of the droplet, to make certain that the droplet was stabilised on the calcite surface. A minimum of three drops, from three measurements were taking for each brine. An average of these values were analysed before final conclusion was reached as results.

5.4.3 Zeta potential measurements

The role of electrostatic interactions in wettability alteration was analyzed by taking zeta potential measurements. The zeta potential measurements, Section 4.2.4, were performed with milled carbonate samples suspended in several brine solutions of interest, using the Malvern Zetasizer Nano machine shown in Figure 5.11a. The Zetasizer uses the laser doppler velocemetry technique (LDV) for nano particle analysis. Using LDV, the system measures the velocity of the particles (electrophoretic mobility), as they move through a fluid. The velocity of the particle is proportional to the rate of fluctuation which is being captured by the optics and

reference beam systems of the Zetasizer. These movements are thus, combined with the Smoluchowski's approximation from Henry's equation Section 3.3, to determine the zeta potential.

According to Equation 3.21 in Section 3.3, $f(K_a)$ is 1.5 which is known as the Smoluchowski approximation. This approximation is relevant in this measurement as its an aqueous solution. The folded capillary cell, Figure 5.11b was used to house the milled powder and brine, before being placed in the Zetasizer. The sample was milled, using the Vibratory Disc Mill RS 200, and particle size was arrived at, as 8 microns.

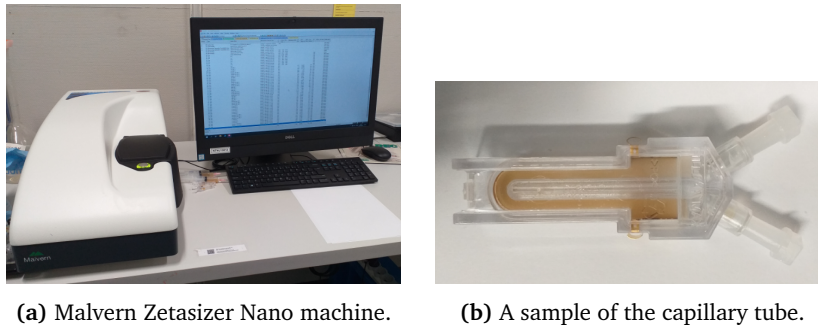


Figure 5.11: Zeta potential measurement experimental set-up.

Two sets of zeta potential measurements were carried out with all 6 brines used in this experiment. Pure carbonate sample was used in one set, while carbonate sample, aged in crude oil for 30 days at 96°C was used in another set. 0.5 gram of the pure carbonate sample is added to 95 ml of the particular brine of interest. This makes it a 1 wt % sample in brine solution. The solution is then stirred using a magnetic stirrer, as shown in Figure 5.12, for a minimum of 48 hours (not more than 55 hours), at room temperature.



Figure 5.12: One of the solutions being stirred on the magnetic stirrer.

The aim of stirring is to ensure the adequate suspension of the particles in the brine solution. After stirring, the pH value of each solution is measured using the pH meter. The most important parameter that affects the zeta potential is pH, therefore a quoted pH value is required for adequate analysis of results. About 1

ml of the solution is then put into the cell, which is then inserted into the Zetasizer machine, which then gives the zeta potential measurements. For each brine, 3 measurements were taken at zetasizer temperature of 23°C and 70°C, which is the highest temperature the machine was designed for. The zeta potential values were recorded along with an error bar based on the standard deviation of measurements made. Brine viscosity at each measurement temperature is captured in the zetasizer software, so the effect of temperature is observed.

The procedure enumerated below, was used to prepare the crude oil aged carbonate sample.

1. Prepare 50-50 % concentration of toluene and n-heptane each. This concentration is going to preserve the organic molecules contained in the crude oil from dissolving. Also, diluting with this concentration, would make the crude oil less viscous. Toluene alone would wash away the active ingredients but n-heptane would diminish this effect. However, a moderate concentration of both is ensured.
2. Add a 20 % solution of crude oil (with powder), for microscopic analysis.
3. Put a pint of the mixture on a microscope slide, to see if there is asphaltene precipitation or not, Figure 5.13. Asphaltene tend to show as flocculate particles under microscope.
4. If there is none, the original sample (aged powder) is then spitted into two parts. One for the zeta potential, while the other is used as a backup.
5. One of the splitted sample is then diluted with the 20 % of toluene and n-heptane sample, and filtered using a 0.45 mesh filter while using the same set up as Section 5.1.
6. After the first stage filtration, another concentration of toluene and n-heptane is added to make the separated particles cleaner. This was done twice.
7. The 0.45 filter, with filtered powder is carefully removed and put in a glass vial to dry. This drying is done by heating the filtered particle with nitrogen in a heating block.
8. After drying, the particles are mixed with different test brines, and allowed to stirr on the magnetic stirrer for 48 hours, after which pH measurements are done, then zeta potential measurements are followed.



Figure 5.13: Checking for asphaltene precipitation, using the microscope.

5.4.4 Oil saturation

The irreducible water saturation of the core plugs was determined by oil saturation using the Beckman centrifuge; precisely the Beckman Coulter Optima L-80 XP Ultracentrifuge model. The oil drainage process is achieved during the rotation of the core holders inside the centrifuge machine. The process was carried out at an RPM of 5000 for the Ainsa cores and 7000 RPM for the Angola core at room temperature and 10 hours. All inputs were made in an adjacent computer connected to the centrifuge machine which had a centas program installed in it. A total of 7 core plugs (4 Ainsa cores and 3 Angola cores) were used in three rounds of the centrifuging process.



(a) The Beckman Coulter Optima L-80 XP Ultracentrifuge



(b) Core holders housing 3 cores in the centrifuge machine.

Figure 5.14: Centrifuge apparatus.



Figure 5.15: Components set-up for the centrifuging process

Once 10 hours was elapsed, the operation was stopped and the centrifuge machine is opened to collect the core holders. The water displaced is collected in the calibrated polycarbonate receiving tube which is part of the core holding assembly. The water is then poured into a burette and the volume of water displaced is determined. Afterwards, the irreducible water saturation is then calculated using the

Equation 5.11 and the mass balance equation 5.12;

$$\text{Residualwatervolume} = V_{pore} - V_w \quad (5.10)$$

V_{pore} is the pore volume and (V_w) is the net produced water.

$$S_{wirr} = \frac{\text{Residualwatervolume}}{V_{pore}} \quad (5.11)$$

$$W_w - W_o = M_t - M_i \quad (5.12)$$

W_w is the weight of 100 % FW saturated core plug, W_o is the weight of an irreducible water saturated core, M_t is the total mass of produced FW, after the process and M_i is the total mass of the initial FW introduced into the core at the beginning of the process.

5.5 Core aging

This section describes the experimental procedures and overall set-ups of several aging procedures explored in this experiment. All aging procedures were carried out at an elevated temperature of 96°C.

5.5.1 Component set-ups

The experimental set-up was carried out at an elevated temperature in the heating cabinet in the laboratory. A suitable set-up fit for purpose was designed, assembled, and tested before commencement. The objective of the set-ups is to ensure an efficient core restoration through the aging processes. Also, the design was made such that unnecessary interruption of the aging processes is completely avoided.

In this experiment, the static and dynamic aging processes were explored. The static aging process entails the core plug being fully submerged into the crude oil, usually in a stainless steel aging cell. The dynamic aging process entails that there is a continuous crude oil flowing through the core plug, with or without the presence of a sleeve pressure. The options of both sleeve and non-sleeve pressure were explored in this experiment. Below are the different components assembled together to ensure a working set-up.

Pumps

The peristaltic pump was used for the dynamic aging without the presence of a sleeve pressure. The choice of this pump is its availability, easy to operate and its portability. Although, the least injection rate that could be provided by the pump was about 15cm³/hr, which is quite high. The pump was placed outside of the heating cabinet.

The vindum and Isco pumps were used for the dynamic aging with the presence of sleeve pressure. The choice of the vindum pump is motivated by the fact that it is pulse free and is able to pump continually. It has a pressure limit of about 29,000 psi, which makes it suitable for laboratory experiments. Furthermore, a desired pump rate as low as 1ml/hr can be reached compared to the peristaltic pump.

The Teledyne D-series pump (Isco pump) was also used for the dynamic aging with sleeve pressure. This pump ensures a continuous fluid delivery like the vindum pump. The controller refills one pump while the other is delivering fluid, using a special inbuilt algorithm. The Isco pump ensures accurate flow rate and pulse free delivery. However, its mode of operation is quite complex compared to the other two pumps used in the experiment.

Brine lines

A 'white' transparent line was used for crude oil flow. In both dynamic aging processes, the flow line connects the oil reservoir, the pump, the core holder, and the collection points (Effluent crude oil).

Core holders and oil reservoirs

Plastic and stainless steel materials were used as oil reservoirs and core holders. Most importantly, it was confirmed prior to the experiment that all selected materials are able to withstand the elevated temperatures. Furthermore, a larger volume of effluent crude oil collection was selected such as the frequent need to empty is prevented.

5.5.2 Experimental set-up

During the static aging process, the core plug is simply immersed in a crude oil containing stainless steel container and placed in the heating oven at an elevated temperature of 96°C. For the dynamic aging process without the sleeve pressure, Figure 5.16 the pump and the oil reservoir are placed outside of the heating cabinet. Fresh crude oil flows from the reservoir through the pump at an assigned flow rate and then into the core holder which is placed inside the heating cabinet. The injection rate is set at 15cm³/hr which is the lowest limit that can be reached by the peristaltic pump. The flow lines that connect the outlet of the pump to the core holder are made to be long enough to ensure that the crude oil is heated up to the required temperature before it enters the core holder where the plugs are placed.

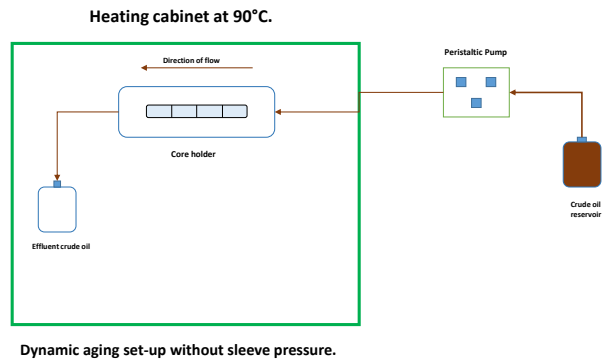


Figure 5.16: Schematic of dynamic aging set-up without sleeve pressure.

The introduction of sleeve pressure and back pressure in the subsequent aging process is to ensure the need of the crude oil to forcefully flow through the core plug into the core holder. The introduction of the back pressure is to ensure the removal of air pressure and also the reduction of gas size. Therefore, the setup with the introduction of these components becomes more complex. Figure 5.17 shows a schematic of the dynamic aging process in the presence of sleeve and back pressures. To prevent the pumps coming in direct contact with crude oil, Exsso D-60 is used to inject the crude oil into the core holders where the plugs are already placed. Hence, the crude reservoir used in this set-up has a piston in it.

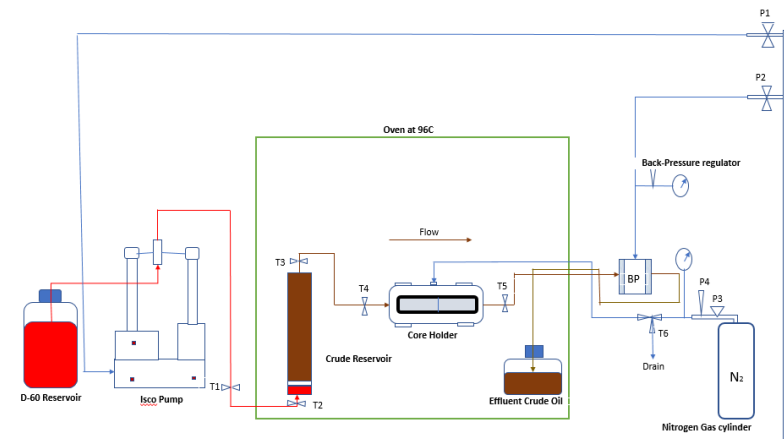


Figure 5.17: Schematic of dynamic aging set-up with sleeve pressure.

Outside of the heating cabinet, the D-60 reservoir is placed in a fumehood, and the Isco pump is used to pump the D-60 into the crude oil reservoir which is placed in the cabinet as shown in Figure 5.17. The sleeve and back pressures are regulated from outside of the heating cabinet, which are set 30 bars and 2 bars, respectively. The core was mounted in the core holder using the vacuum from the flowing water installed in the laboratory. Leakage tests were carried out before the beginning of the experiment. The choke on the gas bottle allows for a maximum of 60 bar pressure. The valve is mounted between the regulator and the sleeve, which allows for slow pressurization and accurate readings of pressure leaving the gas bottle to the core holders. Safety pressures were also set at the pumps, and any pressure exceeding the set pressures activates an alarm and shut down of the system if no intervention is done. To prevent plugging of the flowlines, the oil used were filtered at room temperature to enable the removal of possible wax particles.

5.6 Spontaneous Imbibition experiment.

This section describes the experimental procedure and set-up for the high temperature spontaneous imbibition (SI) test carried out in the laboratory. The test temperature is 96°C. Core plugs with similar petro physical properties are imbibed with the same brines to have arrived at comparative results and reasonable conclusions.

5.6.1 Experimental and component set-up.

The design of the set-up was finally arrived at after several phases of modification. From the conceptual design on paper, to risk analysis/assessment, to the eventual building of the rig. All phases have the same guiding design principles and the overall objective remains the same. The final set-up was developed, keeping in mind the objectives of the project while also considering availability of equipment, laboratory safety, and time (COVID-19 lockdowns).

A test run was carried out before the main experiment which involves the core samples used in this experiment. All glass-made components that forms part of the set-up are properly cleaned with ordinary and distilled water, soap, and acetone where necessary, before being dried at 60°C. Furthermore, all components with o-rings are replaced with new o-rings to maintain the integrity of the experiment. O-rings are fluid sealing components placed between two solid surfaces.

The set-up consists of two Amott cells with a metal clutch and a metal core stand, designed to withstand high temperatures and pressure of up to 2 bar. Other components used are vindum pump 5.5.1, conductivity and salinity measurement tool called hanna, flowlines 5.5.1, graduated cylinder, 3-way valves, pressure relief valve and brine reservoirs 5.5.1. Hanna is an handheld multi 340i meter from

geotech. All flowlines used in the experiment are properly measured to ensure not too short to cause tension on the equipment, and not too long to cause unnecessary untidiness or accident.



(a) (A) and (B) Upper and lower component of Amott Cell respectively, (C) Metallic core stand and (D) Metal Clutch.



(b) Handheld conductivity and salinity measuring tool - Hanna.

Figure 5.18: Some of the components used in the high temperature imbibition experiments.

The spontaneous imbibition (SI) set-up is shown in Figure 5.19. One of the guiding principle or the objective of this set-up is to minimize to the barest minimum, the number of times the heating oven is opened during the course of the experiment. This is to ensure an interruption free test. Therefore, the designed set-up is totally controlled externally, i.e., from outside of the heating cabinet. All brines for the experiment are pre-heated and stored in the reservoirs from the beginning of the experiment. To avoid brine evaporation, the brines were filled to the brim of the reservoirs. Consistent pressure and temperature is needed for an effective SI process.

Therefore, the graduated tube set-up outside of the oven, is not only used to collect oil recovered but also to remove air from the system to avoid pressure build-up. Drastic or fluctuating temperature from the heating cabinet was also avoided by setting the temperature at 96°C and manipulating the settings to ensure the temperature remains so throughout the course of the experiment. The overall idea of the set-up as illustrated in Figure 5.19, the vinding pump, placed between the Exsol-D60 reservoir and the heating cabinet is used to inject D-60 into the flowline, then into the brine reservoirs, which then helps to inject brines into the imbibition cells via the flowlines.

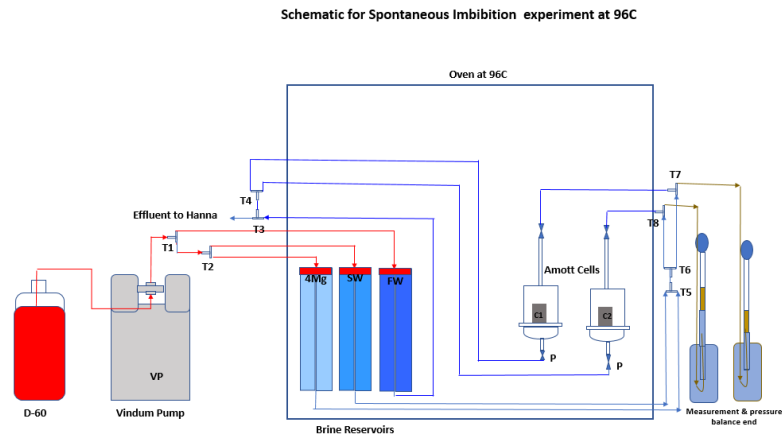


Figure 5.19: Schematic of spontaneous imbibition (SI) setup.

The flowlines and equipment are connected at room temperature. The core was then removed from the aging cells and rolled uniformly over a tissue paper to remove excess oil from the core surface. This process was uniformly carried out for all core samples. The core sample is then placed on the metallic core stand, already placed on the bottom component of the Amott cell which seat on the bottom component of the Amott cell. Afterwards, the upper component of the Amott cell is connected to the lower component using the metal clutch. All connections are then double checked for accuracy.

After the core has been mounted as described above, the experiment is then initiated as the first brine is injected at a rate of 5 ml/min and safety pressure of 400 psi, simultaneously the heating cabinet is turned on and temperature set at 96°C. The brine is injected to a level slightly above the neck of the Amott cell. Oil recovered were collected in the Amott cell or the graduated tube placed at ambient temperature outside of the oven. The graduated cylinder; aside from helping to collect the oil recovered, it also helps to eject air from the system and to avoid pressure build-up. Oil recovery readings are made every 24 hours, while also monitoring the liquid level in the Amott cells. After sometime, the graduated cylinder; though cleaned with acetone, becomes oil-wet thereby allowing the oil to spread over its surface leading to erroneous readings. Therefore, the preference is to take oil readings in the Amott cells via the window in the oven.

Three SI experiments were carried out. The first SI experiment involve using cores B1 and B8 from the Ainsa samples. Both cores have similar petrophysical properties and this forms the basis for selection, furthermore, both cores will be imbibed with FW and SW successively. Also, cores B1 and B8 have been aged dynamically and statically respectively. Therefore, SI results, will enable me make recommendations on the different aging methods. The second SI experiment will involve using

cores B2 and B3 from the Angola samples. These samples will be imbibed with FW, SW, SW-0.1NaCl and SW-0.1NaCl-2S-4Mg successively. The third SI experiment will involve using cores C1 and C2 from the Angola samples. These samples will be imbibed with FW, SW, SW-0.1NaCl-2S-4Mg and SW-0.1NaCl-2S-8Mg successively.

Replacement of high salinity brine with low salinity brines

The guiding principle behind brine replacement is utilizing the density difference and segregation by gravity potentials between the old brine (high salinity) and new brine (low salinity). With the old brine still in the Amott cell, the new brine is now injected from the top of the Amott cell at a rate of 5 ml/min through the flowlines connecting valves T5, T6 and T7 as illustrated in Figure 5.19. Valves T4 and T3 are then opened to effluent connecting reservoir placed outside of the oven.

While the injection and ejection of new brine is going on, the liquid level in the Amott cell is closely monitored. Oil recovered remains in the Amott cell and the new brine droplets move into the Amott cell. Density difference allows the new brine move past the oil at the top of the liquid level in the Amott cell. The liquid level is kept high enough, such that no disturbance is caused to the core gently placed in the cell. A level of segregation is expected between both brines; due to density differences, visible enough to be seen from outside of the heating cabinet.

The conductivity and salinity measurements of all brines were taken shortly before the beginning of the experiment. In addition, the volume of the Amott is estimated at about 350 ml. Therefore, the values were used to estimate when the new brines fully contained in the Amott cell. Periodic measurements of conductivity and salinity were taken with the hanna tool at the effluent end and this can be used to determine when the old brine has been fully ejected from the Amott cell, i.e., when the readings at the effluent end is similar to those of the old brine taken before the experiment. To double check, when the volume of liquid at the effluent end is greater than 350 ml, then we can be sure the new brine is contained in the Amott cell.

Replacement of brines with comparative salinity.

Figure 5.20, shows the schematic for the replacement of brines with comparative density as in the case of SW-0.1NaCl-2S-4Mg and SW-0.1NaCl-2S-8Mg. The procedure is similar to that described in Section 5.6.1. The difference is the new brine is now being injected from beneath the Amott cell at the rate of 5 ml/minute. Simultaneously, the old brine which is contained in the Amott cell, is being ejected and collected in an effluent containing beaker and the Hanna tool is used as described above to know when the new brine is totally contained in the Amott cell.

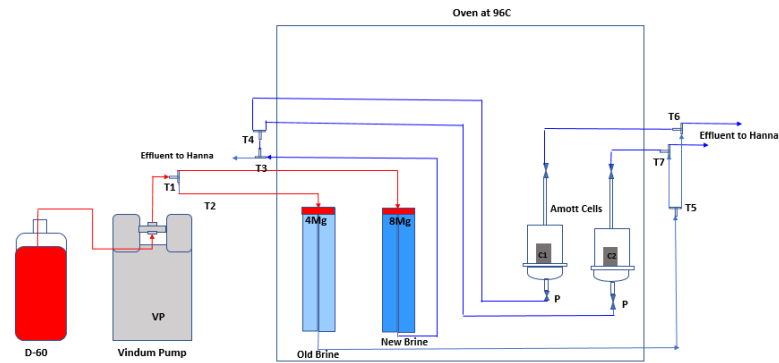


Figure 5.20: Schematic of spontaneous imbibition (SI) setup for the replacement of brines with comparative densities.

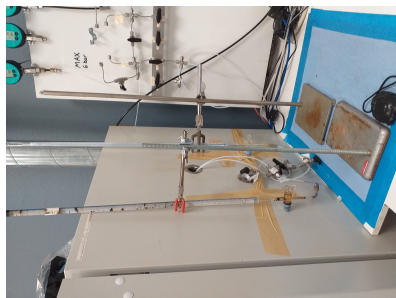


(a) The vindium pumps



(b) Inside of the SI oven.

Figure 5.21: Images of the imbibition rig.



(a) The external oil recovery section in the set-up.



(b) View of the spontaneous imbibition (SI) experiment.

Figure 5.22: External view of the imbibition rig.

Chapter 6

Results and discussion

The results obtained after applying the methods described in Section 5, are reported here. This section begins with fluid properties such as the acid and base numbers of the considered crude oil, viscosity, density, mineralogy results e.t.c. This is followed by core analysis results. In addition, the contact angle and zeta potential results are documented in this section. Finally, spontaneous imbibition (SI) results are described.

6.1 Fluid data

Table 6.1 lists the Heidrun oil parameters. The acid and base numbers, colour were provided in a document provided by Equinor. The oil density was calculated by following the procedure in Section 5.2.1.

Parameter	Value
Acid Number	3.3 mgKOH/g
Base Number	1.2 mgKOH/g
Oil Density	0.889 g/cc
Colour	Dark Brown

Table 6.1: Heidrun oil parameters.

Parameter	Value
IFT	11.1 mN/m
FW Density	1.12 g/cc
Salinity (ppm)	247,793

Table 6.2: Formation water (FW) parameters.

6.1.1 Density

Results of fluid density measurements taken at room temperature are displayed in Table 6.3. These density results are necessary for the brine replacement process in the SI experiments. For brines with significant differences in salinity, like FW and SW. The less saline brine, SW would be injected from the top of the Amott cell as no form of mixing is expected. However, for brines with comparative density, such as SW-0.1NaCl-2S-4Mg and SW-0.1NaCl-2S-8Mg. A bit of mixing is expected and this can be minimised by injecting the latter from the bottom of the Amott cell.

	FW	SW	SW-0.1NaCl-2S-4Mg	SW-0.1NaCl-2S-8Mg
Density (g/cc)	1.120	0.972	0.969	0.990

Table 6.3: Results from density measurements at room temperature.

6.1.2 Viscosity

The volume sufficient for the annulus containing the crude oil is about 20ml and 10ml for spindle 31 and spindle 18 respectively. As shown in the Table 6.4, the viscosity is reduced with increasing temperature. In addition, the trust region of this apparatus is when the torque is between 10 % to 30 %. Thus, all the results presented here, are obtained within this torque range. In addition, the 0.39 cp difference for measurements taken at 96°C is not expected to be a major cause of uncertainty in the SI experiments.

Temperature	RPM	Torque [%]	Viscosity [cp]
22.3°C	100	24.5	7.35
	120	29.3	7.32
Average			7.34
96°C	100	20.6	6.21
	120	23.3	5.82
Average			6.02

Table 6.4: Results from viscosity measurements.

6.2 Core data

6.2.1 Core cutting and core dimensions

A total of 11 cores were used in this experiment, but only 6 of them were used in the SI experiments. 5 Angola cores and 6 Ainsa cores. The Ainsa cores were already cut before the commencement of the project, hence only the Angola cores were cut solely for this project. All cutting procedures were followed as described in Section 5.3.1.

The 5 core plugs gotten from the Angola whole core are named C1, C2, C3, C4, and C5. C5 is an end-cap of C3, hence it is of a shorter length. All core plugs were cleaned, dried, and stored as described in Section 5.3.2. Core dimensions are listed in Table 6.5. The least pore volume was recorded for C5 which is 1.20 cm^3 . The bulk volume of cores C4 and C5 is significantly smaller which can be attributed to their reduced length.

Core ID	Diameter	Length	Bulk Volume	Matrix Volume
	D(cm)	L(cm)	Vb(cm ³)	Vm(cm ³)
Angola				
C1	3.73	4.52	49.52	41.5
C2	3.76	4.49	49.96	42.6
C3	3.77	4.59	51.26	45.3
C4	3.77	3.13	34.86	32.9
C5	3.76	2.61	29.1	27.9
Ainsa				
B1	3.8	4.62	52.33	41.45
B2	3.81	4.59	52.43	41.8
B3	3.82	4.61	52.68	41.9
B5	3.71	4.6	49.75	43.1
B6	3.8	4.42	50.15	40.9
B8	3.81	4.56	52.03	42

Table 6.5: Core dimensions.

Since one of the objectives of this thesis, is to carry out a SI experiment at elevated temperature, the pore volume of the cores are highly significant for quantifiable results. Cores C1 and C2 have the highest pore volume of the Angola cores, and is about 8.02 cm^3 and 7.36 cm^3 respectively. Core plugs B5 and B6 have the least pore volumes of the Ainsa samples. Therefore, cores C1, C2, B1, B2, B3 and B8 were the 6 plugs eventually used in the SI experiment. This selection was not made based on pore volume only but pore volume played an important role. It is worthy to note that plugs B5 and B6 were neither used in SI experiments in Azizov (2019).

6.2.2 Porosity

The porosity results obtained from the procedures described in Section 5.3.3, are listed in Tables 6.6 and 6.7. The results calculated for the Ainsa cores were similar to those gotten Azizov (2019), though small variations were noticed. Cores B5 and B6, showed exactly the same helium porosity results as in Azizov (2019). One reason could be that cores B5 and B6 were not eventually used for the SI experiments carried out in Azizov (2019).

However, for cores B1, B2, B3 and B8 which were used for the previous SI experiments; the newly obtained porosity results were a slightly smaller than the previous ones. The maximum difference is about 4.14 %. The liquid porosity obtained for core B1 is more than the helium porosity, the reason for this can be attributed to excess liquid on the surface of the core during measurement.

For the Angola cores, the highest porosity is recorded for core C1 with 16.19 %, with a pore volume of 8.02 cm³. Generally, these results validates the cleaning process carried out as described in Section 5.3.1.

Core ID Ainsa	PV cm ³	Old helium ϕ %	New helium ϕ %	$\Delta in \phi$ %	Liquid ϕ %
B1	10.88	20.80	19.93	4.14	19.96
B2	10.63	20.27	19.89	1.88	19.53
B3	10.78	20.46	19.70	3.37	19.64
B5	6.63	13.33	13.33	0.00	0.00
B6	9.25	18.44	18.44	0.00	0.00
B8	10.03	19.27	18.70	2.99	18.52

Table 6.6: Data for old and new helium and liquid porosity measurements for the Ainsa cores. The old values are those gotten in (Azizov, 2019), while the new values are results from this experiment. PV is pore volume.

Core ID	C1	C2	C3	C4	C5
PV (cm ³)	8.02	7.36	5.96	1.96	1.20
Helium ϕ (%)	16.19	14.72	11.63	5.62	4.11

Table 6.7: Data for pore volume (PV) and helium porosity measurements for the Angola cores.

6.2.3 Permeability

Air permeability were calculated according to Equation 5.8. These results were then plotted against the inverse of the mean pressures gotten in the measurements described in Section 5.3.4. The resulting graph was extrapolated to obtain liquid permeabilities. The obtained liquid permeabilities are reported in Table 6.8.

Core ID Ainsa	B1	B2	B3	B5	B6	B8
New $K_l(mD)$	35.54	30.24	42.66	89.58	19.16	48.35
Old $K_l(mD)$	41.00	52.00	62.00	86.00	30.00	53.00
Core ID Angola	C1	C2	C3	C4	C5	
$K_l(mD)$	15.38	1.73	1.00	0.30	14.24	

Table 6.8: Data of permeability measurements. The old values are those gotten by (Azizov, 2019) while the new values are results from this experiment.

There was a difference in the calculated permeability results for the Ainsa cores except core B5 which increased by 3.58 mD, compared to (Azizov, 2019). The Ainsa cores have considerably better pore volume and liquid permeability, Table 6.8, than the Angola cores. Hence, a quantifiable amount of production is expected during the SI experiments. Lastly, the similarities in the measurements of core plugs B1, B2 and B3 is indicative of the homogeneity of the core material.

Core ID Ainsa	B1	B2	B3	B5	B6	B8
Pore Volume (cm^3)	10.43	10.43	10.38	6.63	9.25	9.73
$K_l(mD)$	35.54	30.24	42.66	89.58	19.16	48.35
Core ID Angola	C1	C2	C3	C4	C5	
Pore Volume (cm^3)	8.02	7.36	5.96	1.96	1.20	
$K_l(mD)$	15.38	1.73	1.00	0.30	14.24	

Table 6.9: Pore volume and liquid permeability results for core materials.

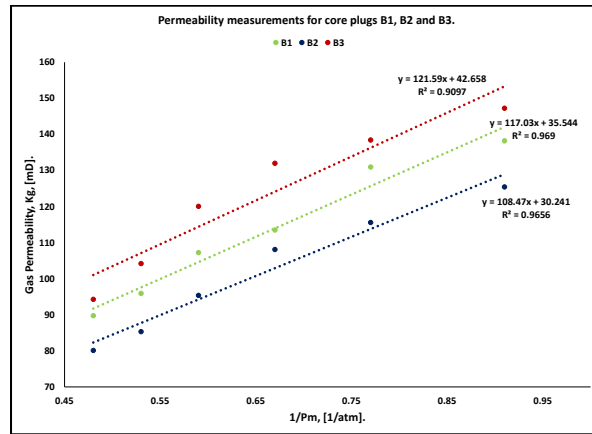


Figure 6.1: Gas permeability against inverse of mean pressure plot for core plugs B1, B2 and B3.

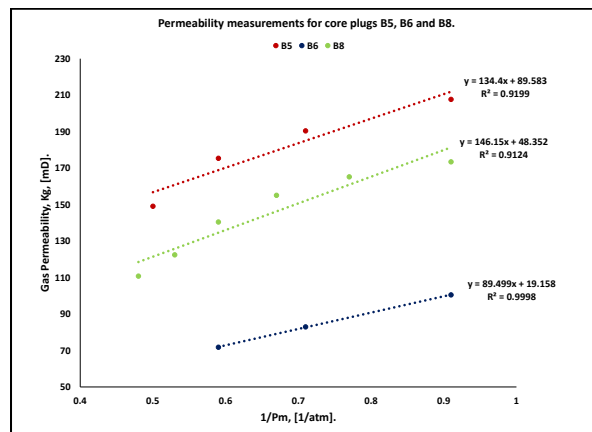


Figure 6.2: Gas permeability against inverse of mean pressure plot for core plugs B5, B6 and B8.

The permeability values gotten from the Angola cores are quite low. As shown in Table 6.8 and 6.9, the highest permeability value is 15.38 mD (Core B1) while the lowest was C4 with 0.30 mD. The Angola cores are classified as heterogeneous. The low pore volumes and liquid permeability results of cores C4 and C5 might lead to low production during the SI experiments.

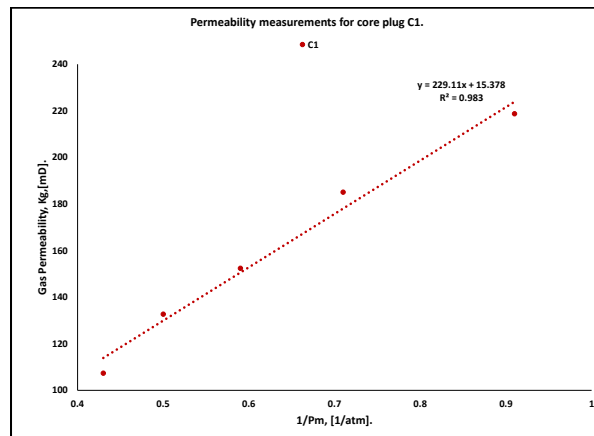


Figure 6.3: Gas permeability against inverse of mean pressure plot for core plug C1.

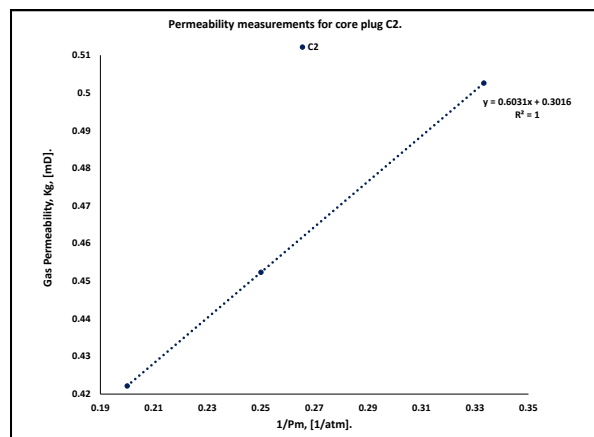


Figure 6.4: Gas permeability against inverse of mean pressure plot for core plug C2.

6.2.4 Core mineralogy

The outcrop cores' mineralogy have been analysed by thin sections and scanning electron microscope (SEM). The reason for using the SEM imaging is the elemental breakdown results that it delivers, which in turn would give ideas of mineral compositions in the cores. End caps of cores C1 and C3 were used to make thin sections E1 and E3 respectively, as shown in Figure 6.5a. The thin sections were used for the SEM analysis.

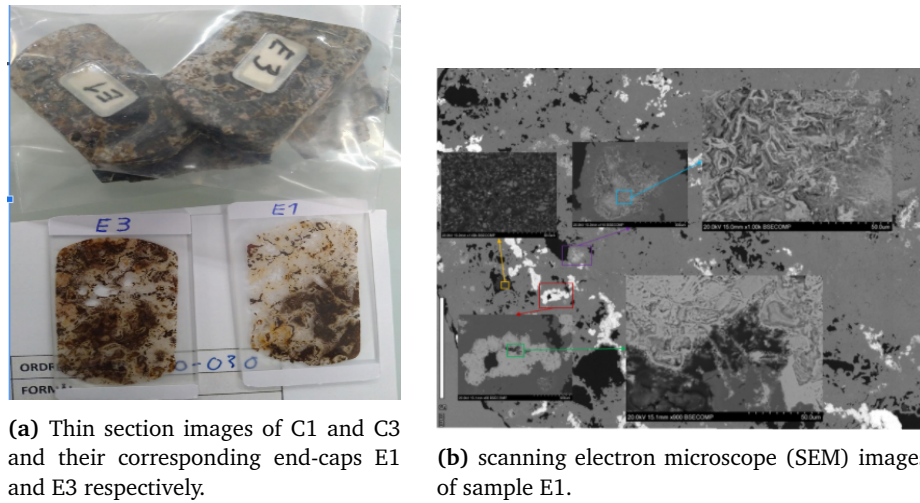


Figure 6.5: Core mineralogy.

The procedure for the SEM analysis was carried out as described in Section 5.3.5. Several areas were picked based on different grey level values. The grey levels correspond to the densities of the elements contained in the sample. Figure 6.5b shows a cut piece from one of the thin sections, the major points and the magnified areas (minor areas). 4 and 3 major areas were picked from sections E1 (E1.1, E1.2, E1.3 and E1.4) and E3 (E2.1, E2.2 and E3.3) respectively. Each areas were then magnified to pick several smaller areas. In total, about 51 smaller areas were analysed.

	Fe	O	C	Si	Ca	Mg	Ba	S
E1.1	47.87	23.23	6.19	1.00	8.26	2.51	0.00	0.00
E1.2	0.90	24.98	20.92	0.00	17.13	7.85	0.00	0.00
E1.3	10.79	26.82	30.47	0.81	8.32	3.84	0.00	0.00
E1.4	42.05	23.99	16.30	0.74	0.00	0.00	0.00	0.00
	25.40	24.75	18.47	0.85	11.24	4.73	0.00	0.00
	Fe	O	C	Si	Ca	Mg	Ba	S
E3.1	45.74	18.19	10.15	2.12	9.99	3.57	0.00	0.00
E3.2	35.54	19.54	5.78	6.06	9.67	0.68	41.33	8.29
E3.3	47.31	26.67	10.70	1.06	22.10	3.05	0.00	0.00
	42.86	21.47	8.88	3.08	13.92	2.43	41.33	4.15

Table 6.10: Elements by weight percentage from SEM analysis.

The energy dispersive spectrometry (EDS) analysis are given in Table 6.10. The magnesium concentration shows the possible presence of dolomite and the small content of Si and Al, which results in low clay content in the core materials. In ad-

dition, the table lists the average weight % of the most occurring elements in the minor areas selected. The amount of magnesium present is not enough to classify the core as dolomite. Figure 6.6a shows the random areas picked in section E1.1 and the elemental results got from the SEM analysis. Figure 6.6b shows the SEM analysis for section E1.1.

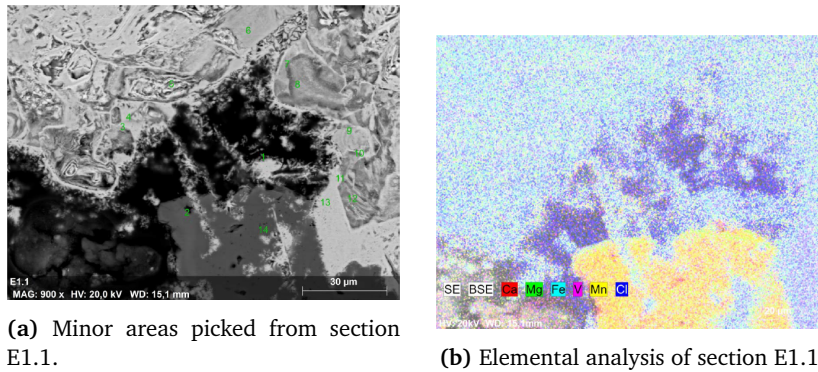


Figure 6.6: SEM analysis of section E1.1.

The possibilities of barium precipitation is also anticipated because of its concentration in section E3.2. The mineralogy analysis of the Ainsa cores were carried out by Azizov (2019). Four thin sections were analysed by the microscope, and there were suggestions of potential anhydrite grains. However, SEM analysis showed no anhydrite on the limestone cores.

6.2.5 Saturation of core plug

Core plugs were first saturated with FW according to the procedures stated in Section 5.4.1. This was followed by saturating the samples using Heidrun oil. This saturation was carried out according to Section 5.4.4. The oil drainage process is achieved by the rotating of the core holders inside the centrifuge machine. While preparing the core holders, a high level of meticulousness ensured a good centrifuging process. Following laboratory procedures, all core holders should have a weight difference of $\pm 0.08\text{g}$. However, ± 0.05 was achieved during this experiment. Furthermore, no spills were seen on the walls of the centrifuge machine after the first set of centrifuging.

The water produced after the experiment was collected in a burettes in order to carry out S_{wirr} calculations, as described in Section 5.11. The S_{wirr} results are presented in Table 6.11. All the calculated S_{wirr} values are lower than those previously gotten in Azizov (2019). The old S_{wirr} values for cores B1, B2 and B3 are 34 %, 40 % and 46 % respectively. No observable problems were seen during the centrifuging process of the Ainsa cores. Furthermore, the mass was also conserved as seen from the mass balance calculations. The Angola cores were not as untroubled. The Angola cores (C1, C2 and C3) were centrifuged according to the

CORE 1D	B1	B2	B3	B8	C1	C2
Pore volume [cm^3]	10.43	10.43	10.38	9.73	8.02	7.36
OOIC [cm^3]	8.85	9.23	9.10	8.72	5.61	4.41
SWIRR [%]	15.23	9.88	12.02	9.45	23.70	40.10

Table 6.11: A table showing the SWIRR calculation results.

process detailed in Section 5.4.4.

The operations of core plug C2 was as smooth as for the Ainsa cores. For cores C1 and C3, the produced FW were far less than the initial volume (8g), introduced at the beginning of the process. A further probe of the equipment was done, and not only were salt deposits found in the centrifuging machine, Figure 6.8b, the cups also had cracks which would have led to leakages, Figure 6.8b, which resulted in fluid loss. C3 produced the least FW as seen in Figure 6.7, hence more leakages are expected to have occurred therein, compared to core plug C1.

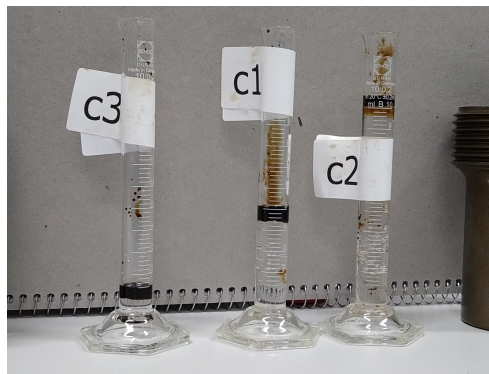


Figure 6.7: Produced FW, after the centrifuging process.

The Beckman Coulter Optima L-80 XP Ultracentrifuge was designed to withstand rotations per minute (RPM) of up to 12,000. The maximum RPM reached in this experiment is 7,000, which is within the designed limit. The decision to use 7,000 RPM for the Angola cores was because of their tight properties, therefore more centrifugal force is needed for an effective saturation to occur. The cracks on the core holders might have resulted from the combination of the tight nature of the core and the centrifugal force as a result of the high RPM.

Another possible explanation is the care of the centrifuging plastic cups. Per the manufacturers' manual, iso-propane should be used to clean the cup after use. However, toluene have been used in the laboratory, in the absence of iso-propane. Also, when toluene is used to clean the cups, a bit of melting is noticed and when further dried at 60°C, the transparency of the cups keeps eroding. This practice might have made the cup weaker overtime. The weakness of the cup, tight nature



(a) Patches of salts seen from one of the cups.

(b) Salt and oil droplets seen in the centrifuge machine.

Figure 6.8: Problems encountered during the oil saturation of Angola cores.

of the core and high RPM could possibly explain the reason for the cracks which led to the leakages.

6.2.6 Contact angle

Two phases, with four rounds of contact angle measurements were taken with the Goniometer as described in Section 5.4.2. In phase 1, we considered the effect of selective dilution of NaCl in seawater (SW) on contact angles. The measurement sequence and conditions are listed in Tables 6.12 for phase 1 and in Table 6.13 for phase 2.

Phase 1: Impact of selective dilution of NaCl in seawater.

Chip	Crude oil aging / T ($^{\circ}$ C)	Brine aging / T ($^{\circ}$ C)	Sequence of brines used
1	20 days /96	3 days /96	SW SW-0.1NaCl

Table 6.12: Contact angle measurement sequence and aging conditions for phase 1.

The impact of selective dilution of NaCl in SW, was scrutinized in this phase of the measurements. Chip 1 was first statically aged in crude oil for 20 days, at 96° C. Then, the chip was aged in each test brine at 96° C for 3 days. Contact angle measurements at 3 different sites on the chip were made at room temperature in the first brine SW, and another measurement is made in the second brine SW-0.1NaCl, after 3 days of aging. Average values of left and right angles, from the measurements were used to illustrate the results as shown in Figure 6.9. In all cases, a reduction in contact angle was recorded, which indicates that SW-0.1NaCl is able to alter the wettability of the calcite surface towards more water wetness.

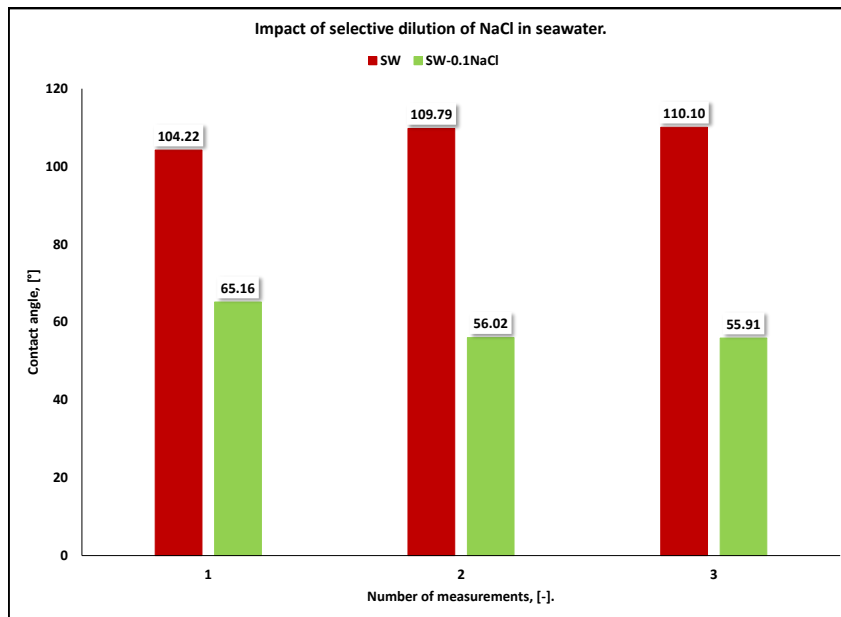


Figure 6.9: Contact angle (CA) measurements after calcite surface contact with SW and then, SW-0.1NaCl brine.

A total angle reduction of about 39.06, 53.77 and 54.19 were recorded in measurements 1, 2 and 3 respectively. SW-0.1NaCl showed a change in contact angle from an average value of 108.03 recorded for SW to 59.03. This shows an alteration in the wettability from completely oil-wet towards water-wet according to the criteria in (Santos et al., 2006), thereby rendering the calcite surface towards more water-wet.

Similar experiments were conducted in (Rashid et al., 2015; Yousef, Al-Saleh, Al-Jawfi et al., 2012), however, in their experiments changes in NaCl^+ was unable to alter the rock wettability. On the other hand, Honarvar et al. (2020) obtained results similar to ours. In Honarvar et al. (2020) the concentration of NaCl^+ in the initial brine was increased. The angle change from 70.4 to 129.8, after the brine salinity reached about 120,000ppm. Therefore, the presence of NaCl^+ rendered the rock surface towards oil-wet. According to the experiment in (Anderson, William G et al. 1986), 4 sites were observed to be water wet in NaCl^+ -diluted SW whereas all sites in SW remained relatively oil wet. This shows that selective dilution of NaCl^+ in SW improves the activity of PDIs in improving the wettability state.

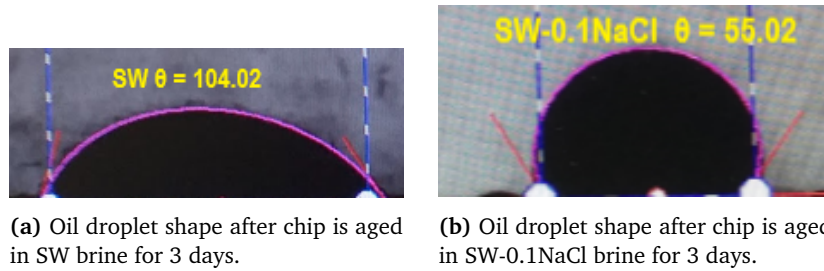


Figure 6.10: Contact angle (CA) measurements to determine the impact of selective dilution NaCl in seawater (SW).

Phase 2: Impact of brines with varying magnesium concentrations on contact angle measurements

Chip	Crude oil aging / T ($^{\circ}$ C)	Brine aging / T ($^{\circ}$ C)	Sequence of brines used
2	20 days / 96	24 hours / 96	FW SW SW-0.1NaCl-2S-4Mg SW-0.1NaCl-2S-8Mg
1	15 days / 96	24 hours / 23	FW SW SW-0.1NaCl-2S-4Mg SW-0.1NaCl-2S-8Mg
2	15 days / 96	24 hours / 96	FW SW-0.1NaCl-2S-8Mg

Table 6.13: Contact Angle: Measurement sequence and conditions for phase 2.

The objective of the first test in this phase, is to determine the effect of varying magnesium concentrations and its combined effect with sulphate in an NaCl diluted SW. In addition, the first two sets in this phase investigates the effect of temperature on the brine aging of the polished chips. Having investigated the effect of NaCl in SW as discussed in phase 1, it is quite imperative to study the effect of this potential determining ion (PDI) at varying temperature. A polished chip (Chip 2) was first statically aged in crude oil for 20 days, at 96° C. Afterwards, the chip was aged in each test brine at 96° C for 24 hours. Contact angle measurements at 3 different sites were made at room temperature in the same brine. The results are illustrated in Figure 6.11, where, the average left and right contact angles were plotted against the brine types.

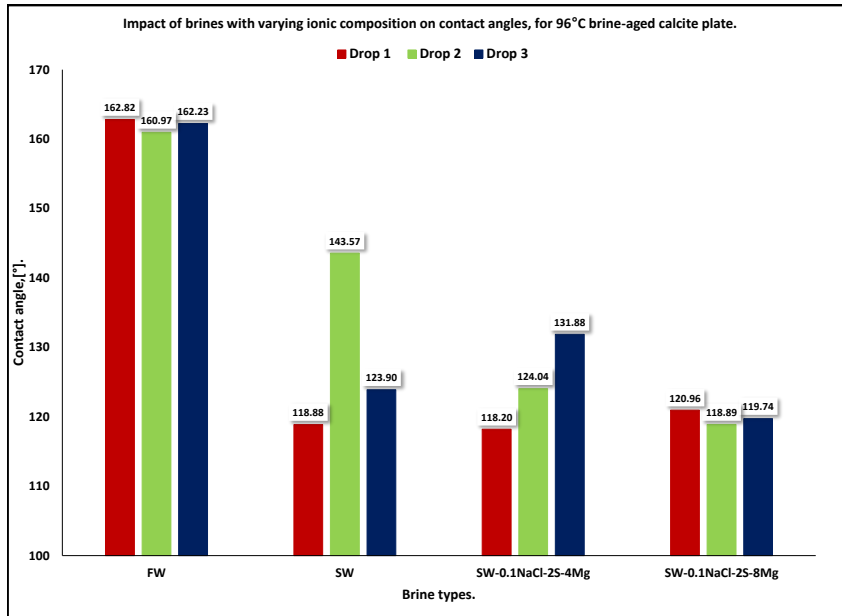


Figure 6.11: Contact angle measurements after calcite surface were aged in varying salinity and ionic brine concentrations at 96°C.

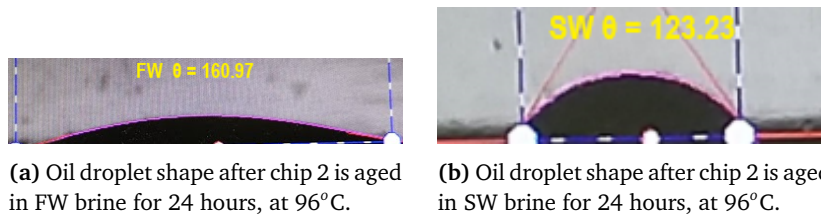


Figure 6.12: Contact angle measurements with chip 2, brine (FW and then aged at 96°C.

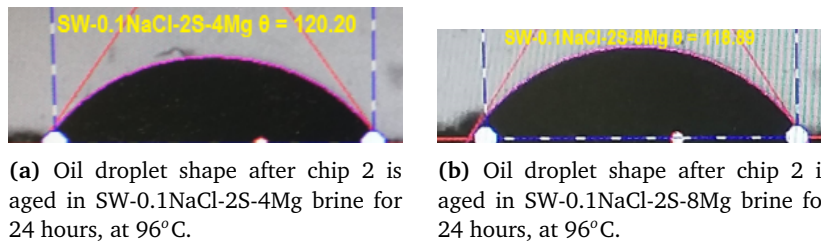


Figure 6.13: Contact angle measurements with chip 2, have contact with FW, SW, SW-0.1NaCl-2S-4Mg and then SW-0.1NaCl-2S-8Mg aged at 96°C.

A general trend of improving water wetness was observed by reduced contact angle values after sequential contacts with varying brines with lower salinity. Average angles changed from 162.0 to 128.5 to 127.3 to 118.11 after the calcite surface sequentially contacted FW, SW, SW-0.1NaCl-2S-4Mg and SW-0.1NaCl-2S-8Mg for 24 hours. After SW, small changes in contact angles were observed. These results further confirms, the effectiveness of PDIs, on the surface of calcite material. These results suggests that magnesium and sulphate could be PDIs to a carbonate surface. And their combined effect is able to render the carbonate surface less oil-wet.

To determine if the wettability alteration process was reversible or not, the same chip was aged in a FW brine for 24 hours after it was immersed in SW-0.1NaCl-2S-8Mg, and contact angle measurements taken. It was noticed that the surface remained less oil-wet, with similar contact angles as observed after the SW-0.1NaCl-2S-8Mg measurements. We therefore concluded that the wettability alteration process is irreversible. For the wettability alteration process to be reversible, oil presence is needed. But in this case the chip has been in contact with SW-0.1NaCl-2S-8Mg, and lower active components are expected to be present on the rock surface. Therefore, to view a more oil wet surface, the chip should be exposed to oil.

As a further test under phase 2, similar experiment was conducted but this time the calcite surface was aged in each test brine at room temperature. The results are displayed in Figure 6.14. This time, chip 1 was cleaned with toluene until

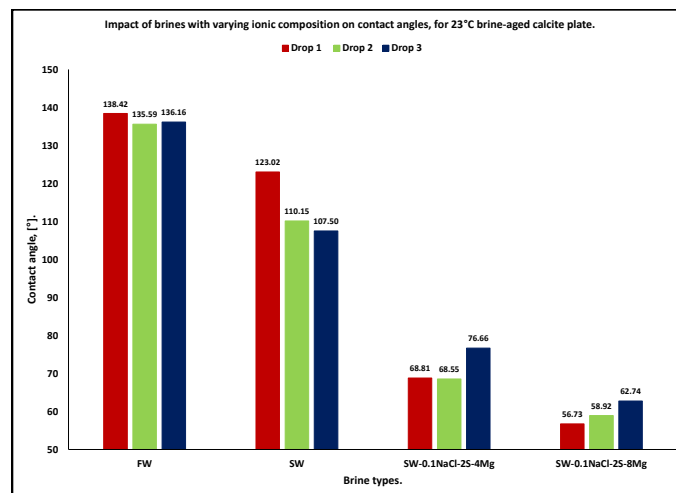


Figure 6.14: Contact angle measurements after calcite surface were aged in varying salinity and ionic brine concentrations at 23°C.

a clear effluent was observed. It was then further cleaned with methanol. Both cleaning process was done for about 3 days. The chip was then dried at 60°C until a constant weight was observed before being aged in crude oil at 96°C for 15 days. The chip was then aged in each test brine at room temperature, and measurements were taken every 24 hours. The general trend gotten were similar to those of similar experiment, discussed above. The calcite surface became less oil-wet with decreasing brine salinity. Average contact angles changed from 136.2 to 39.4 between FW and SW-0.1NaCl-2S-8Mg. However, this time, significant changes to less oil-wetness was seen after contact with SW. An angle reduction of about 42.2 was recorded between the calcite plates' contact with SW and then SW-0.1NaCl-2S-4Mg. In addition, it was confirmed that this wettability alteration is irreversible, as observed in the previous measurement, where the calcite plate was brine aged at 96°C.

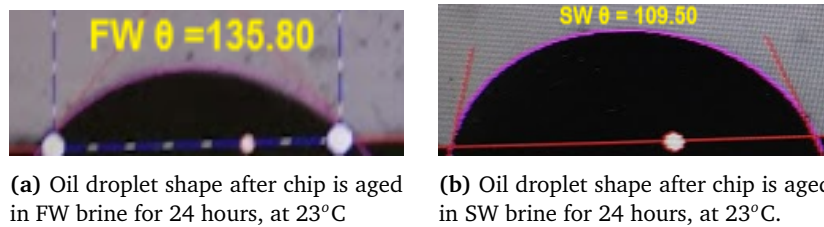


Figure 6.15: Contact angle measurements with chip, brine (FW and then aged at 23°C).

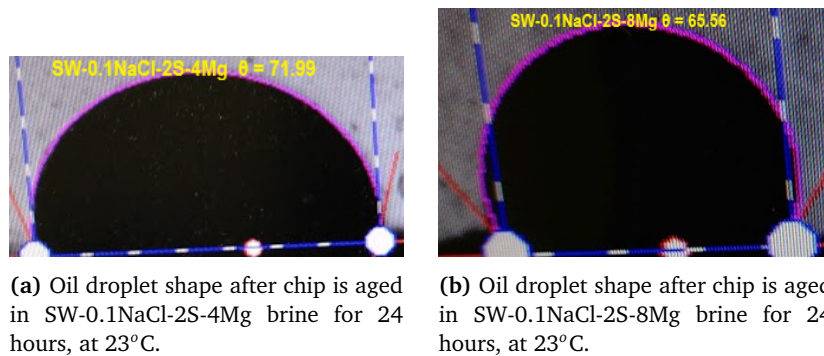


Figure 6.16: Contact angle measurements with chip 2, have contact with FW, SW, SW-0.1NaCl-2S-4Mg and then SW-0.1NaCl-2S-8Mg aged at 23°C.

One more contact angle measurement was taken with chip 2, to quantify the effect of SW-0.1NaCl-2S-8Mg on the chip, after direct contact with FW. The chip was cleaned with methanol and toluene as described previously for chip 1. As depicted in Figure 6.17, SW-0.1NaCl-2S-8Mg was able to reduce the contact angle by up to 57.62 degrees. Tending the calcite surface towards immediate water wetness.

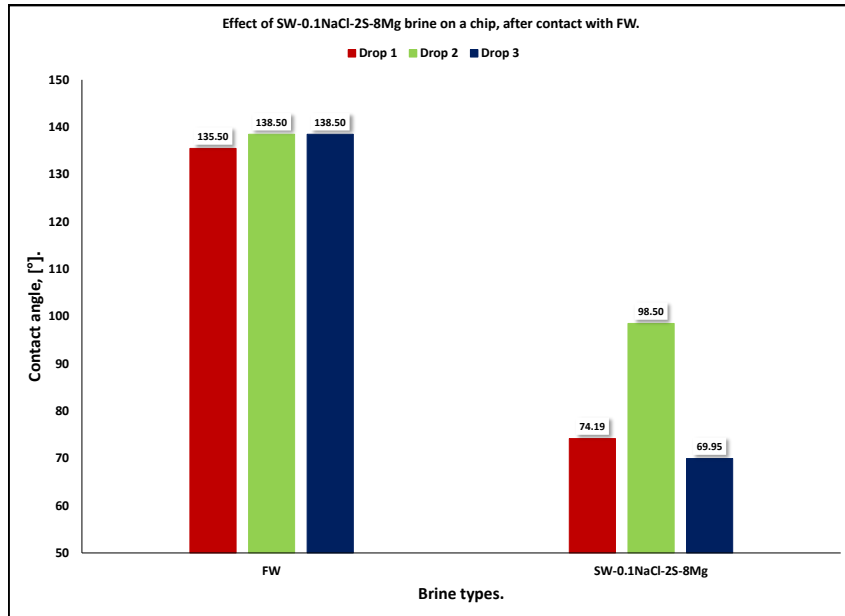


Figure 6.17: Contact angle measurements, after 3 drops on a calcite surface, exposed to SW-0.1NaCl-2S-8Mg, after contact with FW. Brine aging was done at 96°C.

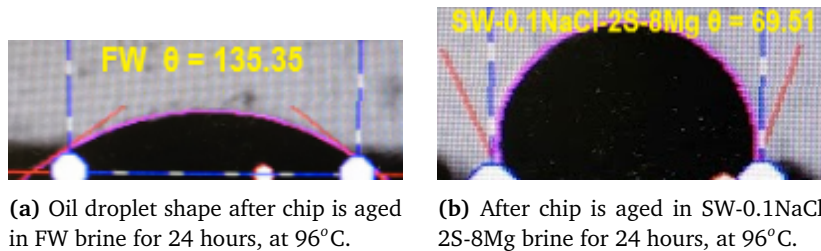


Figure 6.18: Contact angle measurements with chip, brine (FW and then SW-0.1NaCl-2S-8Mg) aged at 96°C.

Results observed in this experiment are in agreement to those in Rashid et al. (2015), where a $Mg^{2+} + SO_4^{2-}$ brine changed the contact angle towards water-wet values. As reported in Karimi et al. (2016), the addition of 5 times magnesium to SW reduced by 28 degree of contact angle, and a combined effect of Mg^{2+} and SO_4^{2-} , further reduced by 14 degrees of contact angle. This confirms that magnesium alter the surface of carbonate rock towards more water wet, especially in the presence of SO_4^{2-} . The presence of SO_4^{2-} increases the concentration of magnesium close to the carbonate surface by reducing the electrostatic repulsive

forces, thereby allowing magnesium release the carboxylic materials from the carbonate surface Rashid et al. (2015). Thus, SO_4^{2-} acts as a catalyst for the process of wettability alteration.

6.2.7 Zeta potential

A change in the surface charge of a rock will lead to an expansion of the double layer, which can result in wettability alteration of the rock Tetteh, Janjang, Barati et al. (2018) and Mahani et al. (2015). The surface charge between the rock/brine and oil/brine are affected by brine pH, temperature, salinity and composition Mahani et al. (2015). Disjoining pressure is necessary for wettability alteration to occur. The electrostatic force is the most important contributor to the disjoining pressure necessary for wettability alteration Tetteh, Janjang, Barati et al. (2018). Other forces include Van der Waals (VDW) and structural forces Gopani et al. (2021).

The expansion of the double layer is caused by the electrostatic repulsion between the rock/brine and oil/brine interfaces, which will lead to development of stable water film between these interfaces and therefore result to water wet conditions, i.e., an adequate electrostatic repulsion between these interfaces, which stabilizes the water film and contributes to water wet conditions.

The rock/brine measurements were taken within the pH range of 7.75 - 8.40 for all the brines except FW, whose pH stands at 6.74. As reported by Mahani et al. (2015), below the pH of 5, ζ potential measurements were impossible due to the dissolution of carbonates. Therefore we have tried to keep the pH values above this range. However, according to Strand, Høgnesen and Tor Austad (2006), at pH values within 7.5 - 8.0, carbonate dissolution occurs in under-saturated low salinity brines. Since the pH range for the low salinity brines are within an acceptable range, comparison analysis can thus be done.

For measurements with pure limestone powder, the ζ potential for FW and SW are recorded as 5.66 mV and 6.53 mV respectively at 25°C. While, the ζ potential for FW and SW are recorded as 7.38 mV and 5.24 mV respectively at 70°C. The difference in pH values of both brines might have contributed to more positive values recorded for SW at the lesser temperature. According to Mahani et al. (2015), at higher temperatures ζ potential moves towards the origin, i.e, from more negative values to less negative, and from more positive to less positive values. Though this trend was not observed for FW but for SW. The presence of sulphate in the SW, which adsorbs more on the rock surface at high temperature, could also explain the potential difference of 1.29 mV between the two test temperatures.

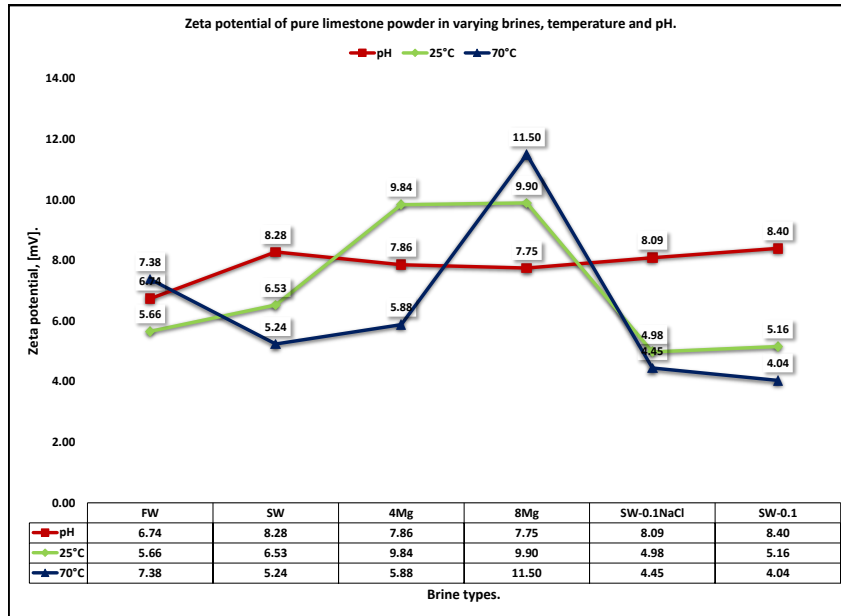


Figure 6.19: ζ potential results of pure limestone powder in varying brines, temperature and pH. 4Mg represents SW-0.1NaCl-2S-4Mg and 8Mg represents SW-0.1NaCl-2S-8Mg.

Usually, less positive values should be observed for SW compared to FW because of more sulphate concentration in SW is expected to contribute to lower ζ potential values. However, the higher pH of which the SW measurement was carried out at the lesser temperature might have contributed to higher values recorded. The absence of sulfate would give room for other positively charged divalent ions to react with the rock surface, thereby making it more positive. Sulphate renders the rock surface less positive, i.e, induces more negative potential. This trend was observed in Gopani et al. (2021), and it can be attributed to the affinity of sulphate for $CaSO_4$ precipitates. Furthermore, Gopani et al. (2021) noted that the decrease in ζ values with increasing sulphate concentration is not indefinite.

Similar ζ potential value for FW, within the same pH range was recorded in Mahani et al. (2015). The effect of pH on ζ potential is dependent on salinity. Smaller gradient in ζ potential values are expected with increased pH, with an increasing salinity. This is because the interaction between H^+ and OH^- (pH), and the PDI on the rock surface would affect the structure of the EDL, which would in turn affect the ζ potential measurements Mahani et al. (2015).

At both temperatures there was a spike in ζ potential values for brines with additional magnesium concentration. 6.53 mV, 9.84 mV and 9.90 mV were recorded for SW, SW-0.1NaCl-2S-4Mg and SW-0.1NaCl-2S-8Mg respectively at 25°C, while 5.24 mV, 5.88 mV and 11.5 mV were recorded at 70°C. An increase in magnesium concentration would make the ζ potential value more positive Gopani et al. (2021).

According to Mahani et al. (2015), selective increments of specific ions in smart water composition, have the ability to alter the surface chemistry between the rock and brines, and this will therefore alter the wettability towards water-wet conditions. Kasha et al. (2015) noted water-wet conditions in brines with additional concentrations of sulphate and magnesium. With an increasing magnesium concentration. The electrostatic force between the oil/brine and rock/brine interface reaches a minimum and this facilitates the desorption of oil molecules from the oil surface.

Least positive ζ potential values were recorded with brines SW-0.1NaCl and SW-0.1 at both test temperatures as shown in Figure 6.19. 4.98 mV and 5.16 mV were recorded for SW-0.1NaCl and SW-0.1 respectively at 25°C, while 4.45 mV and 4.04 mV were recorded at 70°C. Low salinity, drives the ζ potential value to less positive values which is indicative of a strong double layer Gopani et al. (2021). With increasing dilution with respect to SW, ions around the rock became less dense. Hence, the repulsive force between the oil/rock/brine interface increases and helps to detach oil molecules faster.

The measurements with crude oil aged powder were taken within the pH range of 7.74 - 8.30 for all the brines except from FW, whose pH stands at 7.14. According to Strand, Høgnesen and Tor Austad (2006), within the pH range of 6.5 – 7.5. The rock surface possesses a positive net charge, which then sticks with the polar components in the crude oil which are negatively charged. The negatively charged carboxylic materials present in the crude oil drives the ζ potential values to even less positive and more negative potentials as observed in Tetteh, Janjang, Barati et al. (2018) and Karimi et al. (2016). The presence of these carboxylic materials would allow for the oil molecules to attach to the rock surface. A negatively charged surface, is a good ground for desorption for these oil molecule due to higher repulsive forces between oil/brine and rock/brine interfaces. A more negative ζ potential values is indicative of a more negative surface charge Gopani et al. (2021), which supports a strong double layer that drives the system towards water wet conditions Honarvar et al. (2020).

At both test temperatures, negative zeta potential values were recorded for brine, SW-0.1NaCl and SW-0.1. This could also suggest the effectiveness of brine dilution compared to introduction of potential determining ion (PDI)s. The negative charge on the rock surface, due to the existence of (-COOH-), drives the desorp-

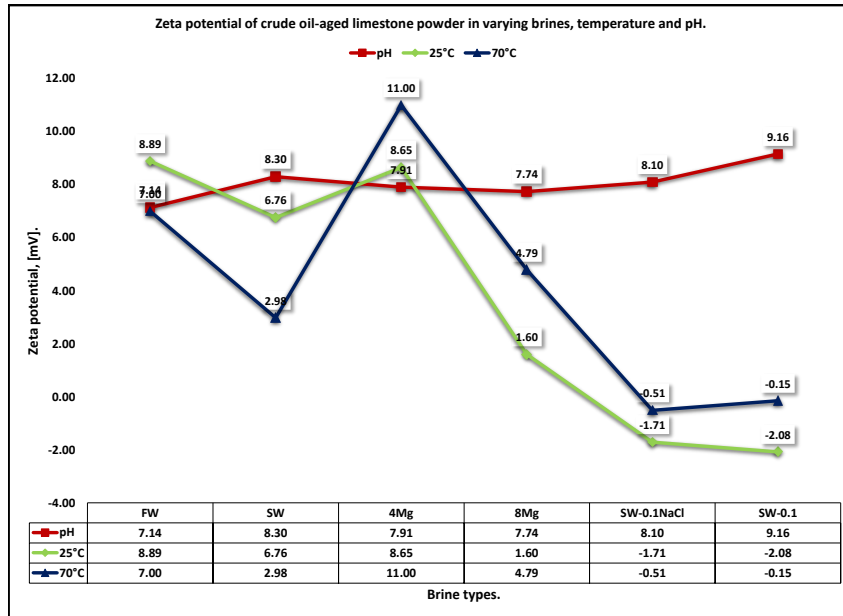


Figure 6.20: ζ potential results of crude-oil aged limestone powder in varying brines, temperature and pH. 4Mg represents SW-0.1NaCl-2S-4Mg and 8Mg represents SW-0.1NaCl-2S-8Mg.

tion of oil molecules from the rock surface, thereby tending the surface towards water-wet conditions Gopani et al. (2021). The trends for brines with additional magnesium concentration were dissimilar for measurements with pure and crude oil aged powder.

At both temperatures, ζ potential values reduced for SW but increased for SW-0.1NaCl-2S-4Mg and SW-0.1NaCl-2S-8Mg. This is as expected as magnesium is more reactive at higher temperature. Although this was not the trend for the pure limestone measurement, therefore the presence or absence of crude oil maybe the factor for this variation in results. According to Gopani et al. (2021), as more cations are adsorbed on a negatively charged rock surface, the electrostatic force between the oil/brine and rock/brine interfaces reaches a minimum and this results into desorption of oil molecules, due less positive ζ potential values. Furthermore, as reported in Mahani et al. (2015), the interaction between the divalent cations and the polar components in the crude oil, is more pronounced at higher temperatures.

The zeta potential results at 25°C may not overly represent the situation at 96°C, which is the temperature of the spontaneous imbibition experiments. However, this gives a general idea of the effect of ions on surface charge. According to Mahani et al. (2015), relative zeta potential values are not expected to change at varying temperature, though, the magnitude might vary.

6.3 Core aging

Ainsa core B8 was randomly picked to be aged statically at 96°C for 90 days. Ainsa cores B1, B2, and B3 were aged dynamically without sleeve pressure with an injection rate of 15ml/hr with a peristaltic pump, for a total of 90 days. Angola cores C1 and C2 were aged dynamically with sleeve pressure at an injection rate of up to 2ml/hr for 20 days.

In the first 12 days of aging dynamically with sleeve pressure of 30 bars, back pressure of 2 bars, and injection rates of 1ml/hr, there was throughput and no forms of leakages were experienced in the set-up. However, after the 12th day, no observable throughput was noticed and leakages were visible in the set-up. The Angola samples are known to be very tight. Readings from the Isco pump showed increasing pressure in the system. Therefore, a point was reached when the injection pressure was higher than the system could hold, and resulted in leakage.

The injection rate was then halved to 1ml/hr, throughput resumed but the pressure in the system remained high, and leakage resumed after about four days. A separate set-up was then created for each core, with each core having its own core holder, pumps and sleeve pressure. The individual aging set-up worked for an additional six days before leakages resumed again. In total, the dynamic aging with sleeve pressure was successful for about 20 days. We decommissioned the set-up after the 6 days of aging. Based on the work in Fernø et al. (2010), which concluded that dynamically aging for up to 8 days is sufficient to improve the core restoration.

6.4 Spontaneous imbibition

The spontaneous imbibition experimental process worked as described in Section 5.6. A lot was learnt during the pre-tests, and this prepared us for the 3 SI experiments. All brines used in the experiment were preheated at the experimental temperature to avoid gas in the system. However, the Exsol D-60 injected into the pistons was mixed with the magnetic stirrer a few hours before the experimental procedure, and some air were seen in the flow lines that connect the D-60 container to the reservoir brines via the pump. This might have introduced some air into the system. Air bubbles were only observed during one of the experiments for a short period of time (about 4 hours).

The process of brine changing was effective as initially planned. For brines with significant difference in salinity, such as FW and SW, a piston like displacement can be viewed from outside of the oven as shown in Figure 6.21. The conductivity tool, Section 5.6, was used to double check when the low salinity brine is fully contained in the Amott cell as described in Section 5.6.



Figure 6.21: Segregation due to density difference, seen when changing to brines with lower salinity.

For brines with comparative salinity, although the piston displacement is not visible enough as compared to the former, the conductivity tool was used to confirm the full presence of the low salinity brine in the system. It is important to highlight that, after each brine has been replaced, we can confirm that the amount of oil produced before the brine is replaced is the same as the amount of oil right after brine replacement. This confirms that no oil production occurred during the brine changing process. Especially in the first spontaneous imbibition experiment, some leakages were observed in the brine reservoir flowlines, which led to some salt precipitation. However, the salt clogged the leakage within an hour and caused no further issue.

6.4.1 Static and dynamic aging results.

The effectiveness of two aging types have been tested by carrying out spontaneous imbibition experiment on two Ainsa cores, B1 and B8, which has been aged dynamically and statically, respectively, as described in Section 5.5. Petro-physical properties of both samples are listed in Table 6.15. Both cores were aged at an elevated temperature of 96°C , for 90 days, and SI experiments were carried out

on both cores at similar conditions. The dynamic aging process for sample B1 was done without a back or sleeve pressure as described in Section 5.5.2, therefore this set-up is slightly different from that described in Fernø et al. (2010). Furthermore, both cores were spontaneously imbibed with Formation water (FW) and seawater (SW) successively.

Property	B1	B8
Porosity (%)	19.96	18.52
Permeability (mD)	35.54	48.35
SWIRR (%)	15.23	9.45
PV (cm ³)	10.43	9.73
Ultimate recovery (%)	28.2	33.3

Table 6.14: Petrophysical properties of the Ainsa cores used for SI experiments at elevated temperature.

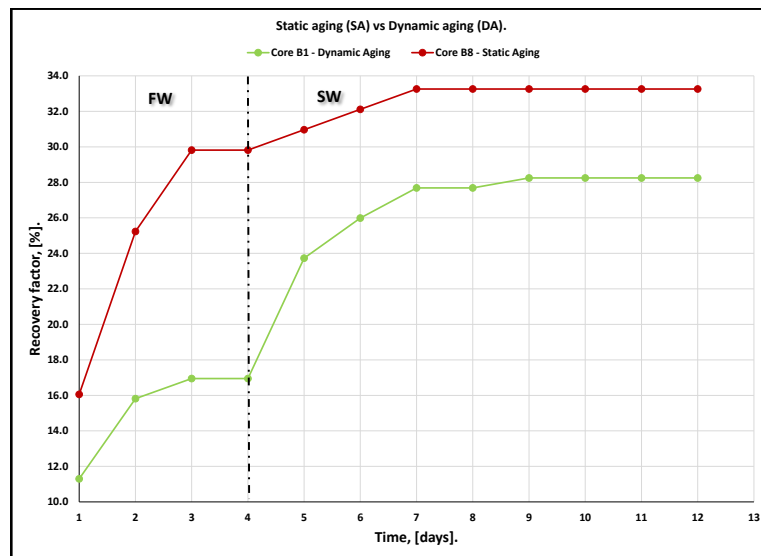


Figure 6.22: Spontaneous imbibition experimental results of two limestone cores, after being imbibed by FW and SW successively and aged statically (B8) and dynamically (B1).

As shown in Figure 6.22, the ultimate recovery of sample B1 was 28.2 % of OOIP, compared to 33.3 % of OOIP for B8. This suggests that sample B1 tends to be more oil-wet. Additionally, the significant reaction of core B8 to FW indicates a larger wettability. As observed in Figure 6.23, more spread of oil droplets were seen on the surface of the dynamically aged core, when compared to its statically aged counterpart.

When a less saline brine (SW), replaced the initial brine (FW), using the steps described in Section 5.6.1, a more evident response was recorded in the core which was dynamically aged (B1), i.e., a recovery from 16.9 % to 23.7 % of OOIP, compared to 29.6 % to 31 % of OOIP, recorded for B8. This observation is in accordance with the work in Fernø et al. (2010). The degree at which the PDIs in SW respond to wettability is a function of the oil-wetting state of the core sample. That is, the higher the response, the higher the oil wetness of the core. Furthermore, during the experiment, the induction time, defined in Section 2.4, was faster for core B1, and this is also in agreement with the work in Fernø et al. (2010). Therefore, it can be suggested that the dynamic aging process is a more efficient process in core restoration than the static aging process.

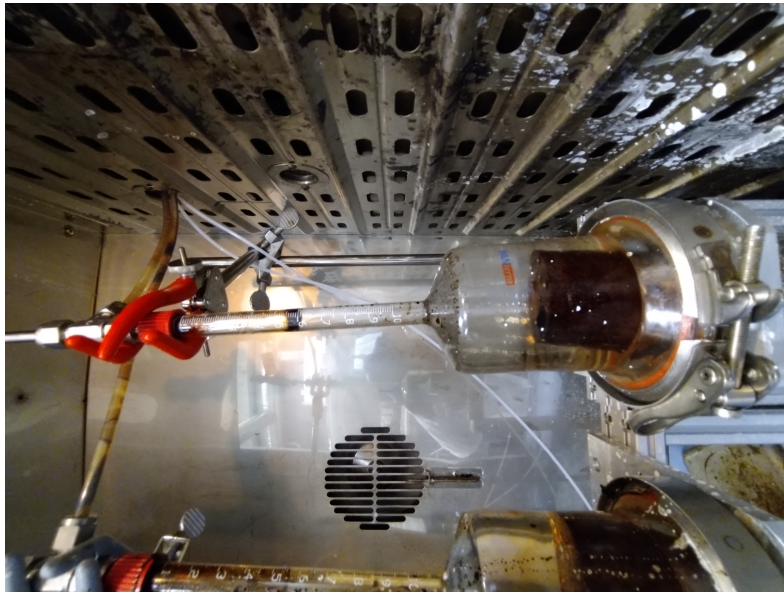


Figure 6.23: Observation of oil droplet spread on the surface of core sample B1.

The dynamic aging set-up in Fernø et al. (2010) was done at 90°C, slightly lower than that of this experiment at 96°C. No sleeve pressure was used when dynamically aging core B1, which is different from the set-up in Fernø et al. (2010). The absence of a confining pressure means that the injected crude oil is more liable to flow through the space between the core holder and the core sample. The core plug is assumed to be initially water-wet, polar compounds contained in the crude oil reaches the mineral surface via diffusion through the water film. The

polar compounds thus adsorb on the rock surface until equilibration is reached, and this adsorption process is controlled by temperature, quantity of polar components, and the degree of diffusion between the inject crude oil and the core.

The adsorption of this polar compounds on the rock surface makes the core oil-wet Donaldson and Alam (2013, p.204). Hence, diffusion between the injected crude and the core explains the wettability alteration process during aging. In addition, the optimal injection rate as suggested in Fernø et al. (2010) was 3ml/hr. In this experiment the injection rate used was 15 ml/hr, which was the lowest rate, allowed by the peristaltic pump. No conclusion can be made as to the most optimal injection rate for flooding without sleeve pressure, because just one rate was used in this experiment. In the later aging procedures, more sophisticated pumps were used and a lower injection rate was possible.

6.4.2 Examining the individual roles of NaCl, magnesium and sulphate.

Capillary imbibition is retarded when the core wettability is oil preferring, therefore, when the initial brine is replaced by a 'smart water' in a spontaneous imbibition process, the additional oil recovery is an evidence of wettability change Song et al. (2020). In developing a smart water to optimize oil recovery, the concentration of active ions, amongst other factors, are very important. The NaCl concentration in seawater was diluted by 10 %, denoted SW-0.1NaCl, and this same brine was enhanced with 2x times concentration of sulphate and 4x times concentration of magnesium as in seawater, this is denoted as SW-0.1NaCl-2S-4Mg. The effect of these two brines, on oil recovery were tested in this spontaneous imbibition experiment. For this experiment we used Ainsa cores B2 and B3, Table 6.15. The cores were imbibed with SW-0.1NaCl, and then SW-0.1NaCl-2S-4Mg after FW and SW successively. The results of the spontaneous imbibition tests are shown in Figure 6.25.

Property	B2	B3
Porosity (%)	18.89	19.70
Permeability (mD)	30.24	42.66
SWIRR (%)	9.88	12.02
PV (cm ³)	10.43	10.38
Ultimate recovery (%)	41.7	30.2

Table 6.15: Petrophysical properties of the Ainsa cores, B2 and B3, used for SI experiments at elevated temperature.

The oil recovery by FW was low. About 16.8 % and 11.0 % of OOIP for cores B2 and B3 respectively. The absence of sulphate to alter any wettability change, could suggest the reason for the low recovery Zhang, Tor Austad et al. (2005). In fact, the recoveries made could be attributed to capillary effects, initial wetting

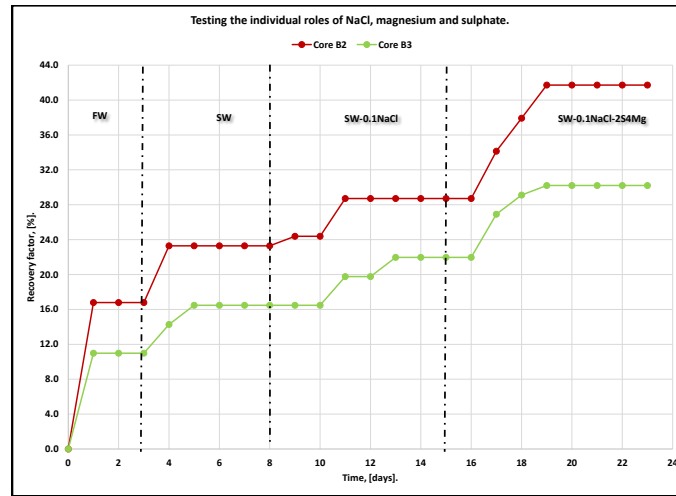


Figure 6.24: Oil recovery by spontaneous imbibition into cores B2 and B3 using different imbibing brines.

conditions of the rock, and temperature effects. Song et al. (2020) recorded very low recoveries in brines depleted of sulphate.

The additional recovery when the imbibing fluid was changed to SW can be attributed to various reasons. One is the sulphate concentration in SW is more than that of FW, and the presence of this potential determining ion (PDI) to play a role in wettability alteration was therefore confirmed. The recoveries by SW brine were about 6.5 % and 5.5 % OOIP for cores B2 and B3 respectively. The plateau recovery after imbibition of SW for cores B2 and B3 are 23.3 % and 16.5 % OOIP respectively. This further confirms studies claiming that SW is about to alter wettability, towards water-wet conditions Strand, Høgnesen and Tor Austad (2006) and S. Shariatpanahi et al. (2016). Also, the salinity of SW is about 35,000 ppm compared to 247,000 ppm for FW.

To investigate the effect of low salinity on oil recovery, the cores were then imbibed with SW-0.1NaCl with a salinity of about 13,000 ppm. Additional recovery was made for both cores. The imbibition rate was slow in both, but slower for core B3. The recovery was similar for both brines, about 5.4 % and 5.5 % of OOIP for cores B2 and B3 respectively. The plateau recovery after imbibition of SW-0.1NaCl brine for cores by B2 and B3 are 28.7 % and 22.0 % OOIP respectively. S. Shariatpanahi et al. (2016) reported about 13 % of OOIP additional oil recovery when a core sample that was imbibed with NaCl depleted SW, after the imbibition of ordinary seawater. The work in S Jafar Fathi, Tor Austad and Strand (2011) was

also in agreement with our observation, where additional oil recovery was made when using an NaCl depleted SW in a spontaneous imbibition experiment.

None of Na^+ or Cl^- is a potential determining ion (PDI) to a chalk surface, and this is also applicable to limestone Strand, Tor Austad et al. (2008). Therefore Na^+ and Cl^- do not belong to the stern layer of the double layer, where other PDI are commonly located. However, NaCl is active in the double layer. Their presence reduces the activities of the PDIs, which are present in SW, in releasing the carboxylic materials from the calcite surface, resulting in wettability alteration towards water-wetness. The presence of Cl^- would limit the access of SO_4^{2-} on the rock surface, while the presence of Na^+ , would limit the access of Mg^{2+} and Ca^{2+} . The reduced ionic strength, is able to reduce the concentration of NaCl, this allows the PDI have a better access to the double layer and therefore able to alter the wettability of the rock surface Seyed Jafar Fathi, Tor Austad, Strand et al. (2012).

According to Liu et al. (2018), Na^+ has a strong influence to alter inter facial water structure compared to other ions because it resides closest to the calcite surface. Likewise, Guo and Kovscek (2019) noted that Na^+ tampers with the innermost water structure by limiting the decay length of short-range non- repulsion. Therefore, the increased concentration of NaCl reduced the adhesion energy between the brine/rock interface and makes it less water-wet. The reduction of NaCl is thus able to trigger wettability towards more water-wet. Section 3.2.1, describes this mechanism.

After noticing additional recovery in an NaCl reduced SW brine, the impact of sulphate and magnesium on the recovery potential of imbibing brines were examined with brine SW-0.1NaCl-2S-4Mg. With this brine is, there is less NaCl concentration to impede the access of the additional active ions (4x magnesium and 2x sulphate) to access the double layer to alter wettability to more water-wet conditions. The improved oil recovery after a day delay in both cores signified the effect of the new brine. The recoveries by SW-0.1NaCl-2S-4Mg brine were about 13 % and 8 % of OOIP for cores B2 and B3, respectively.

The plateau recovery after imbibition of SW-0.1NaCl-2S-4Mg brine for cores B2 and B3 are 41.7 % and 30.2 % of OOIP respectively. These results show the combined effects of sulphate and magnesium as wettability modifiers for carbonate rocks. SW-0.1NaCl-2S-4Mg is effective at releasing the carboxylic materials which are strongly attached to the rock surface and thereby reducing the oil-wet conditions of the rock. The response of core B2 was more profound than core B3 for all imbibing brines, and no conclusive reason was decided upon. A further investigation about the combination of magnesium with sulphate is tested with Angola cores in the next spontaneous imbibition (SI) experiment.

6.4.3 Spontaneous imbibition results on varying magnesium content

Property	C1	C2
Porosity (%)	19.19	14.72
Permeability (mD)	15.37	1.73
SWIRR (%)	23.699	40.100
PV (cm ³)	8.02	7.36
Ultimate recovery (%)	34.7	47.6

Table 6.16: Petrophysical properties of Angola cores, C1 and C2 used for SI experiments at elevated temperature.

Angola cores, C1 and C2 with petrophysical properties displayed in Table 6.16, were successively imbibed with FW, SW, SW-0.1NaCl-2S-4Mg and SW-0.1NaCl-2S-8Mg. The efficiency of SW to improve oil recovery was confirmed in Section 6.4.1 while the effectiveness of SW-0.1NaCl-2S-4Mg was investigated in Section 6.4.2 of the SI experiments. In this section, the implication of double the magnesium content in SW-0.1NaCl-2S-4Mg was explored, i.e., changing to SW-0.1NaCl-2S-8Mg. Results are shown in displayed in Figure 6.25.

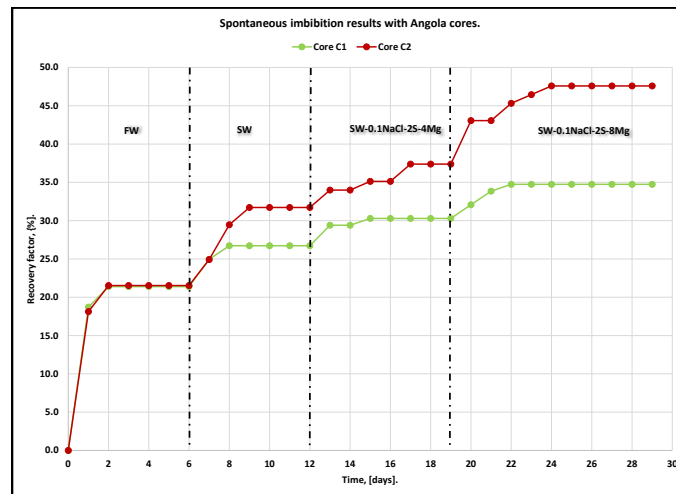


Figure 6.25: Oil recovery by spontaneous imbibition (SI) into cores C1 and C2 using different imbibing brines.

Both cores behaved similarly after the imbibition with FW. 21.4 % of OOIP and 21.5 % of OOIP were recovered for cores C1 and C2, respectively. Both cores plateaued after the second day of imbibition. Once again, SW proved to be an efficient wettability modifier. Additional recovery of 5.3 % of OOIP and 10.2 % of OOIP

was recovered from core C1 and C2 respectively. The response from core C2 was more profound than C1. The ultimate recovery after the imbibition with SW stands at 26.7 % of OOIP and 31.7 % of OOIP for cores C1 and C2, respectively.

Additional recovery was made for both cores after imbibition with SW-0.1NaCl-2S-4Mg brine. As observed before, the combined effect of additional sulphate and magnesium concentration in an NaCl diluted SW was confirmed in this experiment. An incremental oil recovery of 3.6 % of OOIP and 5.7 % of OOIP was made from core C1 and C2, respectively. Core C1 peaked on the 3rd day of imbibition, while C2 peaked on the 5th day.

Karimi et al. (2016) reported additional recoveries when using brines with magnesium, sulphate and combined effect of both PDIs. Additional oil recoveries when imbibing brine was enhanced with sulphate have been reported in Zhang, Tor Austad et al. (2005), Hognesen, Strand, Tor Austad et al. (2005), Tor Austad, Seyed Farzad Shariatpanahi et al. (2015) and Puntervold, Strand and Tor Austad (2007) have all reported additional. Specifically, Zhang, Tor Austad et al. (2005) reported that the effectiveness of the combined effect of magnesium and sulphate increased with temperature and magnesium is a wettability modifier in the presence of sulphate.

A further confirmation of the effect of this combination of PDI was confirmed, after the cores were imbibed with SW-0.1NaCl-2S-8Mg. A fast imbibition was observed from both cores. Also, an incremental recovery of 4.5 % of OOIP and 10.2 % of OOIP was made from core C1 and C2 respectively. These observations confirm that sulphate and magnesium are PDI towards a carbonate surface, and assumed to alter the wettability of the rock surface. The ultimate recovery from C1 is 34.7 % of OOIP and 47.6 % of OOIP for C2.

Chapter 7

Conclusion and future work

Part of the goals of this thesis is to probe the effect of varying salinity brines and ionic compositions on the wettability alteration of two different sets of carbonate core samples, Ainsa cores and Angola cores, which are representatives of carbonate fields in Brazil operated by Equinor. In addition, the efficiency of two different types of aging methods, static and dynamic aging, were also tested, and the results of spontaneous imbibition experiments were used to arrive at several conclusions listed below. A total of 6 brines, namely, FW, SW, SW-0.1, SW-0.1NaCl, SW-0.1NaCl-2S-4Mg, and SW-0.1NaCl-2S-8Mg were used in the spontaneous imbibition experiments. The acid number (AN) of the Heidrun oil used in our experiments is 3.3 mg KOH/g.

The SI results were supported by zeta potential and contact angle measurements. The core mineralogy was analysed by SEM/EDS experiments. The following conclusions have been drawn from the completion of this project;

1. The core samples were confirmed to be limestone with no traces of anhydrite.
2. The dynamic aging process is a more efficient process in core restoration and a more oil-wet core responds better, i.e, gives more oil recovery, when changing from FW to SW. This is also supported in literature.
3. During dynamic aging, it is advisable to age tight cores (<1mD) in parallel, while higher permeability cores with comparable properties could be aged in series.
4. Choice of injection rate needs to be compatible with the permeability of the core (cores with permeability <1mD needs a flow rate less than 1.5 ml/hr).
5. In contact angle measurements, NaCl diluted brine is able to reduce contact angle to 59.03 from 108.3 recorded for SW.
6. A general trend of improving water wetness was observed by reduced contact angles after successive contacts of chip with FW, SW, SW-0.1NaCl-2S-4Mg, and SW-0.1NaCl-2S-8Mg. Average angles changed from 165.3 to 128.5 to 127.3 to 118.11 respectively. Though, the changes were small after contact with SW.

7. As noted in literature, magnesium and sulphate are potential determining ion (PDI)s for limestone samples, and able to alter wettability towards more water wetness.
8. The wettability alteration observed in this thesis is irreversible, in the absence of oil. As confirmed by repeated contact angle measurements.
9. When the polished chip was aged in each test brine at room temperature, more visible reduction in angles were observed compared to brine aging at 96°C. Note that the chips used for these tests are different.
10. About 56 degree of contact angle reduction was observed when a chip was first contacted with FW and then with SW-0.1NaCl-2S-8Mg.
11. For pure limestone powder, presence of sulphate renders the rock surface less positive, and the reduction of NaCl in SW reduced the surface potential to less positive values at both test temperatures (25°C and 70°C).
12. For crude oil aged powder, negative potentials were recorded for brines SW-0.1 and SW-0.1NaCl. A negative potential is indicative of a strong double layer.
13. SW can improve the spontaneous imbibition of water into limestone cores. In all phases of SI experiments carried out, SW was able to improve oil recovery by a total of 14.8 %, 12 % and 12 % of OOIP in the first, second and third phases, respectively. These incremental recoveries is attributed to the interplay between the potential determining ions contained in SW.
14. Low salinity brine, SW-0.1NaCl, resulted in a cumulative incremental recovery of 9.9 % of OOIP. This further confirms the efficiency of NaCl reduced brines to improve oil recovery in carbonate rocks.
15. The combined reaction of sulphate and magnesium or calcium is necessary to improve oil recovery. Brines SW-0.1NaCl-2S-4Mg resulted in cumulative incremental oil recovery of 21 % of OOIP in Section 6.4.2 and 9.3 % of OOIP in Section 6.4.3. Brines SW-0.1NaCl-2S-8Mg resulted in cumulative incremental oil recovery of 14.6 % of OOIP in Section 6.4.3.

7.0.1 Future work

Having spent a lot of time carrying out these experiments in the laboratory, and although a lot of the set up behaved as predicted, there are still some improvements that can be made in case of future work to be done in this subject.

1. SI experiments should be carried out at varying temperature so as to properly quantify the effect of temperature on oil recovery.
2. As an improvement to the current set up, a better and more efficient way to retrieve the oil recovered externally, should be explored. An improved measurement must ensure that the set-up is not disturbed while running, and also that little or no oil is lost on the walls of the flowlines.
3. Just one type of oil was used in this experiment, therefore the impact of acid number was not investigated. Further work could explore the possibilities of varying acid number, to quantify its effect on SI experiments.

4. The range of brine salinity and ionic composition could be expanded for contact angle experiments, so as to determine the most optimal composition for carbonate rocks.
5. The direct effect of sleeve pressure in dynamic aging processes could be explored to determine if the effect is significant enough compared to a set-up without a sleeve pressure.
6. A SI set up that totally eliminates air bubbles moving through the Amott cell would greatly improve the integrity of production results. Such set-up should be explored in future works.

Bibliography

- Abdallah, Wael et al. (1986). 'Fundamentals of wettability'. In: *Technology* 38.1125-1144, p. 268.
- Adejumo, Gbadebo (2020). *Experimental study on the effect of low water salinity and ionic salinity and ionic composition on wettability alteration in carbonates*. https://drive.google.com/file/d/1Z7eFg1g1uqSaXF3a3GfR0SD_yvNkvH0/view?usp=sharing.
- Austad, T et al. (2012). 'Conditions for a low-salinity enhanced oil recovery (EOR) effect in carbonate oil reservoirs'. In: *Energy & fuels* 26.1, pp. 569–575.
- Austad, Tor, Seyed Farzad Shariatpanahi et al. (2015). 'Low salinity EOR effects in limestone reservoir cores containing anhydrite: a discussion of the chemical mechanism'. In: *Energy & Fuels* 29.11, pp. 6903–6911.
- Austad, Tor, Skule Strand and Tina Puntervold (2009). 'Is wettability alteration of carbonates by seawater caused by rock dissolution'. In: *Paper SCA2009-43 presented at the International Symposium of the Society of Core Analysts held in Noordwijk, The Netherlands, September*, pp. 27–30.
- Azizov, Ilgar (2019). 'Effect of Water Quality on Wettability Alteration in Carbonates'. MA thesis. NTNU.
- Bowles, Oliver (1956). *Limestone and dolomite*. Vol. 7738. US Department of the Interior, Bureau of Mines.
- Bruna Alves Jul 14, 2020 (2020). 'Brazil: oil production 2008-2019'. In: www.statista.com.
- Butt, Hans-Jürgen, Karlheinz Graf and Michael Kappl (2013). *Physics and chemistry of interfaces*. John Wiley & Sons.
- Chandrasekhar, Sriram (2013). 'Wettability alteration with brine composition in high temperature carbonate reservoirs'. In:
- Chilingar, GV and TF Yen (1992). 'Some notes on wettability and relative permeability of carbonate reservoir rock'. In: *Energy Sources* 7.1, pp. 21–27.
- Costa Fraga, CT da et al. (2003). 'Campos basin-25 years of production and its contribution to the oil industry'. In: *Offshore Technology Conference*. Offshore Technology Conference.
- Darling, Toby (2005). *Well logging and formation evaluation*. Elsevier.
- Donaldson, Erle C and Waqi Alam (2013). *Wettability*. Elsevier.
- Dubey, ST, MH Waxman et al. (1991). 'Asphaltene adsorption and desorption from mineral surfaces'. In: *SPE Reservoir Engineering* 6.03, pp. 389–395.

- Fathi, S Jafar, Tor Austad and Skule Strand (2011). 'Water-based enhanced oil recovery (EOR) by "smart water": Optimal ionic composition for EOR in carbonates'. In: *Energy & fuels* 25.11, pp. 5173–5179.
- Fathi, Seyed Jafar, Tor Austad, Skule Strand et al. (2012). 'Water-based enhanced oil recovery (EOR) by "smart water" in carbonate reservoirs'. In: *SPE EOR Conference at Oil and Gas West Asia*. Society of Petroleum Engineers.
- Fathi, Seyed Jafar, Tor Austad, Skule Strand and Tina Puntervold (2010). 'Wettability alteration in carbonates: The effect of water-soluble carboxylic acids in crude oil'. In: *Energy & fuels* 24.5, pp. 2974–2979.
- Feldmann, Felix et al. (2020). 'An experimental and numerical study of low salinity effects on the oil recovery of carbonate rocks combining spontaneous imbibition, centrifuge method and coreflooding experiments'. In: *Journal of Petroleum Science and Engineering* 190, p. 107045.
- Fernø, MA et al. (2010). 'Dynamic laboratory wettability alteration'. In: *Energy & Fuels* 24.7, pp. 3950–3958.
- Gandomkar, Asghar and Mohammad Reza Rahimpour (2017). 'The impact of monovalent and divalent ions on wettability alteration in oil/low salinity brine/limestone systems'. In: *Journal of Molecular Liquids* 248, pp. 1003–1013.
- Gopani, Paras H et al. (2021). 'Role of Monovalent and Divalent Ions in Low-Salinity Water Flood in Carbonate Reservoirs: An Integrated Analysis through Zeta Potentiometric and Simulation Studies'. In: *Energies* 14.3, p. 729.
- Graue, A, T Bognø, BAr Baldwin et al. (2001). 'Wettability effects on oil-recovery mechanisms in fractured reservoirs'. In: *SPE Reservoir Evaluation & Engineering* 4.06, pp. 455–466.
- Graue, A, T Bognø, RW Moe et al. (1999). 'Impacts of wettability on capillary pressure and relative permeability'. In: *SCA9907, Reviewed Proc.: 1999 International Symposium of Core Analysts, Golden, Co., USA*.
- Guo, Haoli and Anthony R Kavscek (2019). 'Investigation of the effects of ions on short-range non-DLVO forces at the calcite/brine interface and implications for low salinity oil-recovery processes'. In: *Journal of colloid and interface science* 552, pp. 295–311.
- Gupta, R and KK Mohanty (2011). 'Wettability alteration mechanism for oil recovery from fractured carbonate rocks'. In: *Transport in porous media* 87.2, pp. 635–652.
- Al-Hadhrami, Hamed S and Martin J Blunt (2001). 'Thermally induced wettability alteration to improve oil recovery in fractured reservoirs'. In: *SPE Reservoir Evaluation & Engineering* 4.03, pp. 179–186.
- Han, Kenneth N (2002). *Fundamentals of aqueous metallurgy*. SME.
- Hirasaki, GJ et al. (1991). 'Wettability: fundamentals and surface forces'. In: *SPE Formation Evaluation* 6.02, pp. 217–226.
- Hognesen, Eli Jens, Skule Strand, Tor Austad et al. (2005). 'Waterflooding of preferential oil-wet carbonates: Oil recovery related to reservoir temperature and brine composition'. In: *SPE Europec/EAGE annual conference*. Society of Petroleum Engineers.

- Honarvar, Bizhan et al. (2020). 'Smart water effects on a crude oil-brine-carbonate rock (CBR) system: further suggestions on mechanisms and conditions'. In: *Journal of Molecular Liquids* 299, p. 112173.
- Hopkins, Paul Andrew et al. (2016). 'Adsorption of acidic crude oil components onto outcrop chalk at different wetting conditions during both dynamic adsorption and aging processes'. In: *Energy & Fuels* 30.9, pp. 7229–7235.
- Jordan, MM, K Sjursaether, IR Collins et al. (2004). 'Scale Control Within North Sea Chalk/Limestone Reservoirs. The Challenge of Understanding and Optimizing Chemical Placement Methods and Retention Mechanism:-Laboratory to Field.' In: *SPE international symposium and exhibition on formation damage control*. Society of Petroleum Engineers.
- Karimi, Mahvash et al. (2016). 'Wettability alteration and oil recovery by spontaneous imbibition of low salinity brine into carbonates: Impact of Mg^{2+} , SO_4^{2-} and cationic surfactant'. In: *Journal of Petroleum Science and Engineering* 147, pp. 560–569.
- Kasha, Ahmed et al. (2015). 'Effect of Ca^{2+} , Mg^{2+} and SO_4^{2-} ions on the zeta potential of calcite and dolomite particles aged with stearic acid'. In: *Colloids and Surfaces A: Physicochemical and Engineering Aspects* 482, pp. 290–299.
- Lashkarbolooki, Mostafa, Shahab Ayatollahi and Masoud Riazi (2014). 'Effect of salinity, resin, and asphaltene on the surface properties of acidic crude oil/smart water/rock system'. In: *Energy & fuels* 28.11, pp. 6820–6829.
- Liu, Jian et al. (2018). 'Wettability alteration and enhanced oil recovery induced by proximal adsorption of Na^+ , Cl^- , Ca^{2+} , Mg^{2+} , and SO_4^{2-} ions on calcite'. In: *Physical Review Applied* 10.3, p. 034064.
- Lucia, F Jerry (2007). *Carbonate reservoir characterization: An integrated approach*. Springer Science & Business Media.
- Mahani, Hassan et al. (2015). 'Insights into the mechanism of wettability alteration by low-salinity flooding (LSF) in carbonates'. In: *Energy & Fuels* 29.3, pp. 1352–1367.
- Al-Mahrooqi, SH et al. (2005). 'Wettability alteration during aging: The application of NMR to monitor fluid redistribution'. In: *Society of Core Analyst*, pp. 21–25.
- Mamonov, Aleksandr, Tina Puntervold, Skule Strand et al. (2017). 'EOR by smart water flooding in sandstone reservoirs-effect of sandstone mineralogy on initial wetting and oil recovery'. In: *SPE Russian Petroleum Technology Conference*. Society of Petroleum Engineers.
- Mohanty, KK, S Chandrasekhar et al. (2013). 'Wettability Alteration with Brine Composition in High Temperature Carbonate Reservoirs'. In: *SPE Annual Technical Conference and Exhibition*. Society of Petroleum Engineers.
- Morrow, Norman R et al. (1990). 'Wettability and its effect on oil recovery'. In: *Journal of petroleum technology* 42.12, pp. 1–476.
- Nasralla, Ramez A et al. (2018). 'Low salinity waterflooding for a carbonate reservoir: Experimental evaluation and numerical interpretation'. In: *Journal of Petroleum Science and Engineering* 164, pp. 640–654.

- Petrovich, R and AA Hamouda (1998). 'Dolomitization of Ekofisk oil field reservoir chalk by injected seawater'. In: *Proceedings of the Ninth International Symposium on Water-Rock Interactions, Taupo, New Zealand*. Vol. 30.
- Punternold, Tina, Skule Strand and Tor Austad (2007). 'New method to prepare outcrop chalk cores for wettability and oil recovery studies at low initial water saturation'. In: *Energy & Fuels* 21.6, pp. 3425–3430.
- Rao, Dandina N (1999). 'Wettability effects in thermal recovery operations'. In: *SPE Reservoir Evaluation & Engineering* 2.05, pp. 420–430.
- Rashid, Saeed et al. (2015). 'Wettability alteration in carbonates during "Smart Waterflood": Underlying mechanisms and the effect of individual ions'. In: *Colloids and Surfaces A: Physicochemical and Engineering Aspects* 487, pp. 142–153.
- RezaeiDoust, A et al. (2009). 'Smart water as wettability modifier in carbonate and sandstone: A discussion of similarities/differences in the chemical mechanisms'. In: *Energy & fuels* 23.9, pp. 4479–4485.
- Romanuka, Julija et al. (2012). 'Low salinity EOR in carbonates'. In: *SPE Improved Oil Recovery Symposium*. Society of Petroleum Engineers.
- Santos, Ronaldo G dos et al. (2006). 'Contact angle measurements and wetting behavior of inner surfaces of pipelines exposed to heavy crude oil and water'. In: *Journal of Petroleum Science and Engineering* 51.1-2, pp. 9–16.
- Shariatpanahi, Seyed Farzad, Skule Strand and Tor Austad (2010). 'Evaluation of water-based enhanced oil recovery (EOR) by wettability alteration in a low-permeable fractured limestone oil reservoir'. In: *Energy & Fuels* 24.11, pp. 5997–6008.
- (2011). 'Initial wetting properties of carbonate oil reservoirs: effect of the temperature and presence of sulfate in formation water'. In: *Energy & fuels* 25.7, pp. 3021–3028.
- Shariatpanahi, SF et al. (2016). 'Water based EOR by wettability alteration in dolomite'. In: *Energy & Fuels* 30.1, pp. 180–187.
- Sohal, M Adeel, Geoffrey Thyne and Erik G Sogaard (2016). 'Review of recovery mechanisms of ionically modified waterflood in carbonate reservoirs'. In: *Energy & Fuels* 30.3, pp. 1904–1914.
- Song, Jin et al. (2020). 'Effect of salinity, Mg²⁺ and SO₄²⁻ on "smart water"-induced carbonate wettability alteration in a model oil system'. In: *Journal of colloid and interface science* 563, pp. 145–155.
- Standnes, Dag C and Tor Austad (2000). 'Wettability alteration in chalk: 2. Mechanism for wettability alteration from oil-wet to water-wet using surfactants'. In: *Journal of Petroleum Science and Engineering* 28.3, pp. 123–143.
- Strand, Skule, Tor Austad et al. (2008). "'Smart water" for oil recovery from fractured limestone: a preliminary study'. In: *Energy & fuels* 22.5, pp. 3126–3133.
- Strand, Skule, Eli J Høgnesen and Tor Austad (2006). 'Wettability alteration of carbonates—Effects of potential determining ions (Ca²⁺ and SO₄²⁻) and temperature'. In: *Colloids and Surfaces A: Physicochemical and Engineering Aspects* 275.1-3, pp. 1–10.

- Tetteh, Joel, Nazirah Mohd Janjang, Reza Barati et al. (2018). 'Wettability alteration and enhanced oil recovery using low salinity waterflooding in limestone rocks: a mechanistic study'. In: *SPE Kingdom of Saudi Arabia Annual Technical Symposium and Exhibition*. Society of Petroleum Engineers.
- Thomas, Michele Moio, Jamie A Clouse and John M Longo (1993). 'Adsorption of organic compounds on carbonate minerals: 1. Model compounds and their influence on mineral wettability'. In: *Chemical geology* 109.1-4, pp. 201–213.
- Torsæter, Ole and Manoochehr Abtahi (2003). 'Experimental reservoir engineering laboratory workbook'. In: *Norwegian University of Science and Technology*.
- Van Cappellen, Philippe et al. (1993). 'A surface complexation model of the carbonate mineral-aqueous solution interface'. In: *Geochimica et Cosmochimica Acta* 57.15, pp. 3505–3518.
- Yi, Zhang, Hemanta Kumar Sarma et al. (2012). 'Improving waterflood recovery efficiency in carbonate reservoirs through salinity variations and ionic exchanges: A promising low-cost " Smart-Waterflood" approach'. In: *Abu Dhabi International Petroleum Conference and Exhibition*. Society of Petroleum Engineers.
- Yousef, Ali A, Salah Al-Saleh, Mohammed Saleh Al-Jawfi et al. (2012). 'Improved/enhanced oil recovery from carbonate reservoirs by tuning injection water salinity and ionic content'. In: *SPE improved oil recovery symposium*. Society of Petroleum Engineers.
- Yousef, Ali A, Salah Al-Saleh, Abdulaziz Ubaid Al-Kaabi et al. (2010). 'Laboratory investigation of novel oil recovery method for carbonate reservoirs'. In: *Canadian Unconventional Resources and International Petroleum Conference*. Society of Petroleum Engineers.
- Zhang, P, Tor Austad et al. (2005). 'The relative effects of acid number and temperature on chalk wettability'. In: *SPE International Symposium on Oilfield Chemistry*. Society of Petroleum Engineers.
- Zhang, Peimao and Tor Austad (2006). 'Wettability and oil recovery from carbonates: Effects of temperature and potential determining ions'. In: *Colloids and Surfaces A: Physicochemical and Engineering Aspects* 279.1-3, pp. 179–187.
- Zhang, Peimao, Medad T Tweheyo and Tor Austad (2007). 'Wettability alteration and improved oil recovery by spontaneous imbibition of seawater into chalk: Impact of the potential determining ions Ca²⁺, Mg²⁺, and SO₄²⁻'. In: *Colloids and Surfaces A: Physicochemical and Engineering Aspects* 301.1-3, pp. 199–208.

Appendix A

Additional material

A.1 Raw measurement data

A.1.1 Core dimensions

Core ID	Diameter	Length	Area
	(cm)	(cm)	(cm ²)
Angola			
C1	3.73	4.52	10.93
C2	3.76	4.49	11.11
C3	3.77	4.59	11.16
C4	3.77	3.13	11.16
C5	1.00	1.00	0.79
Ainsa			
B1	3.80	4.62	11.34
B2	3.81	4.59	11.40
B3	3.82	4.61	11.46
B5	3.71	4.60	10.81
B6	3.80	4.42	11.34
B8	3.81	4.56	11.40

Figure A.1: Core Dimensions for all cores used in the experiment.

A.1.2 Porosity and permeability measurements

CORE ID	P1 (bar)	P2 (bar)	Change in P (bar)	Q (cm ³ /s)	Q (ml/s)	Mean pressure (Pm) (atm)	1/Pm (atm ⁻¹)	(P1 ² -P2 ²)/A	K D	K mD
B1	1.2	1	0.2	0.25	4.17	1.1	0.91	4.9907528	0.138195849	138.1958489
	1.4	1.2	0.2	0.28	4.67	1.3	0.77	5.8981624	0.130955926	130.9559262
	1.6	1.4	0.2	0.28	4.67	1.5	0.67	6.805572	0.113495136	113.495136
	1.8	1.6	0.2	0.3	5	1.7	0.59	7.7129816	0.107219237	107.2192367
	2	1.8	0.2	0.3	5	1.9	0.53	8.6203912	0.095933001	95.93300128
	2.2	2	0.2	0.31	5.17	2.1	0.48	9.5278008	0.089747607	89.74760681
B2	1.2	1	0.2	0.23	3.83	1.1	0.91	5.017054482	0.12544278	125.4427797
	1.4	1.2	0.2	0.25	4.17	1.3	0.77	5.929246206	0.115566596	115.5665857
	1.6	1.4	0.2	0.27	4.5	1.5	0.67	6.84143793	0.108063857	108.0638572
	1.8	1.6	0.2	0.27	4.5	1.7	0.59	7.753629654	0.095368109	95.36810926
	2	1.8	0.2	0.27	4.5	1.9	0.53	8.665821378	0.085329361	85.32936092
	2.2	2	0.2	0.28	4.67	2.1	0.48	9.578013102	0.080119304	80.11930364
B3	1.2	1	0.2	0.27	4.5	1.1	0.91	5.043426288	0.147255279	147.2552794
	1.4	1.2	0.2	0.3	5	1.3	0.77	5.960411704	0.138445134	138.4451345
	1.6	1.4	0.2	0.33	5.5	1.5	0.67	6.87739812	0.131984362	131.9843616
	1.8	1.6	0.2	0.34	5.67	1.7	0.59	7.794384536	0.120056363	120.0563631
	2	1.8	0.2	0.33	5.5	1.9	0.53	8.711370952	0.10419818	104.1981802
	2.2	2	0.2	0.33	5.5	2.1	0.48	9.628357368	0.094274544	94.27454396

Figure A.2: Permeability measurement data for Ainsa cores B1, B2 and B3.

CORE ID	P1 (bar)	P2 (bar)	Change in P (bar)	Q (cm ³ /s)	Q (ml/s)	Mean pressure (Pm) (atm)	1/Pm (atm ⁻¹)	(P1 ² -P2 ²)/A	K D	K mD
B5	1.2	1	0.2	0.36	6	1.1	0.91	4.757148242	0.207704269	207.7042694
	1.5	1.3	0.2	0.42	7	1.4	0.71	6.054552308	0.19039556	190.3955803
	1.8	1.6	0.2	0.47	7.83	1.7	0.59	7.351956374	0.175387929	175.3879287
	2.1	1.9	0.2	0.47	7.83	2	0.5	8.64938044	0.149079739	149.0797394
B6	1.2	1	0.2	0.19	3.17	1.1	0.91	4.9907528	0.100507507	100.5075066
	1.5	1.3	0.2	0.2	3.33	1.4	0.71	6.3518672	0.082956061	82.95606054
	1.8	1.6	0.2	0.21	3.5	1.7	0.59	7.7129816	0.071804398	71.80439793
B8					0					
	1.2	1	0.2	0.32	5.33	1.1	0.91	5.017054482	0.173430813	173.4308135
	1.4	1.2	0.2	0.36	6	1.3	0.77	5.929246206	0.165196041	165.1960411
	1.6	1.4	0.2	0.39	6.5	1.5	0.67	6.84143793	0.155100727	155.1007275
	1.8	1.6	0.2	0.4	6.67	1.7	0.59	7.753629654	0.140432831	140.4328306
	2	1.8	0.2	0.39	6.5	1.9	0.53	8.665821378	0.122447943	122.4479428
2.2	2	0.2	0.39	6.5	2.1	0.48	9.578013102	0.110786234	110.7862339	

Figure A.3: Permeability measurement data for Ainsa cores B5, B6 and B8.

CORE ID	P1 (bar)	P2 (bar)	Change in P (bar)	Q (cm ³ /s)	Q ml/s	Mean pressure (Pm) (atm)	1/Pm (atm ⁻¹)	(P1*2P2*2) A	K D	K mD
C1	1.2	1	0.2	0.39	6.5	1.1	0.91	4.806576496	0.218735004	218.7350041
	1.5	1.3	0.2	0.42	7	1.4	0.71	6.120006452	0.165083465	165.083465
	1.8	1.6	0.2	0.42	7	1.7	0.59	7.431436406	0.152421677	152.4216771
	2.1	1.9	0.2	0.43	7.17	2	0.5	8.74286636	0.132704844	132.7048444
	2.4	2.2	0.2	0.4	6.67	2.3	0.43	10.05429631	0.10734841	107.3484097
C2	5	1	4	0.05	0.83	3	0.33	266.5220352	0.000502591	0.502591339
	6	2	4	0.06	1.00	4	0.25	355.3627136	0.000452332	0.452332206
	7	3	4	0.07	1.17	5	0.20	444.203392	0.000422177	0.422176725
	6	1	5	0.07	1.17	3.5	0.29	388.677968	0.000482488	0.482487686
	7	2	5	0.09	1.50	4.5	0.22	499.728816	0.000482488	0.482487686
	7	1	6	0.1	1.67	4	0.25	533.0440704	0.000502591	0.502591339
C3	5	1	4	0.14	2.33	3	0.33	267.9415908	0.001430976	1.430976053
	6	2	4	0.16	2.67	4	0.25	357.254544	0.001226551	1.226550902
	7	3	4	0.21	3.50	5	0.20	446.569318	0.001287878	1.287878448
C4	4	1	3	0.97	16.17	2.5	0.40	167.4634943	0.01081752	10.81751981
	5	2	3	1.22	20.33	3.5	0.29	234.448892	0.009718243	9.718243129
	6	3	3	1.48	24.67	4.5	0.22	301.4342897	0.00916949	9.169489874
	7	4	3	2.18	36.33	5.5	0.18	368.4196874	0.0110507	11.05069971
C5	4	1	3	0.66	11.00	2.5	0.40	11.7825	0.033422449	33.42244855
	5	2	3	0.78	13.00	3.5	0.29	16.4955	0.028213755	28.21375527
	6	3	3	0.88	14.67	4.5	0.22	21.2065	0.024757369	24.75736929
	7	4	3	1	16.67	5.5	0.18	25.9215	0.023018215	23.01821525

Figure A.4: Permeability measurement data for Angola cores.

A.2 Porosity measurements

Core ID	Diameter	Length	Bulk Volume	Core holder	Core holder	Core +core holder	Core +core holder
	d(cm)	L(cm)	Vb(cm ³)	V1(cm ³)	V1(New)	V2(cm ³)	V2(New)
Angola							
C1	3.73	4.52	49.52	64.00		22.50	
C2	3.76	4.49	49.96	64.00		21.40	
C3	3.77	4.59	51.26	64.00		18.70	
C4	3.77	3.13	34.86	48.00		15.10	
C5	3.76	2.61	29.10	48.00		20.10	
Ainsa							
B1	3.80	4.62	52.33	68.00	61.00	26.55	19.10
B2	3.81	4.59	52.43	68.00	61.00	26.20	19.00
B3	3.82	4.61	52.68	68.00	61.00	26.10	18.70
B5	3.71	4.60	49.75	69.00		25.90	25.90
B6	3.80	4.42	50.15	69.00		28.10	28.10
B8	3.81	4.56	52.03	69.00	61.00	27.00	18.70

Figure A.5: Porosity measurement data for all cores.

	Matrix Volume	Matrix Volume	Pore Volume	Pore Volume	Porosity	Porosity	Difference Vp
	Vm(cm ³)	Vm(New)	Vp(cm ³)	(New)		New	(%)
Angola							
C1	41.50		8.02		16.19		
C2	42.60		7.36		14.72		
C3	45.30		5.96		11.63		
C4	32.90		1.96		5.62		
C5	27.90		1.20		4.11		
Ainsa							
B1	41.45	41.90	10.88	10.43	20.8	19.93	4.14
B2	41.80	42.00	10.63	10.43	20.27	19.89	1.88
B3	41.90	42.30	10.78	10.38	20.46	19.70	3.71
B5	43.10	43.10	6.63	6.63	13.33	13.33	0.00
B6	40.90	40.90	9.25	9.25	18.44	18.44	0.00
B8	42.00	42.30	10.03	9.73	19.27	18.70	2.99

Figure A.6: Final porosity measurement data for all cores.

		Liquid Porosity					
	Liquid Porosity	Dry weight	Wet weight	Weight Difference	Pore volume	PV Difference	%
Angola							
C1	16.76	122.60	131.89	9.29	8.30	0.28	3.50
C2	12.21	123.24	130.07	6.83	6.10	-1.26	-17.06
C3	10.11	129.83	135.64	5.80	5.18	-0.78	-13.11
C4	10.17	88.34	92.31	3.97	3.54	1.59	80.94
C5	10.23	73.85	77.18	3.33	2.98	1.78	149.10
Ainsa							
B1	19.96	112.30	123.99	11.70	10.44	0.01	0.12
B2	19.53	113.29	124.76	11.47	10.24	-0.19	-1.81
B3	19.64	113.45	125.04	11.59	10.35	-0.03	-0.31
B5	0.00						
B6	0.00						
B8	18.52	111.87	122.66	10.79	9.64	-0.09	-0.96
Water density		1.12 g/cc					
Oil density		0.886 g/cc					

Figure A.7: Liquid Porosity Measurements

A.3 Viscosity and irreducible water saturation data

Crude Oil Viscosity					
Temp. (°C)	Torque (%)	RPM (-)	Viscosity (Cp)	Spindel (-)	Density (g/cc)
23	29.3	120	7.32	31 (20ml)	0.886
23	24.5	100	7.35		
23	37	160	7.22		
		Ave.	7.30		
96	23.3	120	5.82	18 (10ml)	
96	20.6	100	6.21		
96	30.5	150	5.76		
		Ave.	5.93		

Figure A.8: Viscosity measurement data

Irreducible Water Saturation, Swirr							
Core ID	Initial FW-Cup (g)	Total FW-Cup (cm³)	Total FW-Cup (g)	Produced FW (g)	Produced FW (cm³)	OOIC (cm³)	Swirr
B1	8.00	14.20	15.904	7.90	8.85	8.85	15.23
B2	8.00	14.50	16.24	8.24	9.23	9.23	9.88
B3	8.00	14.40	16.128	8.13	9.10	9.10	12.02

Figure A.9: Irreducible water saturation results

A.4 Contact angle data

		Drop 1	Drop 2	Drop 3	Drop 4	Drop 5	Drop 6
SW	Left	101.56	106.05	105.89			
	Right	106.87	113.53	114.31			
SW-0.1NaCl	Left	64.56	71.68	55.22	53.37	76.67	75.2
	Right	65.76	71.73	56.82	58.44	76.85	78.02

Figure A.10: Contact angle measurement results for SW, then SW-0.1NaCl sequence

Left Angle Plot				
	Drop 1	Drop 2	Drop 3	Drop 4
FW	162.82	160.97	162.23	
SW	118.88	143.57	123.90	
SW-0.1NaCl-2S-4Mg	118.20	124.04	131.88	136.08
SW-0.1NaCl-2S-8Mg	120.96	118.89	119.74	127.81

Right Angle Plot				
	Drop 1	Drop 2	Drop 3	Drop 4
FW	169.39	168.52	168.06	
SW	122.29	141.80	120.97	
SW-0.1NaCl-2S-4Mg	117.63	124.54	147.64	149.55
SW-0.1NaCl-2S-8Mg	120.11	110.45	118.51	129.66

Figure A.11: Contact angle measurement results for FW - SW-0.1NaCl-2S-8Mg sequence at high temperature.

FW						SW					
Left	Right	Circle	Left	Right	Circle	Left	Right	Circle	Left	Right	Circle
46.58	41.11	48.24	133.42	138.89	131.76	82.00	84.32	82.20	98.00	95.68	97.80
43.18	39.98	39.58	136.82	140.02	140.42	68.56	71.15	65.18	111.44	108.85	114.82
58.89	53.63	57.51	121.11	126.37	122.49	76.68	76.34	77.27	103.32	103.66	102.73
49.31	52.09	50.35	130.69	127.91	129.65	56.88	57.09	57.78	123.12	122.91	122.22
44.16	44.67	52.01	135.84	135.33	127.99	83.96	82.99	79.30	96.04	97.01	100.70
						75.22	69.78	74.54	104.78	110.22	105.46

SW-0.1NaCl-2S-4Mg						SW-0.1NaCl-2S-8Mg					
Left	Right	Circle	Left	Right	Circle	Left	Right	Circle	Left	Right	Circle
109.56	112.83	104.62	70.44	67.17	75.38	117.46	117.06	98.42	62.54	62.94	81.58
108.01	114.90	112.27	71.99	65.10	67.73	113.81	114.81	97.16	66.19	65.19	82.84
101.23	105.45	136.06	78.77	74.55	43.94	120.41	121.44	100.01	59.59	58.56	79.99
						121.50	125.04	105.23	58.50	54.96	74.77
						119.30	122.86	99.29	60.70	57.14	80.71
						117.73	118.02	104.70	62.27	61.98	75.30

Figure A.12: Contact angle measurement results for FW - SW-0.1NaCl-2S-8Mg sequence at room temperature.

FW						SW-0.1NaCl-2S-8Mg					
Left	Right	Circle	Left	Right	Circle	Left	Right	Circle	Left	Right	Circle
17.18	10.61	17.88	162.82	169.39	162.12	107.26	104.37	89.57	72.74	75.63	90.43
19.03	11.48	17.73	160.97	168.52	162.27	53.51	64.15	59.60	126.49	115.85	120.40
17.77	11.94	17.76	162.23	168.06	162.24	111.73	108.38	108.13	68.27	71.62	71.87

Figure A.13: Contact angle measurement results for direct FW - SW-0.1NaCl-2S-8Mg sequence

A.5 Zeta potential data

Limestone powder at 25 °C						
Brine	FW	SW	4Mg	8Mg	SW-0.1NaCl	SW-0.1
	5.94	5.32	7.76	9.11	4.64	5.49
	5.96	6.81	6.7	9.9	5.04	4.85
	5.08	6.25	6.06	10.1	5.26	5.14
Average	5.66	6.53	9.84	9.9	4.98	5.16
Limestone powder at 70 °C						
Brine	FW	SW	4Mg	8Mg	SW-0.1NaCl	SW-0.1
	6.22	5.53	3.67	11.5	5.21	4.06
	9.15	7.12	5.46	10.4	5.03	5.41
	6.77	3.07	8.51	7.76	5.1	4.38
Average	7.38	5.24	5.88	11.5	4.45	4.04
pH values at 25°C (Limestone powder)						
Brine	FW	SW	4Mg	8Mg	SW-0.1NaCl	SW-0.1
pH	6.74	8.28	7.86	7.75	8.09	8.40
25°C	5.66	6.53	9.84	9.90	4.98	5.16
70°C	7.38	5.24	5.88	11.50	4.45	4.04
			4Mg	SW-0.1NaCl-2S-4Mg		
			8Mg	SW-0.1NaCl-2S-8Mg		

Figure A.14: Zeta potential data for pure limestone powder.

A.6 Spontaneous imbibition data

Crude oil aged powder at 25°C						
Brine	FW	SW	4Mg	8Mg	SW-0.1NaCl	SW-0.1
	10.08	7.1	10.2	1.27	-1.78	-2.17
	7.78	6.21	8.73	1.45	-1.87	-2.15
	8.08	6.97	7.02	2.09	-1.49	-1.92
Average	8.89	6.76	8.65	1.6	-1.71	-2.08
Crude oil aged powder at 70°C						
Brine	FW	SW	4Mg	8Mg	SW-0.1NaCl	SW-0.1
	5.70	3.85	11.10	7.74	-0.67	-0.32
	7.38	4.05	12.80	2.65	-0.68	-0.08
	7.83	1.05	9.18	3.99	-0.19	-0.06
Average	7.00	2.98	11.00	4.79	-0.51	-0.15
pH values at 25C (Crude oil aged powder)						
Brine	FW	SW	4Mg	8Mg	SW-0.1NaCl	SW-0.1
pH	7.14	8.30	7.91	7.74	8.10	9.16
25°C	8.89	6.76	8.65	1.60	-1.71	-2.08
70°C	7.00	2.98	11.00	4.79	-0.51	-0.15
			4Mg	SW-0.1NaCl-2S-4Mg		
			8Mg	SW-0.1NaCl-2S-8Mg		

Figure A.15: Zeta potential data for crude oil aged powder.

Time (Days)	Production (Cm3)	Cum. Prod (Cm3)	RF (%)	Production (Cm3)	Cum. Prod (Cm3)	RF (%)
	B1	B1	B1	B8	B8	B8
1	1.00	1.00	11.30	1.40	1.40	16.06
2	0.40	1.40	15.82	0.80	2.20	25.23
3	0.10	1.50	16.95	0.40	2.60	29.82
4	0.00	1.50	16.95	0.00	2.60	29.82
5	0.60	2.10	23.73	0.10	2.70	30.96
6	0.20	2.30	25.99	0.10	2.80	32.11
7	0.15	2.45	27.68	0.10	2.90	33.26
8	0.00	2.45	27.68	0.00	2.90	33.26
9	0.05	2.50	28.25	0.00	2.90	33.26
10	0.00	2.50	28.25	0.00	2.90	33.26
11	0.00	2.50	28.25	0.00	2.90	33.26
12	0.00	2.50	28.25	0.00	2.90	33.26

N for B1	8.85
N for B8	8.72
RF	Recovery Factor

Figure A.16: Spontaneous Imbibition data for cores B1 and B8

Time [Days]	C1		RF [%]	C2		RF [%]	Brines
	Production [cm3]	Tot_Produced [cm3]		Production [cm3]	Tot_Produced [cm3]		
0	29/03/2021	0.00	0.00	0.00	0.00	0.0	FW
1	30/03/2021	1.05	1.05	0.80	0.80	18.1	
2	31/03/2021	0.15	1.20	0.15	0.95	21.5	
3	01/04/2021	0.00	1.20	0.00	0.95	21.5	
4	02/04/2021	0.00	1.20	0.00	0.95	21.5	
5	03/04/2021	0.00	1.20	0.00	0.95	21.5	
6	04/04/2021	0.00	1.20	0.00	0.95	21.5	
7	05/04/2021	0.20	1.40	0.15	1.10	24.9	SW
8	06/04/2021	0.10	1.50	0.20	1.30	29.5	
9	07/04/2021	0.00	1.50	0.10	1.40	31.7	
10	08/04/2021	0.00	1.50	0.00	1.40	31.7	
11	09/04/2021	0.00	1.50	0.00	1.40	31.7	
12	10/04/2021	0.00	1.50	0.00	1.40	31.7	
13	11/04/2021	0.15	1.65	0.10	1.50	34.0	SW-0.1NaCl-2S-4Mg
14	12/04/2021	0.00	1.65	0.00	1.50	34.0	
15	13/04/2021	0.05	1.70	0.05	1.55	35.1	
16	14/04/2021	0.00	1.70	0.00	1.55	35.1	
17	15/04/2021	0.00	1.70	0.10	1.65	37.4	
18	16/04/2021	0.00	1.70	0.00	1.65	37.4	
19	17/04/2021	0.00	1.70	0.00	1.65	37.4	
20	18/04/2021	0.10	1.80	0.25	1.90	43.1	SW-0.1NaCl-2S-8Mg
21	19/04/2021	0.10	1.90	0.00	1.90	43.1	
22	20/04/2021	0.05	1.95	0.10	2.00	45.3	
23	21/04/2021	0.00	1.95	0.05	2.05	46.5	
24	22/04/2021	0.00	1.95	0.05	2.10	47.6	
25	23/04/2021	0.00	1.95	0.00	2.10	47.6	
26	24/04/2021	0.00	1.95	0.00	2.10	47.6	
27	25/04/2021	0.00	1.95	0.00	2.10	47.6	
28	26/04/2021	0.00	1.95	0.00	2.10	47.6	
29	27/04/2021	0.00	1.95	0.00	2.10	47.6	

Figure A.17: Spontaneous Imbibition data for cores C1 and C2

Time [Days]	Date	B2		B3		B2		B3		Brines
		Produced [cm3]	Tot_Produced [cm3]	RF [%]	Produced [cm3]	Tot_Produced [cm3]	RF [%]	Produced [cm3]	Tot_Produced [cm3]	
0	26/03/2021	0.00	0.00	0.00	0.00	0.00	0.00	0.00	0.00	FW
1	27/03/2021	1.55	1.55	16.80	1.00	1.00	10.98	1.00	10.98	
2	28/03/2021	0.00	1.55	16.80	0.00	1.00	10.98	1.00	10.98	
3	29/03/2021	0.00	1.55	16.80	0.00	1.00	10.98	1.00	10.98	
4	30/03/2021	0.60	2.15	23.30	0.30	1.30	14.28	1.30	14.28	SW
5	31/03/2021	0.00	2.15	23.30	0.20	1.50	16.48	1.50	16.48	
6	01/04/2021	0.00	2.15	23.30	0.00	1.50	16.48	1.50	16.48	
7	02/04/2021	0.00	2.15	23.30	0.00	1.50	16.48	1.50	16.48	
8	03/04/2021	0.00	2.15	23.30	0.00	1.50	16.48	1.50	16.48	
9	04/04/2021	0.10	2.25	24.38	0.00	1.50	16.48	1.50	16.48	SW-0.1NaCl
10	05/04/2021	0.00	2.25	24.38	0.00	1.50	16.48	1.50	16.48	
11	06/04/2021	0.40	2.65	28.71	0.30	1.80	19.77	1.80	19.77	
12	07/04/2021	0.00	2.65	28.71	0.00	1.80	19.77	1.80	19.77	
13	08/04/2021	0.00	2.65	28.71	0.20	2.00	21.97	2.00	21.97	
14	09/04/2021	0.00	2.65	28.71	0.00	2.00	21.97	2.00	21.97	
15	10/04/2021	0.00	2.65	28.71	0.00	2.00	21.97	2.00	21.97	
16	11/04/2021	0.00	2.65	28.71	0.00	2.00	21.97	2.00	21.97	SW-0.1NaCl-2S-4Mg
17	12/04/2021	0.50	3.15	34.13	0.45	2.45	26.91	2.45	26.91	
18	13/04/2021	0.35	3.50	37.92	0.20	2.65	29.11	2.65	29.11	
19	14/04/2021	0.35	3.85	41.72	0.10	2.75	30.21	2.75	30.21	
20	15/04/2021	0.00	3.85	41.72	0.00	2.75	30.21	2.75	30.21	
21	16/04/2021	0.00	3.85	41.72	0.00	2.75	30.21	2.75	30.21	
22	17/04/2021	0.00	3.85	41.72	0.00	2.75	30.21	2.75	30.21	
23	18/04/2021	0.00	3.85	41.72	0.00	2.75	30.21	2.75	30.21	

Figure A.18: Spontaneous Imbibition data for cores B2 and B3